A novel *miR-328-Bace1* axis ensures brown adipose tissue homeostasis and energy metabolism in mice

Inaugural-Dissertation
zur Erlangung des Doktorgrades
der Mathematisch-Naturwissenschaftlichen Fakultät
der Universität zu Köln

vorgelegt von

MATTEO OLIVERIO

aus Piacenza

KÖLN 2018

Berichterstatter	Dr. Jan-Wilhelm Kornfeld
	Prof. Dr. Thomas Langer
Tag der mündlichen Prüfung	21.12.2017
Jahr der Veröffentlichung	2018

Table of Contents

List of Figures

Colour legend of aforementioned figures

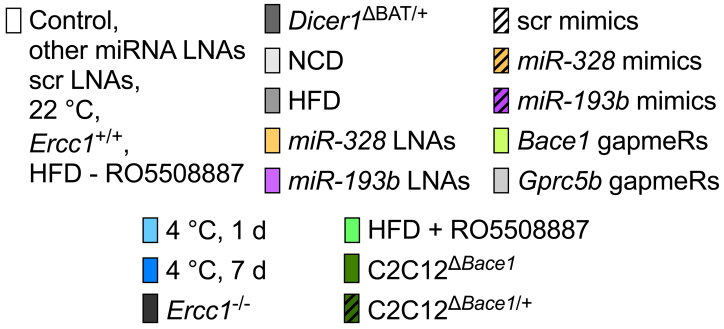

List of Tables

List of Abbreviations

AD	Alzheimer's disease
Amp	Ampicillin resistance cassette
APP	β-amyloid precursor protein
AT	Adipose tissue
ATP	Adenosine-tri-phosphate
Aβ	β-amyloid
Bace1	β-site amyloid precursor protein cleaving enzyme 1
BAT	Brown adipose tissue
bp	Basepair
brite	Brown-in-white
CBh	Chicken β-actin (CBA) promoter
circRNA	Circular RNA
CNS	Central nervous system
CRISPR	Clustered regularly interspaced short palindromic repeats
crRNA	CRISPR RNA
CSC	Cell surface capturing
DIO	Diet-induced obesity
EE	Energy expenditure
ES cell	Embryonic stem cell
FCCP	Carbonyl cyanide-4 (trifluoromethoxy) phenylhydrazon
GFP	Green fluorescent protein
GO	Gene ontology
GPI	Glycosylphosphatidylinisotol
Gprc5b	G-protein coupled receptor family C group 5 member B
gRNA	Guide RNA
GTT	Glucose tolerance test
H&E	Hematoxylin and eosin
HFD	High-fat diet
HMW	High molecular weight
IPA	Ingenuity pathway analysis
iSPECS	Improved secretome protein enrichment with click sugars
ITT	Insulin tolerance test
L	Liver
LMW	Low molecular weight
lncRNA	Long noncoding RNA
miRNA	MicroRNA
mRNA	Messenger RNA
miRNA	MicroRNA
mRNA	Messenger RNA
NCD	Normal chow diet
NEFA	Non-esterified fatty acids
NMR	Nuclear magnetic resonance
nt	Nucleotide
OCR	Oxygen consumption rate
PCR	Polymerase chain reaction
PIBA	Immortalized brown pre-adipocyte
piRNA	Piwi-interacting RNA
pre-miRNA	Precursor microRNA
pri-miRNA	Primary microRNA
PuroR	Puromycin resistance cassette
qPCR	Real-time quantitative RT-PCR
RISC	RNA-induced silencing complex
rRNA	Ribosomal RNA
RT	Reverse transcription
SB	Southern blot
SCAT	Subcutaneous adipose tissue
scr	Scramble (control)
SM	Skeletal muscle

snoRNA	Small nucleolar RNA	U6	U6 promoter
SNS	Sympathetic nervous system	UTR	Untranslated region
TG	Triacylglycerol	VAT	Visceral adipose tissue
TLC	Thin-layer chromatography	WAT	White adipose tissue
tracrRNA	Trans-activating CRISPR RNA	WB	Western blot
TRP	Transient receptor potential	WT or wt	Wild-type

ZUSAMMENFASSUNG

Braunes Fettgewebe (BAT) hat in den letzten Jahrzehnten zur Bekämpfung von Fettleibigkeit und ihrer Folgeerkrankungen als therapeutisches Mittel stark an Aufmerksamkeit gewonnen. Sowohl in Nagern als auch in Menschen schützt aktiviertes BAT mittels Steigerung des Energieumsatzes vor Diät-induzierter Fettleibigkeit und der zugehörigen Beeinträchtigung des Glukose-Metabolismus. Interessanterweise können BAT-ähnliche Eigenschaften auch in Vorläuferzellen der quergestreiften Muskulatur hervorgerufen werden, da diese beiden Gewebe einer gemeinsamen Zelllinie entstammen. Es konnte nachgewiesen werden, dass Differenzierung and Funktion von BAT durch nicht-kodierende RNA-Netzwerke kontrolliert wird. Insbesondere sind verschiedenste microRNAs (miRNAs) dazu in der Lage, sowohl BAT-Homöostase als auch die Zelllinien-Entscheidung zwischen BAT und quergestreifter Muskulatur zu beeinflussen.
In dieser Studie zeigen wir eine neue *miR-328-Bace1* Achse auf, welche an metabolischer Homöostase beteiligt ist, indem sie die Differenzierung und Aktivierung brauner Fettzellen fördert. Wir konnten nachweisen, dass die Expression von *miR-328* mit BAT-Aktivität korreliert und zudem *in vitro* die Differenzierung brauner Fettzellen - unter Benachteiligung von Muskelzell-Entwicklung - begünstigt. Dieser Vorgang wird veranlasst mittels der Inhibition durch die miRNA von der β-Sekretase BACE1, einer Protease, welche für ihre schädliche Rolle in Alzheimer-Entwicklung bekannt ist. In der Tat konnten wir nachweisen, dass sich BACE1 antagonistisch zu *miR-328* verhält. Sowohl *Bace1* Knock-Down als auch Knock-Out führten zu einem pro-adipogenen Phänotyp in braunen Fettzellen und sogar Muskelzellen. Darüber hinaus konnte dem konditionierten Medium von *Bace1* Knock-Out-Myoblasten eine parakrine Wirkung zugewiesen werden, da es das adipogene Potenzial von Wildtyp-Myoblasten steigerte. Komplementäre Proteom-Analysen ermittelten anschließend potenzielle BACE1-Substrate, welche in diesen Vorgang verwickelt sein könnten. Von besonderem Interesse wurde hierbei AOC3 als vermeintliches BACE1-Substrat identifiziert, ein entzündungsförderndes Transmembran-Protein, welches im Zusammenhang mit Typ-2-Diabetes steht. Die lösliche Form des Proteins, sAOC3, ermöglicht diesem parakrine und endokrine Funktionen. Dieser Mechanismus könnte für die vorteilhaften metabolischen Effekte durch BACE1-Inhibition ver-

antwortlich sein, welche wir in fettleibigen Mäusen beobachten konnten. Tatsächlich konnten wir zeigen, dass reduzierte BACE1-Aktivität, welche bekanntermaßen die Pathophysiologie der Alzheimer-Krankheit mindert, auch die Energie-Homöostase des gesamten Körpers verbesserte, indem sie verminderte Gewichtszunahme und einen günstigeren Glukose-Stoffwechsel hervorrief. Des Weiteren führte BACE1-Inhibition zu einer erhöhten BAT-Marker-Expression in braunem Fett und gleichzeitig zu einer globalen Verminderung von Differenzierungs-Markern der quergestreiften Muskulatur. Zusammengefasst stellen BACE1 und dessen Substrate, eventuell einschließlich AOC3, vielversprechende Ansätze zur Bekämpfung von Fettleibigkeit, der Alzeimer-Krankheit und deren Folgeerkrankungen dar. Somit erweitert diese Arbeit das Anwendungsgebiet von BACE1 - über Alzheimer-Krankheit hinaus - zu BAT und Stoffwechselregulation.

Summary

In the last decades brown adipose tissue (BAT) rose to attention as therapeutic target to counteract obesity and its related diseases. In both rodents and humans, activated BAT protects from diet-induced obesity and the associated deterioration of glucose metabolism via enhancing energy expenditure. Interestingly, BAT-related features can also be promoted in skeletal muscle (SM) progenitor cells due to the common cell lineage that these tissue share. Differentiation and function of BAT has been shown to be under control of noncoding RNA networks. In particular, various microRNAs (miRNAs) are able to drive both brown fat homeostasis and BAT/SM cell fate regulation.
Here we show a novel *miR-328–Bace1* axis involved in metabolic homeostasis through a mechanism that promotes brown adipocyte differentiation and activation. We found *miR-328* expression to correlate to BAT activity and to promote brown adipogenesis to the detriment of myogenesis *in vitro*. This process is dependent on the inhibition by the miRNA of the β-secretase BACE1, a protease known for its detrimental role in Alzheimer's disease (AD). We could show this protein to act antagonistically to *miR-328*. Indeed, both knock-down and knock-out of *Bace1* resulted in a pro-adipogenic phenotype in both brown adipogenic and even myogenic cell lines. Moreover, conditioned medium from *Bace1* knock-out myoblasts revealed paracrine effects by stimulating the adipogenic potential of wild-type myoblasts. Complementary proteomic analyses determined potential substrates of BACE1 involved in this process. In particular, AOC3, a pro-inflammatory, type 2 diabetes-related transmembrane protein, was identified as a putative BACE1 target, with potential paracrine and endocrine functions due to its soluble form sAOC3. This mechanism could be responsible for the beneficial metabolic effects of BACE1 inhibition observed in obese mice. In fact, we showed that diminished BACE1 activity, known to reduce the pathophysiology of AD, enhanced whole-body homeostasis, leading to decreased body weight gain and ameliorated glucose metabolism. BACE1 inhibition was furthermore associated with increased BAT marker expression in the adipose tissue and a global decrease in SM-associated differentiation pathways.
Taken together, BACE1 and its substrates, potentially including AOC3, are promising therapeutic targets against obesity, AD and their sequelae. This warrants the broadening of the scientific scope for BACE1 investigation beyond AD and towards BAT and metabolism regulation.

Graphic Abstract

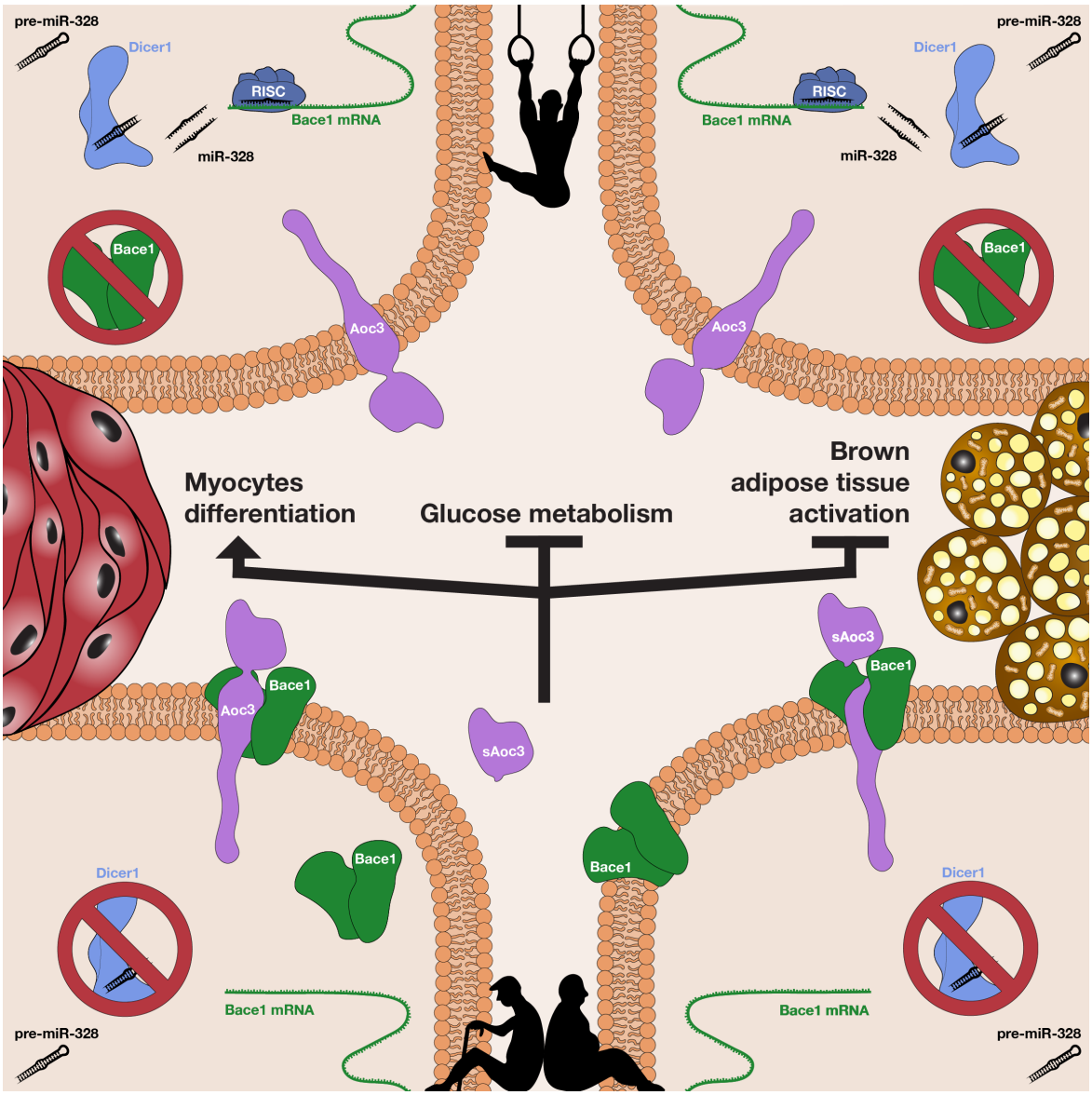

***Dicer1-miR-328-Bace1* axis ensures brown adipose tissue homeostasis and energy metabolism in mice.**

CHAPTER 1

INTRODUCTION

1.1 The obesity pandemic and associated diseases

In the last decades obesity has become a major socio-economic burden in our society, with more than 1.9 billion adults worldwide being overweight in 2014, of which over 600 million were obese [1]. The World Health Organisation (WHO) defines overweight and obesity as abnormal or excessive fat accumulation that may impair an individual‚Äôs health status [1]. To classify these two conditions in adults in an unbiased way, the body mass index (BMI) is utilised. BMI is an index of weight-for-height defined as a person's weight in kilograms divided by the square of his height in meters (kg/m^2). The standard for body mass categorisation considers an adult with a BMI greater than or equal to 25 as overweight and a BMI greater than or equal to 30 as obese [1]. In recent years the obesity pandemic reached such a severe impact worldwide that in every region, except parts of sub-Saharan Africa and Asia, overweight and obesity are linked to more deaths than underweight [1], placing a massive burden on health systems around the globe. This global rise in the prevalence of obesity does not only affect adults, with more than 41 million children under the age of 5 considered overweight or obese [1]. In rodents it has been shown that offspring obesity is dependent on maternal impaired glucose homeostasis during lactation [2], demonstrating a transgenerational occurrence of the metabolic syndrome. Alterations in body fat mass and abnormal fat distribution, known as lipodystrophy, have a major impact on whole-body metabolism and can lead to increased risk of type 2 diabetes mellitus (T2D), cardiovascular diseases, neurodegenerative diseases, some types of cancer [3] [4] [5] and in general all-cause mortality [6].

1.1.1 Obesity and type 2 diabetes mellitus

The main obesity-related disease is unanimously type 2 diabetes mellitus, with more than 422 million adults affected worldwide (Data from 2014) [7]. T2D is a complex metabolic disease characterised by defect insulin signalling and subsequently increased levels of glucose in the serum, known as hyperglycaemia. The peptide hormone insulin acts in a post-prandial manner as it is able to clear plasma of glucose and triacylglycerols by receptor-mediated uptake into cells of peripheral organs. On a molecular level insulin triggers glucose uptake into peripheral organs via binding to the insulin-receptor and inducing a subsequent signalling pathway including phosphatidyl inositol 3-kinase pathway (PI3K). The following downstream cascade includes AKT/protein kinase B (PKB), which in its phosphorylated - and activated - form, regulates the activity of many targets, including kinases, transcription factors and other molecules involved in metabo-regulatory pathways [8]. Chronic activation of the insulin-receptor though may lead to insulin-desensitisation in many organs, including liver, adipose tissue and skeletal muscle. To compensate for the insulin resistance, pancreatic β-cells become constitutively over-productive and may break, leading to a complete lack of endogenous insulin secretion, which manifests in hyperglycaemia and T2D [9].
Risk factors for T2D include not only many genetic, but also epigenetic components caused by environmental triggers such as diet, lifestyle and obesity [10]. The development and pathophysiology of obesity and T2D are so interconnected that is difficult to pinpoint any exclusive causes to each of them.
Although the treatment of T2D is nowadays relatively standardised and careful monitoring of blood sugar levels allows many patients to live a healthy life, impairment of glucose homeostasis can lead to serious complications throughout the body. These complications, that include heart attack, stroke, kidney failure, leg amputation and vision loss, can lead to premature death, making T2D a major cause of deaths worldwide with 1.5 million deaths caused by this disease in 2012 only [7].

1.1.2 Obesity and neurodegenerative diseases

Glucose homeostasis plays a central role in regulating brain metabolism. Indeed, the brain consumes around 25% of total body glucose despite constituting only 2% of body weight [11]. Impairment in glucose regulation and obesity have been associated with a higher risk of developing neurodegenerative diseases like Alzheimer's (AD), Parkinson's (PD), Huntington's diseases and multiple sclerosis [12]. Given the shared deterioration

of glucose homeostasis in the onset both obesity and neurodegenerative diseases, a BMI above 25 is not only considered a risk factor for the development of T2D but also for AD and PD [13]. In fact T2D prevalence has a high epidemiological correlation with AD [14].

1.2 Alzheimer's disease

Alzheimer's disease is the most common among neurodegenerative diseases affecting about 47 million people worldwide, a number which is constantly increasing [15]. The disease is defined by two pathological hallmarks: extracellular amyloid plaques and intracellular neurofibrillary tangles. These features were first described by the German psychiatrist Alois Alzheimer in 1907 (reviewed in [16]) and since then many efforts have been deployed in understanding the mechanism behind this pathology. Neurofibrillary tangles are aggregates of the microtubule-associated protein tau that accumulate when it is aberrantly processed and hyperphosphorylated [17]. The generation of amyloid plaques, on the other hand, arise due to endoproteolysis of amyloid precursor protein (APP), a type I membrane protein. As shown in figure 1.1 APP is subsequently cleaved by the proteases β-secretase (also known as Bace1) and γ-secretase, to liberate β-amyloid (Aβ) peptides. This process also generates a soluble APP ectodomain (sAPPβ), due to β-secretase cleavage, and a membrane bound carboxy (C)-terminal fragment (C59), due to γ-secretase cleavage [17].

1.2.1 Insulin signalling in Alzheimer's disease

As described above, obesity or overweight in midlife is implicated as an independent risk factor of AD in later life. The correlation between this neurodegenerative disease and metabolic malfunctioning is also highlighted by the fact that AD patients show impaired glucose metabolism, hyperinsulinaemia and insulin resistance [18] [19]. Moreover, brain samples from AD patients display reduced insulin levels, insulin receptor density and signalling [20]. The interconnection between the detrimental effects of AD and T2D is so strong that several research groups refer to the neurodegenerative disease as "type 3 diabetes" [21] [22], claiming that AD may represent a neuroendocrine disorder that resembles, yet is distinct from diabetes mellitus. For the importance that insulin implicates in key regulatory pathways of learning and memory in the central nervous system (CNS), impaired insulin activity and signalling in the brain has been proposed to promote and/or exacerbate AD neuropathology [23]. The intercorrelation between AD

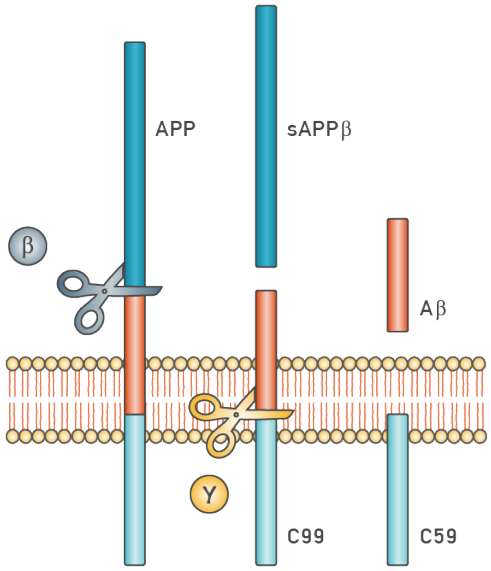

FIGURE 1.1. **APP processing by β- and γ-secretases for the generation of Aβ.** First, the β-secretase Bace1 (β) cleaves APP to create the N-terminus of Aβ, generating the membrane-bound C99 and the secreted sAPPβ ectodomain (blue). Second, C99 is cut by the γ-secretase (γ) to generate the C-terminus of Aβ. The Aβ peptide (red) is then released and secreted extracellularly. An intracellular domain, C59 (light blue), is also produced. Original figure; based on [17].

and obesity was supported by an *in vivo* study in which Ho and colleagues used an AD mouse model to study the effects of diet-induced obesity on the brain. The peripheral insulin resistance that arose with excessive feeding was shown to reduce both the amount and the signalling efficency of insulin in the brain of these mice, leading to an increase of AD symptoms, like β-amyloid peptide generation and subsequent cognitive decline [24].

1.2.2 The β-secretase BACE1

Since the discovery of β-amyloid plaques in the brains of AD patients, a lot of effort has been undertaken in discovering the protease responsible for their generation. It took many years before different research groups identified this protease as the β-secretase BACE1, a 501 amino acid type I transmembrane aspartic protease which is related to the pepsin family and the retroviral aspartic proteases [25] [26] [27] [28] [29]. Despite being majorly expressed in the brain, BACE1 protein is distributed broadly - in low levels - among most peripheral tissues, with the exception of the pancreas which shows robust expression [27]. BACE1 is not only present on the cell membrane, but is also located within acidic intracellular compartments, including endosomes and trans-Golgi

networks, for its optimal enzyme activity at acidic pH [17].
BACE1 role in the proteolytic cleavage of APP was first discovered using *Bace1*-depleted neurones which showed abolished production of Aβ and deposition of β-amyloid plaques [27] [30]. This central relevance for BACE1 in AD pathology is also highlighted by increased BACE1 levels and activity in AD patient's brains [31].
Although early reports on *Bace1* whole-body knock-out mice showed no apparent adverse effects, suggesting that inhibition of the β-secretase should not have any toxic effect due to its physiological not-APP-related role [32], more recent studies have shown a wide range of BACE1-related side effects, including hypomyelination, retinal pathology and others (reviewed in [17]). A physiological role for BACE1 activity has for example been shown in muscle where the secretase is involved muscle spindle maintenance, leading to defects in coordinated movements in mice lacking one or both copies of *Bace1* [33].
In light of the pathological correlation between AD and T2D, the question arose whether BACE1 has a role in glucose metabolism as well. First evidence in this direction came from a study by Meakin *et al.* which showed that whole-body knock-out of *Bace1* displayed improved insulin sensitivity and glucose homeostasis [34]. Additional studies have been performed *in vitro* to further test the effects of BACE1 activity on glucose regulation on a molecular level. In the skeletal muscle cell line C2C12, BACE1 inhibition was shown to directly enhance glucose uptake and metabolism [35]. In line with this, over-expression of *Bace1* in the human neuroblastoma cell line SH-SY5Y reduced cellular glucose metabolism and switched the cellular metabolic profile from oxidative to glycolytic [36].

1.2.3 Therapeutic approaches against Alzheimer's disease

Given the high incidence of AD and the immense therapy costs associated with it, much research has been focusing on a potential cure that could stop or delay the onset of the disease. In 2015 a report by the Alzheimer's Association [37] stated that the market introduction of a treatment in 2025 that could delay the onset of AD by five years could reduce the prevalence of this neurodegenerative disease by approximately 42% in 2050. To date, no reliable biomarkers of AD are known and there are no treatments able to stop the cognitive decline in AD patients. Only moderate symptomatic benefits have been reported by the use of drugs like cholinesterase inhibitors and the NMDA (N-methyl-D-aspartate) receptor antagonist, memantine [38]. As the pathophysiology of AD leads to Aβ overproduction and impaired Aβ clearance, recent approaches to counteract the disease have been focusing on enhancing clearance of β-amyloid peptides from the

brain [39] and blocking Aβ generation in the first place. As a promising example of this approach, BACE1 inhibitors and γ-secretase inhibitors and modulators are thoroughly being investigated [40].

1.2.4 The therapeutical potential of BACE1 inhibitors

Among all therapeutic approaches developed in the last decades, BACE1 inhibitors have shown the highest potential in counteracting AD with many of such compounds in phase II/III human clinical trials [17]. LY2811376 was one of the first drugs tested in humans in the beginning of this millennium [41]. Despite rather modest potency on BACE1 inhibition, this compound showed a robust Aβ lowering activity in both animals and normal healthy volunteers (phase I trials). However, LY2811376 development was terminated due to off-target toxicities in eye and brain. Since then other inhibitors with high affinity binding to BACE1 and the ability to reduce Aβ production *in vivo* have been discovered [42] [43] [44]. Of particular interest is Verubecestat (MK-8931), which was the first BACE1 inhibitor to reach phase III clinical trials in patients with mild to moderate AD [44]. The drug discovered by Kennedy and colleagues is orally administered and shows reduced Aβ and sAPPβ in the cerebrospinal fluid of animal models and humans, both healthy and with AD. Furthermore, Verubecestat did not show any of the side effects previously attributed to BACE1 inhibition by other compounds. However more studies are necessary in the context of BACE1-targeting therapeutics and a really effective cure for AD is still far beyond.

1.3 Metabolic regulation of peripheral tissues

Obesity occurs when energy consumption in form of food intake chronically exceeds energy expenditure. It has been known for many years that body weight is regulated by the central nervous system, in particular the hypothalamic area of the brain [45] and to-date many different nuclei within the hypothalamus have been characterised based on their function in energy homeostasis regulation [46]. Although hormonal and neuronal mechanisms in response to feeding behaviour are finely tuned by neuropeptides produced by the brain, peripheral tissues also play a pivotal role, with pancreas, liver, adipose tissue and skeletal muscle bidirectionally communicating with the brain to maintain the proper body homeostasis [47].

1.3.1 Adipose tissue

Adipose tissue (AT) is an important regulator of global energy homeostasis in the body since it can store and provide energy in the form of lipids. AT is therefore a site of continuous anabolic and catabolic processing of lipids. On the anabolic side lipids are formed through lipogenesis, a process that converts excess carbohydrates into fatty acids, which are then esterified and stored as triacylglycerols (TGs) [48]. Known key players in lipogenesis regulation are fatty acid-binding proteins (FABPs), a family of intracellular lipid chaperones, that regulate lipid trafficking and responses in cells [49]. The adipocyte-specific member of this family is FABP4 (also known as aP2), which is also expressed in macrophages and plays an important role in the development of insulin resistance in relation to metaflammation [49]. FABP4 is fundamental for AT homeostasis, and mice with no or reduced expression of this protein showed increased body weight but unaffected insulin sensitivity and glucose homeostasis [50] [51]. Catabolic processing of lipids in AT on the other hand include the release of fatty acids into the circulation under fasting conditions to provide fuel for energy-supplying β-oxidation both locally and in peripheral tissues.

AT can be divided into three major subgroups (figure 1.2): white adipose tissue (WAT), mainly located in the subcutaneous and intra-abdominal regions, brown adipose tissue (BAT), primarily located in the interscapular region in rodents, and a thermogenically-activated form of WAT named beige or brite (brown in white) adipose tissue [52].

All three adipose tissues arise from a mesodermal origin and pre-adipocytes of all lineages share the expression of preadipocyte factor-1 (PREF1), a transmembrane protein expressed on immature pre-adipocytes, which represses adipogenic differentiation [53]. Once cells undergo growth arrest, *Pref1* expression gets down-regulated, triggering a transcriptional cascade that leads to adipogenic differentiation. This process mainly involves peroxisome proliferator-activated receptor γ (PPARγ) and CCAAT/enhancer-binding proteins (C/EBPα, β and δ) [54]. The transcription factor PPARγ does not only comprise the ability to promote the adipogenic expression cascade but also directly regulates adipocyte metabolism, being able to induce lipogenesis and lipid storage, while repressing lipolysis and the release of non-esterified fatty acids (NEFAs, discussed in 1.4) from adipocytes in a diet-dependent manner [55]. Fully functional adipocytes later-on express FABP4 [49].

Although adipocytes from all depots share a significant overlap in general adipogenic metabolism, BAT and WAT are yet characterised by distinct differences that drive their commitment and activation as will be further described below.

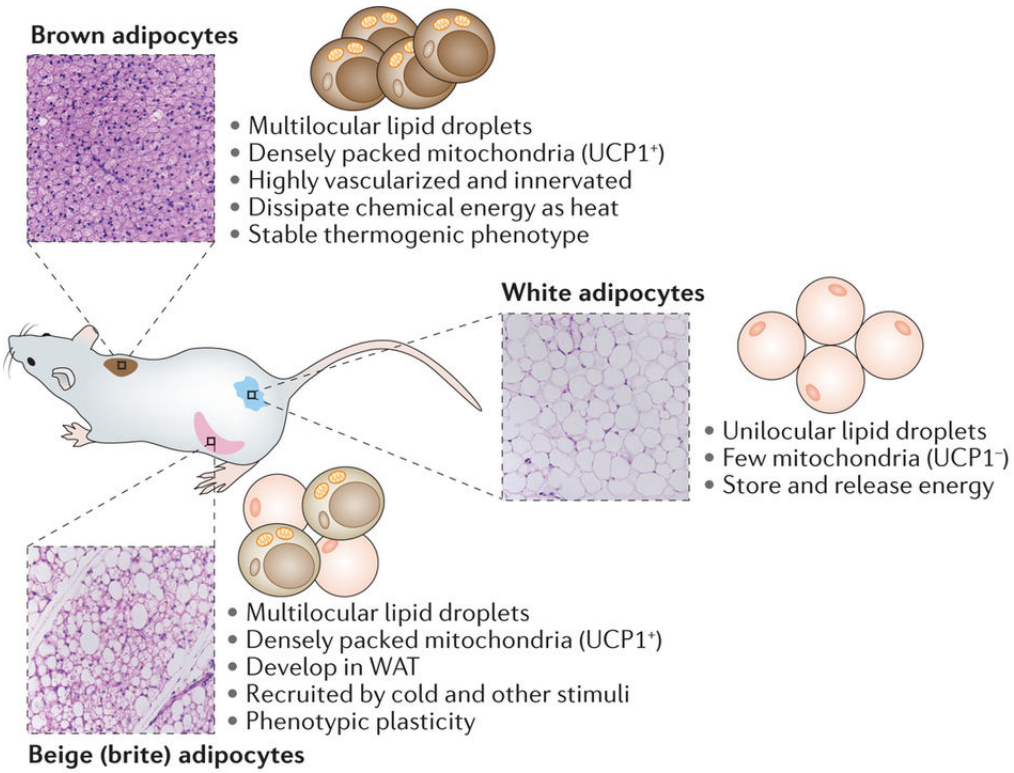

FIGURE 1.2. **The three classes of adipocytes.** Adipose tissue is mainly composed of adipocytes. These are divided into brown, white and beige adipocytes. Brown adipose tissue (BAT), mainly located in the interscapular region, is characterised by adipocytes with multilocular lipid droplets. Thanks to the uncoupling protein 1 (UCP1)-containing mitochondria and its high vascularisation and innervation, BAT is able to dissipate chemical energy as heat. White adipose tissue (WAT), with various subcutaneous and intra-abdominal depots, presents adipocytes with unilocular lipid droplets and is a major organ for the storage and release of energy. Beige adipocytes are present within various WAT depots, in particular in the subcutaneous ones. These cells have BAT-like characteristics and can be recruited by cold exposure and other stimuli. Beige adipocytes show a much higher phenotypic plasticity than BAT, being able to switch between a thermogenic or storage phenotype. From [52].

1.3.1.1 White adipose tissue

White adipose tissue is the most abundant type of AT and is mainly composed of white adipocytes [5]. These cells are characterised by a unilocular lipid droplet which takes up about 90% of the adipocyte mass and confers the cells their typical spheric shape (figure 1.2). In a steady state system the lipid release of white adipocytes equals lipid uptake and lipogenesis. Yet, given the constantly changing nutritional availability during food intake and fasting phases, white adipocytes exhibit a remarkable size plasticity, which is unique for a non-neoplastic tissue [56]. As soon as lipid influx into white adipocytes

exceeds lipid release, the cells are capable of increasing either in size (hypertrophy) or number (hyperplasia) to furthermore constitute a safe storage site for fatty acids [56]. WAT is divided into different depots, the two main ones being subcutaneous adipose tissue (SCAT) and intra-abdominal or visceral adipose tissue (VAT) [57]. The deposition of lipids within the different depots occurs in a hierarchical manner: The primary site for NEFA uptake is SCAT and only after the lipid storage capacity is saturated in this depot, additional excess energy will be taken up by VAT [56]. For SCAT comprising the highest capacity to protect from lipodystrophy, it is considered to be the safest fat depot and accumulation of SCAT has minor detrimental effects on body homeostasis [58]. Increase of VAT mass on the other hand plays a more dominant role in NEFAs release and is often associated with obesity-related diseases, like T2D and cardiovascular complications [59]. Therefore, different WAT localisations implicate different roles in energy and glucose homeostasis regulation.
Next to its role as storage site WAT has also been indicated as the main endocrine organ in the body for it releases a vast range of hormones, known as adipokines [60]. Adipokines can regulate various substantial processes, including appetite, energy expenditure, lipid metabolism and insulin and glucose homeostasis [60]. The endocrine role of adipose tissue with be described in more detail in chapter 1.4.

1.3.1.2 Brown adipose tissue

Brown adipose tissue, the key site for non-shivering thermogenesis, is mainly composed of brown adipocytes, characterised by multilocular lipid droplets (figure 1.2). This tissue was first discovered in hibernating animals and was known to be present in rodents and newborn humans. However recent studies found presence of thermogenically active BAT also in adult humans [61] [62] [63]. Rodents present a main BAT depot in the interscapular region, whereas humans have BAT depots localised in the neck and the supraclavicular and mediastinal regions [64]. Just like WAT, BAT is also an endocrine organ and secretes several hormones (also known as batokines and lipokines) that regulate the cross-talk with the brain and other peripheral tissues [65]. Further details will be given in the next chapter (1.4).
Non-shivering thermogenesis in BAT allows mammals exposed to cold to produce heat apart from shivering [66]. Nutrients and oxygen available in the blood are combusted by BAT and utilised to fuel heat production. This process relies on the activity of uncoupling protein 1 (UCP1) in the inner mitochondrial membrane of brown adipocytes. UCP1 acts as an electron transporter, uncoupling mitochondrial combustion of substrates from ATP

production, instead producing heat and profoundly increasing energy expenditure (EE) [60]. The high vascularisation of BAT allows the tissue to cope with the high demand for nutrients and oxygen and also enables efficient distribution of heat throughout the body [60].

BAT stimulation occurs through activation of the sympathetic nervous system via stimulation of transient receptor potential (TRP) channels in sensory neurons [67]. The sympathetic fibres innervating BAT release norepinephrine (NE) upon cold-exposure to acutely activate thermogenesis [60]. NE binds to β-adrenergic receptors on the cell surface of brown adipocytes, leading to lipolysis of locally stored lipids, which henceforth serve for β-oxidation, and at the same time up-regulation of UCP1 [68]. Among the β-adrenergic receptors the β3-receptor subtype is the most effective activator for BAT thermogenesis [60]. The cell intrinsic signalling upon β-adrenergic stimulation is mediated by intracellular cyclic adenosine monophosphate (cAMP) release and protein kinase A (PKA) activation, which leads to the expression of thermogenic genes. NE-induced genes includes among others *Cebpb*, ELOVL fatty acid elongase 3 (*Elovl3*), which regulates endogenous synthesis of saturated very long chain fatty acids and TG formation, and peroxisome proliferator-activated receptor gamma coactivator 1-alpha (*Ppargc1a*), which is a key driver of mitochondrial biogenesis [60]. Other thermogenic stimuli aside cold-exposure are β-adrenergic pharmaceuticals, hormones and ingestion of caloric energy. Energy intake interestingly triggers diet-induced thermogenesis, i.e. an even higher energy output by BAT than demanded for mere food metabolism [69].

BAT differs from WAT not only in its thermogenic capacity, but also in its development, with brown adipocytes rising from precursors in the embryonic mesoderm, hereby sharing lineage with skeletal muscle cells [70]. These multipotent precursors express transcription factors such as paired box 3 (*Pax3*) [71], *Pax7* [72], engrailed-1 (*En1*) [73] and myogenic factor 5 (*Myf5*) [70], while white adipocytes mainly originate from *Pax3*$^-$, *Pax7*$^-$, *En1*$^-$ and *Myf5*$^-$ precursors. Although it has been implied, that beige adipocytes derive from the *Myf5*$^-$ lineage, it still remains unclear whether the process of browning therefore represents a transdifferentiation phenomenon or whether beige adipocytes develop from a separate precursor lineage [74]. Interestingly, a very low percentage of white adipogenic progenitor cells were also found to be *Myf5*$^+$ [5], underlining the difficulty to identify markers exclusively limited to distinct adipogenic lineages. However the concept of a shared progenitor lineage between brown adipocytes and skeletal muscle cells is indisputable and clearly distinct from white adipogenic precursor pools.

Since the discovery of BAT in adult humans, estimations have been made, that 50%

of the population possess the tissue in a thermogenically active form. Interestingly it could also be shown that BAT activity significantly declines with both age and obesity [75]. Human studies revealed that cold exposure leads to increased BAT activity and decreased body fat mass, with an inverse correlation reported between the amount of BAT and adiposity [76] [77]. This activation of brown fat occurred even in individuals with chronically low basal BAT activity, highlighting the potential that this tissue has in regulating whole-body homeostasis. It is therefore of greatest therapeutic interest to enhance BAT activity in humans as treatment against obesity. Conventional weight loss strategies and physical exercise often result in a hypometabolic state accompanied by impaired release of appetite-suppressing adipokines due to rapid WAT loss. An activation of BAT on the other hand could be able to circumvent the weight loss-induced appetite enhancement and involuntary reduction in energy expenditure [69]. Unfortunately β-adrenergic receptor agonists nowadays implicate low bioavailability [5] and various side effects particularly on the cardiovascular system [78], leaving a potent BAT activator yet to be discovered.

1.3.1.3 Beige adipose tissue

Some adipocytes within WAT have already been shown many years ago to be characterised by a multilocular appearance and high levels of UCP1 when stimulated by cold or β-adrenergic stimuli (figure 1.2) [79] [80]. Induction of these adipocytes strongly correlates with the capacity to reduce obesity in mice [81]. This tissue was later named beige or brite adipose tissue. Beige adipocytes share features of both white and brown ones, having extremely low basal expression of UCP1 (as does WAT), but being able to highly increase UCP1 levels and respiration rates when stimulated (as does BAT) [82]. Despite showing an expression footprint common to both WAT and BAT under specific conditions, beige adipose tissue also has specific gene markers with the most promising being TNF receptor superfamily member 9 (*Tnfrsf9* or CD137), transmembrane protein 26 (*Tmem26*) and T-box 1 (*Tbx1*), which were identified in *in vitro* and *in vivo* studies [83] [84]. However, an unequivocal gene set of beige markers is still debated.
In humans it has been shown that part of BAT depots could be composed of beige adipocytes and stimulating the development of beige adipocytes within white fat (a process known as browning) could reduce the detrimental effects of WAT accumulation, leading to a healthier metabolic phenotype [83].

1.3.2 Skeletal muscle

Skeletal muscle (SM) is one of the three main muscle types, together with cardiac and smooth muscle, and is the major site for insulin-stimulated glucose utilisation, disposing about 80% of total body glucose [85].
Defects in SM insulin homeostasis, with consequent insulin resistance, are a hallmark of the metabolic dysfunctions leading to obesity. This tissue is able to increase glucose transport upon insulin stimulation thanks to insulin-sensitive glucose transporters, with the GLUT4 isoform being the best characterised [86]. It has been suggested that insulin resistance in SM could occur due to defects in the recruitment of these glucose transporters to the sarcolemma, the muscle cell membrane [86]. Physical activity can influence muscle metabolism, with exercise training being shown to increase the number of mitochondria in SM [87].
Necessary for the determination and terminal differentiation of SM, are the members of the myogenic regulatory factors (MRF) family, a basic helix-loop-helix (bHLH) protein family that consists of MYOD1 (myogenic differentiation 1, also known as MYF3), MYOG (myogenin, also known as MYF4), MYF5 (myogenic factor 5) and MYF6 (also known as MRF4 or Herculin) [88]. All four of them are able, when over-expressed, to convert non-muscle cells to the myogenic lineage [88]. For example, ectopic expression of MYOD1 was shown to activate muscle genes in a variety of differentiated cell lines, including dermal fibroblasts, chondrocytes, smooth muscle, retinal pigmented epithelial cells, adipocytes, and melanoma, neuroblastoma, osteosarcoma, and hepatoma cells [89]. These myogenic factors are also involved in myogenesis during development and are expressed in a temporally distinct manner: *Myf5* is the first one to be detected in the somite, than *Myog* and last *MyoD*, which continues to be expressed throughout development. *Myf6* is instead expressed transiently in the myotome and later re-expressed to become the predominant MRF expressed in adult muscle [90]. Both *MyoD* and *Myf5* have are not strictly required for myogenic differentiation, with knock-out mouse models showing no apparent effects on muscle development [91] [92]. *Myog*, on the other hand, is essential for proper skeletal muscle formation and differentiation, with lack of the gene in mice leading to a severe reduction of differentiated skeletal muscle and postnatal death [90]. These experiments suggest that *MyoD* and *Myf5* act to determine the myogenic lineage whereas *Myog* and *Myf6* are important for differentiation and maintenance of the terminally differentiated state.
SM is a highly active tissue and require constant supply of ATP for the working muscles. Creatine kinase (CK) plays a pivotal role in the homeostasis of cellular ATP by catalysing

the conversion of creatine and consuming adenosine triphosphate (ATP) to create adenosine diphosphate (ADP) and phosphocreatine (PCr), with the latter serving as an energy reservoir for the rapid buffering and regeneration of ATP [93]. CK has five different isoenzymes, of which CKM is the muscle specific one. In SM, CKM can form homodimers, named CKMM, or heterodimers with the brain isoenzyme CKB, named CKMB [93]. CKM is considered a late myogenic marker and was shown to be accumulated in fully differentiated myogenic cell cultures [94].

Another important expect of SM physiology is calcium regulation. In this context a pivotal role is played by the troponin complex subunit Troponin T (TnT), which can modulate calcium regulation of actin thin filament function and is essential for the contraction of striated muscles [95]. In vertebrates TnT is encoded by three homologous genes with specific spatial regulation: *Tnnt1* is expressed in low skeletal muscle, *Tnnt2* in cardiac muscle and *Tnnt3* in fast skeletal muscle [95]. The two SM isoforms TNNT1 and TNNT3 are responsible for the binding to tropomyosin and anchoring to the thin filament in the sarcomeres of slow or fast twitch skeletal muscle respectively, which regulates the actin-activated myosin motor function [96].

Among the pathways critical for SM function there are also the ones involving mitochondrial oxidative metabolism and energy transduction. Indeed, decrease is mitochondria has been shown since many decades to be a major effect of long-term muscle atrophy [97]. In this context, the transcriptional coactivator PPARGC1α plays a fundamental role and its expression in SM is sufficient to induce mitochondriogenesis [98].

As stated above SM shares a common lineage with BAT, with progenitor cells being able to differentiate in both tissues. This was also supported by *in vivo* studies showing that mice unable to differentiate skeletal muscle cells present increased brown fat, especially in the dorsal cervical region [90]. This suggests that cells incapable of completing terminal muscle differentiation give rise to brown adipocytes. Recent investigations found specific molecular inter-players involved in this cell fate switch. Among these there is PR domain containing 16 (*Prdm16*), whose ectopic expression in both immortalised and primary myogenic cell lines led to a brown fat-like phenotype upon proadipogenic stimulation [70]. However, it was already known since many years that the master regulators of adipogenesis PPARγ and C/EBPα are able to drive myoblasts to transdifferentiate into mature adipocytes, completely blocking cell myogenesis upon expression of the two transcription factors [99].

In addition to the transdifferentiation between SM and AT, muscle stress (e.g. muscle dystrophies, inflammatory myopathies, or caused by ageing, obesity, diabetes and

other metabolic diseases) can lead to intramuscular fat deposition [100]. This includes both acellular lipid droplets within the myofibers and interstitial adipocytes which are PPARc2 positive [101]. Intra- and interfiber adipocytes are usually white, however also brown adipocytes have been identified, which can support SM in heat production during physical exercise [102].
As well as AT, SM has also been identified as an endocrine organ, which releases soluble factors called myokines [100]. They are synthesised in the tissue especially during contraction and exercise and can act in a paracrine or endocrine manner. Most of these myokines are secreted by AT as well. These shared factors are called adipo-myokines and include, among others, FGF21, IL-6 and myostatin [100].

1.4 Endocrine regulation of energy homeostasis

Energy homeostasis is described by the first law of thermodynamics:

Energy intake – energy expenditure = energy stored

Energy intake consist of all the fuels ingested by an organism, while energy expenditure (EE) is given by basal metabolic rate, thermogenesis and muscle action. As aforementioned excess fuels are stored as glycogen or TGs in different tissues, in particularly WAT, which stores them as fat. This mechanism has a protective function as it prevents ectopic lipid deposition in organs more metabolically active, like liver or SM [48]. The process of maintaining energy homeostasis fulfilled by adipose tissue, referred to as homeostatic regulation of adiposity and body weight, in regulated by the CNS through neuronal and hormonal signals [47]. The release and regulation of peripheral hormones has a central role in balancing whole-body homeostasis.
WAT, being a major endocrine organ, produces many hormones. One of the main WAT-specific hormones is leptin that was first shown to regulate energy balance in mice [103] and later in humans [104]. Leptin is released in the blood by white adipocytes in response to their lipid content and can regulate food intake and EE via activating anorexigenic neurons in the hypothalamus [105]. Suppression of appetite is stimulated by increasing levels of leptin when fat mass increases. This stimulus is lost when WAT lipid content is back to balance [105]. Another adipocyte-specific hormone is adiponectin that, similarly to leptin, is able to repress energy intake while enhancing energy expenditure via the hypothalamic regulation on the CNS [5]. Moreover this hormone can ameliorate fatty

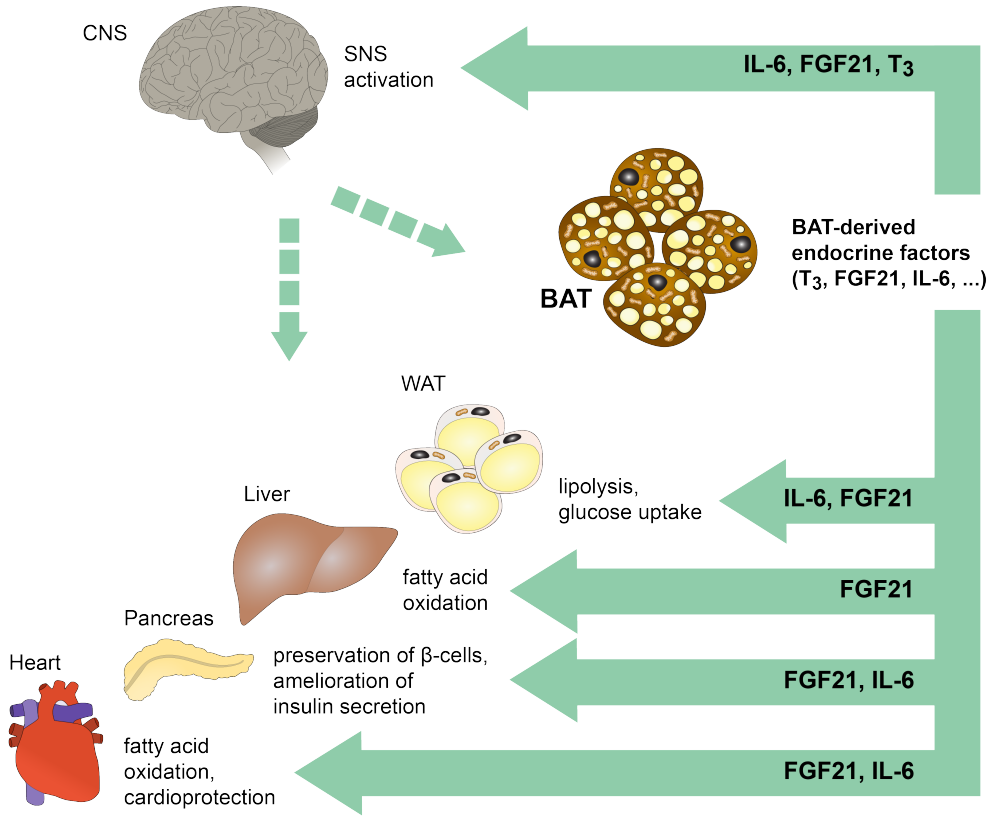

FIGURE 1.3. **Endocrine regulation of brown adipose tissue.** Brown adipose tissue (BAT) releases endocrine factors that are able to target both the central nervous system (CNS) and peripheral tissues (e.g. white adipose tissue, liver, pancreas, heart). Factors such as T_3, FGF21 and IL-6, can regulate organ cross-talk and therefore promote energy homeostasis supplying substrates to fuel thermogenesis. These processes are achieved by BAT via direct targeting of organs in the periphery or indirectly, via stimulating the CNS to trigger systemic effects. The cross-talk between BAT and the CNS is bivalent, with external stimuli (e.g. food intake, cold exposure) promoting the brain to elicit the release of endocrine factors by BAT, generating a regulatory feedback loop. FGF21, fibroblast growth factor-21; IL-6, interleukin-6; SNS, sympathetic nervous system; T_3, triiodothyronine. Original figure; based on [65].

acid oxidation and insulin sensitivity in SM and liver by stimulating AMPK activity [57]. Surprisingly, although adiponectin improves global energy homeostasis in a similar way as leptin, its expression is inversely correlated with fat mass [106]. Also primarily released by WAT, is resistin whose expression follows adipocyte differentiation *in vitro* [107]. This protein is positively regulated by C/EBPα and negatively by PPARγ. In mice it was shown to increase upon HFD, positively correlating to FABP4, and to play a causative role in the development of insulin resistance. In humans resistin was associated with the development of obesity and insulin resistance, yet contradictory findings do not allow

a definitive relationship between these pathology and the circulating adipokine [107]. Adipose tissue also produces non-esterified fatty acids (NEFAs). This adipocyte-derived secreted products have long been known to be released in fasting condition to provide nutrients to the rest of the body [57]. NEFAs circulating in the blood are able to regulate glucose homeostasis via stimulating adipocytes and muscle to reduce glucose uptake and hepatocytes to increase glucose output [57].
The other main hormone involved in whole-body energy regulation is insulin. Insulin is secreted by pancreatic β-cells upon food intake in response to increased glucose levels in the blood [108]. Insulin release promotes the uptake of glucose by peripheral tissues such as liver, adipose tissue and muscle [108] while on the other hand repressing lipolysis [5]. Like leptin, insulin can regulate food intake through stimulation of specific neuronal populations [109].
The thermogenic activity of brown fat, which has been shown to be able to counteract obesity, can be also regulated by a - BAT-specific - hormonal network [110]. This complex regulatory network includes both hormones produced within brown adipocytes and hormones released by other metabolically active organs such as brain, liver, heart, skeletal muscle and WAT. A similar hormonal regulation could regulate as well browning of beige adipose tissue (figure 1.3) [83]. However, brown fat hormonal footprint differs from that of white fat, with the main WAT-released adipokines (e.g adiponectin and leptin) being poorly expressed in this tissue, especially in highly active BAT [60]. This supports the idea that hormones produced by brown and beige adipocytes are actively released under conditions in which these two tissues are thermogenically activated [65]. Before being considered an endocrine organ, BAT was already known to release the thyroid hormone triiodothyronine (T_3) [111]. T_3 is synthesised in brown adipocytes and its production is increased under conditions of high BAT activity [111]. T_3 is converted from its inactive form thyroxine (T_4) by the type 2 deiodinase DIO2, an intracellular enzyme found also in BAT and SM, that regulates energy balance and may influence glucose metabolism [112]. Other hormones have later been found to regulate glucose and insulin homeostasis mainly via influencing hepatic and cardiac function. These include insulin-like growth factor I (IGF-1), interleukin-6 (IL-6) and fibroblast growth factor-21 (FGF21) [65]. IGF-1 was propose to ameliorate diabetes complications via mimicking the actions of insulin [113]. IL-6 is mainly known for its role as a pro-inflammatory agent, but it was also shown to activate BAT by acting on the CNS in a sympathetic nervous system (SNS)-dependent manner [114] and to ameliorate insulin secretion [115]. FGF21 is probably the major BAT hormone and was found to be released also by beige adipose

tissue in both mice and humans [116] [117]. FGF21 endocrine activity regulates energy homeostasis through signalling to many organs, including the CNS where it increases metabolic rate [118]. In the periphery the hormone promotes cardioprotection and fatty acid oxidation in heart [119] and it acts directly on the liver via inducing fatty acid oxidation [120]. FGF21 was also demonstrated to protect from the detrimental effects of diabetes [113].
Taken together, a complex network of hormones released by adipose tissue, especially by brown adipocytes, is able to regulate energy and glucose homeostasis, headlining the endocrine activity of BAT as potential target to counteract obesity and its related diseases.

1.5 Metabolic regulation by microRNAs

In recent years many different strategies have been deployed in order to measure RNA species clinically relevant to various human diseases [121]. New technologies allowed the discovery of many noncoding RNAs, whose regulatory potential is now being exploited to target disease-related pathways (reviewed in [122]), including metabolic ones involved in the development of obesity and its sequelae.

1.5.1 The noncoding genome

Only few decades ago that part of the genome not giving rise to proteins was considered 'junk DNA'. Surprisingly, although only 1-2% of the mammalian genome codes for protein, advances in transcriptome sequencing demonstrated that more than 80% of it is transcribed into RNA, leading to the production of many so-called noncoding RNAs [123] [124] [125] [126] [127]. Noncoding RNAs were first discovered in lower organisms thanks to early studies in plants (e.g. Arabidopsis [128]), invertebrates (e.g. Drosophila [129]) and honey bee ([130]). Further sequencing analyses revealed the presence of many classes of noncoding RNAs, with data from 2011 indicating an amount of 16592 noncoding RNA genes, of which around 30% were long intragenic noncoding RNAs (a class of long noncoding RNAs, lncRNAs), 10% microRNAs (miRNAs) and 9% small nucleolar RNAs (snoRNAs) [131]. Some examples of noncoding RNA families are shown below.
Long noncoding RNAs are a heterogeneous class of regulatory transcripts characterised by a length of more than 200 nt [125]. These noncoding RNAs share many characteristics with protein-coding genes, differing in their inability to translate into protein. Moreover,

in contrast to protein-coding transcripts, lncRNAs are expressed at lower levels, are less evolutionarily conserved and less frequently associate with ribosomes [132]. Interestingly, some lncRNAs do give rise to small peptides and can therefore act as both coding and noncoding transcripts [133]. LncRNAs have multiple ways of action and different roles in various processes, such as epigenetics regulation, cellular differentiation and disease pathogenesis [134].

MicroRNAs are the best characterised class of noncoding RNAs. With a length of about 22 nt, they are estimated to target more than 75% of the gene transcripts through incomplete base-pairing to genes 3' untranslated region (UTR) via a ~7 nt region known as miRNA seed [135]. Further details on miRNA biogenesis and function will be discussed in the following chapters.

Small nucleolar RNAs have an intermediate size, spanning between 60 and 300 nt. SnoRNAs are located in the nuclear compartment within which ribosomes are formed, called nucleolus, where they help facilitating ribosomal RNA (rRNA) folding and stability through sequence-specific 2'-O-methylation and pseudouridylation [136]. In recent years, however, various non-canonical functions have also been described for specific snoRNAs, including regulation of mRNA editing and alternative splicing and post-transcriptional gene silencing by pathways which could involve miRNA-like mechanisms [137].

Another family of noncoding RNAs with size and function similarities to miRNAs, are piwi-interacting RNAs (piRNAs). The biogenesis of piRNAs differs from miRNAs as such is Dicer-independent and involves a subfamily of Argonaute proteins involved in maintaining genome stability in germline cells [138]. These noncoding RNAs are transcribed in genomic regions containing transcribed transposable elements and other repetitive elements [122].

A newly discovered family of noncoding RNAs are circular RNAs (circRNAs). These are characterised by a covalently closed circular RNA molecules, usually spanning exonic sequences and spliced at canonical splice sites [139]. CircRNAs can be found in all eukaryotic species and their expression varies in different cell types and can exceed the abundance of linear mRNA or other noncoding transcripts [137]. These transcript are enriched in the brain and their expression increases during foetal development [137]. Little is known about circRNA function and their tissue specificity, however in some studies they have been found to regulate gene expression acting as miRNA sponges or RNA-binding proteins [139].

1.5.2 The biogenesis of microRNAs

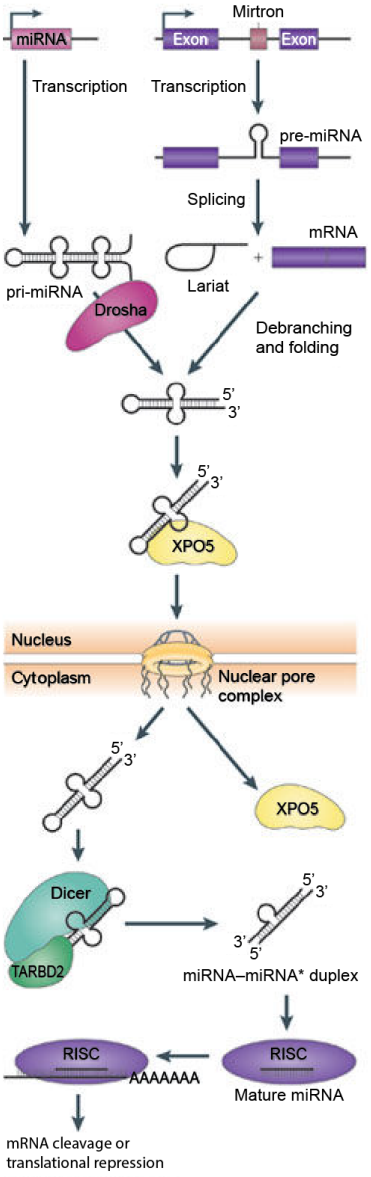

MiRNAs were first discovered as regulatory genes involved in various developmental processes in *C. elegans* [140] [141]. Their processing (Figure 1.4) starts in the nucleus where they are transcribed by RNA polymerase II as primary miRNAs (pri-miRNAs) 1000-3000 nt long. These are then cropped into shorter 60-70 nt long miRNA precursors (pre-miRNAs) by a complex of the RNAse III endonuclease Drosha and the microprocessor complex subunit DGCR8 (also known as Pasha). The ~2 nt long 3' overhang of nuclear pre-miRNAs is recognised by Exportin-5 enabling their nuclear export. In the cytoplasm they are then cleaved into short miRNA duplexes by the RNAse III endonuclease DICER1 (encoded by the *Dicer1* gene). In complex with TAR RNA-binding protein 2 (TARBP2), DICER1 loads the miRNA duplex onto Argonaute (AGO) proteins, AGO1-8 in humans, to form the RNA-induced silencing complex (RISC). One strand of the duplex remains as mature miRNA, whereas the other strand is discarded from AGO. The RISC complex allows miRNAs to actuate degradation of messenger RNAs (mRNAs) or translational repression via base-pairing to the 3' UTR of specific genes [142].

FIGURE 1.4. **MicroRNA biogenesis.** MicroRNAs (miRNAs) are transcribed as individual primary miRNA (pri-miRNA) or together with host genes (mirtrons). After being processed by the Drosha complex or the lariat-debranching enzyme, precursor miRNAs (pre-miRNAs) are exported from the nucleus by exportin 5 (XPO5). Further processing by Dicer and TAR RNA-binding protein 2 (TARBP2) generates mature miRNAs, which, after being loaded into the RNA-induced silencing complex (RISC) can degrade protein-coding transcripts or repress translation. Adapted from [122].

An alternative pathway, discovered in *Drosophila*, generates miRNAs that derive from short intronic hairpins named mirtrons (Figure 1.4) [143]. The biogenesis of these miRNAs differs from the canonical one so that it bypasses cleaving by Drosha and instead involves mRNA splicing and intron lariat-debranching enzymes [144]. In contrast to pri-miRNA hairpins, which generate functional RNAs from both 5' and 3' hairpin arms, mirtron hairpins produce miRNAs only from their 3' arms [143]. After this step, the cleaved mirtrons reenter the canonical pathway and are transported to the cytoplasm by Exportin-5 where they generate mature miRNAs - through DICER1 cleaving - which are then loaded into the RISC complex [144].
MiRNAs have also been shown to derive from snoRNAs, transfer RNAs (tRNAs) or other RNA species via Drosha/DGCR8-independent, Dicer-dependent pathways [145]. The only claimed case, so far, for a Dicer-independent miRNA is *miR-451*, which derives from a short *pre-miR-451* generated by the Drosha/DGCR8 complex. This miRNA is directly cleaved at the 3'-end by AGO2 and further trimmed by 3'-5' exoribonuclease PARN to produce the mature form of *miR-451* [146] [147] [148].
However, all of these miRNAs, through the RISC-mediated inhibitory mechanism, can regulate many biological processes and have been shown to play important roles in the pathophysiology of many diseases [122].

1.5.3 DICER1 and its role in adipose tissue homeostasis

Given its pivotal role in the maturation of miRNAs, DICER1 as been extensively investigated in the past decades in many studies utilising straight or conditional knock-out mouse models. These experiments revealed the enzyme to be required for normal development, differentiation and physiology of most tissues, with the different phenotypes being sometimes causally associated with removal of specific miRNAs [145]. Results from miRNAs studies in AT showed that miRNAs may have important regulatory effects on adipocyte differentiation and regulation. For this reason it was suggested that miRNAs regulation by DICER1 could play a role in this context.
Early studies on the role of DICER1 in adipogenesis showed that the enzyme is required for adipogenic differentiation of embryonic fibroblasts and primary pre-adipocytes in mice [149]. Tamoxifen-induced Cre-driven ablation of *Dicer1* in pre-adipocytes blocked differentiation of these cells, reducing almost completely the expression of adipogenic genes like *Pparg*, *Fabp4* and the glucose transporter *Glut4* [149].
Further studies by Mudhasani and colleagues investigated in an aP2-specific *Dicer1* knock-out mouse line the role of this enzyme in the formation of white and brown adipose

tissue [149]. Depletion of *Dicer1* reduced the level of various adipogenesis-specific transcripts and inhibited lipogenesis in white adipocytes, leading to decreased WAT mass. Interestingly, lipogenesis in BAT was not affected, despite down-regulation of genes involved in thermoregulation, including *Ucp1*, *Cidea* and *Ppargc1a* [149].
Moreover, adipose tissue has shown a global regulation of miRNAs associated with physiological and pathological conditions in mice [150]. In particular, the expression of many miRNAs decreased with ageing in SCAT, with more than 50% of the detected miRNAs being down-regulated. This global down-regulation was associated with defects in the expression of DICER1. Interestingly, this phenotype was completely prevented by caloric restriction [150]. Mori and colleagues utilised a mouse model with an adipose tissue-specific knock-out of *Dicer1* (AdicerKO) to analyse the effects that reduced miRNA processing could have on metabolism [151]. When fed a HFD, these mice exhibited decreased WAT mass in parallel with increased BAT mass due to whitening, leading to the development of lipodystrophy. This phenotype was associated with adipose tissue inflammation, dyslipidemia and insulin resistance [151]. Furthermore, AdicerKO mice showed age-associated detrimental effects, such as accelerated insulin resistance and premature mortality [152]. The WAT-specific depletion of *Dicer1* also affected other organs, with increased mTORC1 activation in WAT and SM [152].
These studies highlight the central role that miRNAs and their DICER1-mediated processing have in regulating multiple processes, including adipose tissue homeostasis.

1.5.4 MicroRNAs and adipose tissue metabolism

As mentioned above, miRNAs are able to regulate adipose tissue metabolism and have been proposed to play a major role in the differentiation and function of both WAT and BAT [153].

1.5.4.1 MicroRNAs in adipose tissue

For the immense regulatory network of miRNAs in tuning specific gene expression, there has been a highly emerging field in the research of adipose tissue-specific miRNAs able to regulate fat homeostasis (figure 1.5).
In this context, one of the first discovered miRNAs was *miR-27*, which was shown to negatively regulate adipogenesis in both mice [155] [156] and humans [157]. Furthermore, its expression was also proven to be reduced in BAT and SCAT upon cold stimulation and additional gain- and loss-of-function experiments *in vitro* could confirm an inhibitory effect of *miR-27* on brown and beige adipogenesis [155] [157].

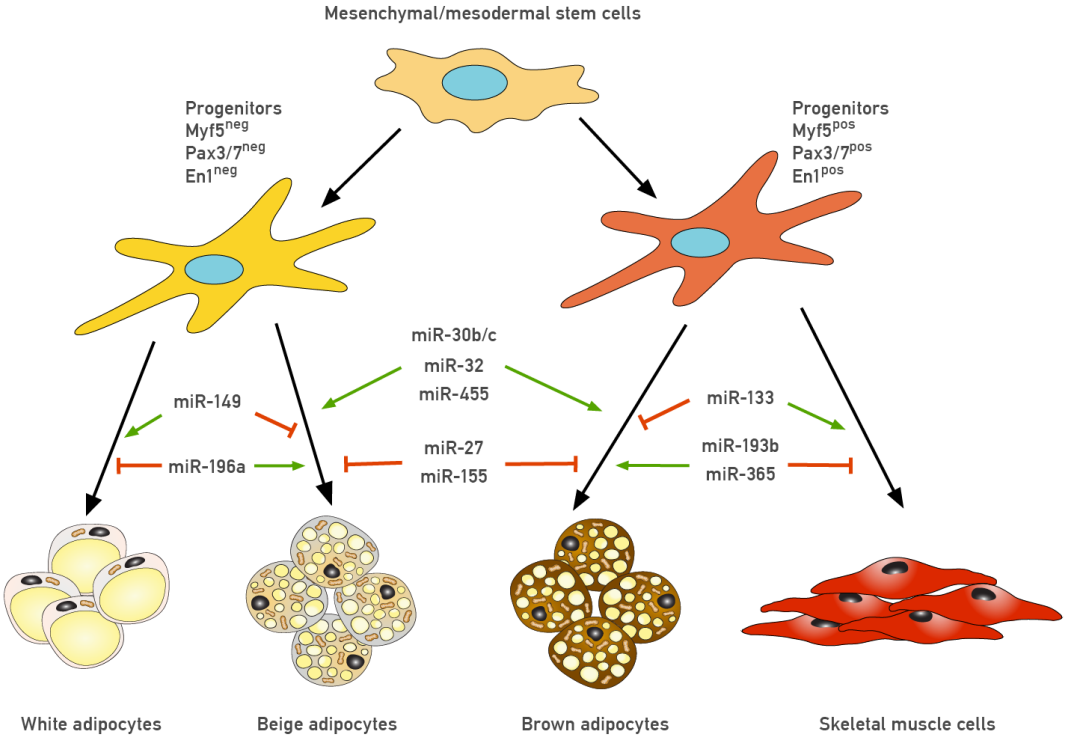

FIGURE 1.5. **MicroRNAs involved in adipose tissue and skeletal muscle differentiation and function.** Various miRNAs are able to positively or negatively regulate the fate of fat and skeletal muscle progenitors, promoting adipocyte lineages or regulating the switch between brown adipocytes and skeletal muscle cells. Original figure; based on [154].

Another negative regulator of adipose tissue metabolism is *miR-149-3p*. Upon fasting this miRNA induces a subcutaneous-to-visceral fat switch, with SCAT acquiring many of the morphological and molecular characteristics of VAT to preserve energy [158]. In turn, knock-down of *miR-149-3p* in primary pre-adipocytes promotes differentiation in beige adipocytes and *in vivo* leads to increased mitochondrial activity and EE. This effect could be attributed to *miR-149-3p* targeting of *Prdm16* [158].

Targeting another fat-specific transcription factor, *Cebpb*, *miR-155* was able to suppress the development of adipogenic and thermogenic programs both *in vitro* and *in vivo* [159]. Indeed, mice lacking *miR-155* showed increased BAT function and browning of WAT when exposed to cold. This was observed in both homozygous and heterozygous *miR-155* knock-out mice. Over-expression of *miR-155* on the other hand triggered the opposite phenotype: mice displayed significantly reduced BAT size and weight along with an impairment of its function, as shown by lower levels of thermogenic markers in this tissue [159].

While *Cebpb* is directly targeted and thus repressed by *miR-155*, it is also an indirect target of *miR-196a*, resulting in opposing effects on the transcription factor. *MiR-196a* activates CEBPβ expression and induces beige adipocyte differentiation through repression of HoxC8, a negative regulator of CEBPβ [160]. This miRNA was shown to be induced in WAT precursor cells after cold exposure or β-adrenergic stimulation and over-expression of *miR-196a* in mice enhances EE and protects them from diet-induced obesity [160].

Notably the regulation of adipogenesis is not only affected by single miRNAs, but also entire miRNA families, such as *miR-30*. *MiR-30c* was shown to promote adipocytes differentiation in humans [161] and, together with *miR-30b*, to enhance the thermogenic capacity of brown and beige adipocytes [162]. Hu and colleagues could show that the pro-adipogenic phenotype elicited by *miR-30b/c* is dependent on their targeting of the 3'-UTR of the receptor-interacting protein 140 (RIP140), a co-repressor of genes involved in glucose uptake, glycolysis and oxidative phosphorylation in major metabolic tissues such as fat, muscle, liver, and heart. Indeed, reinstatement of RIP140 suppressed the up-regulation of BAT markers observed in brown adipocytes upon miRNAs knock-down [162]. Moreover, *miR-30b* expression does not only affect, but it is also affected by cold- and drug-induced BAT and SCAT stimulation in mice [163].

Interestingly several studies have not only identified a role for miRNAs in late differentiation and thermogenic activity, but also in early developmental events of adipogenesis. For example, *miR-455* is a BAT-enriched miRNA that enhances adipocytes' thermogenic potential acting downstream of BMP7 and cold-induced pathways to promote brown adipocyte lineage commitment [164]. Over-expression of this miRNA *in vitro* increases the expression of key regulators of adipogenesis and BAT-markers not only in committed brown and white adipocytes, but also in non-committed multipotent progenitor cells. This phenotype was confirmed *in vivo*, with mice over-expressing *miR-455* under the control of the aP2-Cre (i.e. in FABP4 positive cells) showing an enhanced thermogenic capacity upon stimulation of BAT [164].

One of the most recently discovered BAT-related miRNA is *miR-32*, which was also shown to increase the thermogenic capacity of BAT [165]. Inhibition of the miRNA in mice led to impaired thermogenic response upon cold induction and decreased EE. *MiR-32* is located in close proximity of a BAT specific super enhancer and it acts via the p38/MAPK signalling pathway to increase FGF21 expression in BAT [165].

Interestingly, both WAT and BAT have been shown to generate a major fraction of circulating exosomal miRNAs [151].

1.5.4.2 MicroRNAs in brown adipose tissue/skeletal muscle cell fate regulation

Due to the shared cell lineage of brown adipocytes and skeletal muscle cells and given the ability by various transcription factors to drive transdifferentiation of myogenic and white fat precursors to brown adipocytes, lot of interest rose in last years on the role played by miRNAs in regulating this fate switch. Two main miRNAs, namely *miR-133* and the *miR-193b-365* cluster, came to attention in this context.
MiR-133, comprising the two closely related *miR-133a* and *miR-133b*, is a muscle-specific miRNA (myomiR) which was found to be expressed also in BAT and, to a lower degree, in SCAT [166]. Loss- and gain-of-function experiments in brown pre-adipocytes could prove the miRNA to induce and inhibit brown adipogenesis respectively, herein affecting cell differentiation, but not proliferation. Interestingly, knock-down experiments in primary cells revealed that the pro-adipogenic effect of *miR-133* inhibition was limited to SCAT but not VAT, which is known to be less prone to browning induction in rodents. The negative regulation of BAT by *miR-133* was demonstrated to occur due to the suppression of *Prdm16* expression, as confirmed via luciferase assays [166]. In line with the *in vitro* results, knock-out of *miR-133a* in mice led to increased brown and thermogenic gene programs in SCAT [167]. Furthermore, these mice exhibited enhanced insulin sensitivity and glucose tolerance associated with increased thermogenic capacity upon cold exposure [167].
MiR-193b and *miR-365*, which are encoded within the same miRNA cluster in the genome, were first identified as BAT-enriched after genome-wide miRNA analysis of BAT, SCAT and SM [168]. Expression of these miRNAs was up-regulated during adipogenesis and down-regulated in BAT of genetically obese *ob*/*ob* mice. *In vitro* experiments in primary brown adipocytes revealed decreased brown adipogenesis accompanied by increased expression of myogenic markers upon inhibition of the cluster [168]. The same results were obtained in the myogenic cell line C2C12. *MiR-193b-365* was suggested to act via targeting the adipogenesis inhibitor RUNX1 translocation partner 1 (*Runx1t1*) and the pro-myogenic genes cell adhesion associated, oncogene regulated (*Cdon*) and insulin like growth factor binding protein 5 (*Igfbp5*) [168]. However, further *in vivo* studies on mice lacking the *miR-193b-365* cluster failed to validate the *in vitro* findings observed in BAT [169]. These mice showed no difference in BAT regulatory networks and in their thermogenic response to cold or β3 adrenergic stimulation compared to control littermates. It has been hypothesised that this discrepancy between *in vitro* and *in vivo* indications could rely in a compensatory down-regulation of *miR-133*, whose levels

were reduced in the BAT of the *in vivo* mouse model [169]. In fact, *miR-133* deficiency could completely mitigate the effects of *miR-193b* depletion, leading to an opposite BAT response [166] [167].

All of these studies highlight the multi-faceted role that miRNAs have in regulating adipose tissue differentiation and activity on various levels, making them potential therapeutical targets against obesity-related metabolic impairment.

1.6 Objectives

Obesity is a major burden of our society, with increased adiposity and impaired glucose homeostasis increasing the risk for related diseases such as T2D and neurodegenerative pathologies (1.1). Brown adipose tissue activation has been proposed as a therapeutic target to counteract obesity and its sequelae (1.3.1.2). MicroRNAs have been shown to play an important role in maintaining brown adipose tissue homeostasis, both globally [170] and concerning specific miRNA effects (1.5.4).
In light of this, the aim of this study was to discover and characterise novel miRNAs that could potentially regulate energy homeostasis via enhancing brown adipose tissue metabolism. For this purpose, expression of miRNAs was analysed in models of altered BAT homeostasis and putative targets were tested for *in vitro* functionality, both in brown adipogenesis and myogenesis, two processes that share a common progenitor origin.
MicroRNA-mediated regulation of BAT can trigger metabolic pathways involved in whole-body homeostasis. In order to unravel downstream regulators of candidate miRNAs involved in these pathways *in vitro* and *in vivo* techniques were used to first discover these molecules and then characterise their impact on brown adipose tissue and whole-body homeostasis.

CHAPTER 2

MATERIALS AND METHODS

2.1 Animal care

All experimental animals were maintained on a C57BL/6 background and housed in a pathogen-free facility. A 12 h light/dark cycle and a temperature of 22-24 °C was maintained. Care of animals was within institutional animal-care committee guidelines. All procedures were approved by local authorities (Bezirksregierung Köln) and regional authorities (Tierschutzkommission acc. §15 TSchG of the Landesamt für Natur, Umwelt und Verbraucherschutz North Rhine Westphalia, internal reference number 84-02.04.2014.A184 and 84-02.04,2014.A068) and fulfilled National Institutes of Health guidelines. Unless otherwise indicated, animals were allowed *ad libitum* access to food and drinking water.

2.2 Experimental diets

All mice were fed *ad libitum* normal chow diet (NCD, Teklad Global Rodent no. 5.2018.R12; Harlan). For diet-induced obesity experiments, mice were fed a high-fat diet (HFD, diet identification no. D12492; Research Diets) containing 26.2% carbohydrates, 26.3% protein and 34.9% fat (60% calories from fat) from four weeks of age.
BACE1 inhibitor (RO5508887, Figure 2.1) was supplied by Roche and previously tested for mice experiments [43]. For RO5508887 treatment, C57BL/6 mice were fed HFD for three weeks after weaning and afterwards, cages were randomized and half of the cohort

received HFD supplemented with RO5508887 for an additional 12 weeks. To achieve a RO5508887 dose of 10 mg kg^{-1} body weight per day an average food intake of 3 g per mouse per day of HFD ± RO5508887 was considered.

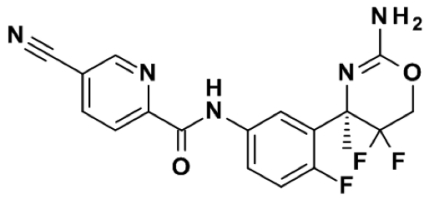

RO5508887

FIGURE 2.1. **Chemical structure of BACE1 inhibitor RO5508887.**

2.3 Experimental mouse models

Specific brown adipose tissue reduction of *Dicer1* expression was achieved using Cre recombinase-mediated excision of LoxP-flanked ("floxed") gene sequences. Therefore, mice homozygous for floxed alleles of *Dicer1* ($Dicer1^{LoxP/LoxP}$) were interbred with mice expressing Cre recombinase under control of the BAT-specific uncoupling protein 1 (*Ucp1*) promoter (*Ucp1*-$Cre^{+/-}$ mice). *Ucp1*-Cre mice were generated as described in [171]. Resulting $Dicer1^{LoxP/+}$; *Ucp1*-$Cre^{+/-}$ knock-out mice ($Dicer1^{\Delta BAT/+}$) were compared with $Dicer1^{LoxP/+}$; *Ucp1*-$Cre^{-/-}$ littermates (controls).
Tissues from mice (C57BL/6) exposed to 4 °C for 1 or 7 days were obtained from the laboratory headed by Jörg Heeren (University Medical Center Hamburg - Eppendorf, Germany).
All other experiments were performed using C57BL/6 mice.

2.4 Genotyping

2.4.1 DNA isolation

Mouse tail biopsies were taken at weaning age and digested overnight at 56 °C and 450 rpm in 300 μl tail lysis buffer. The buffer was composed of 50 mM KCl, 1.5 mM $MgCl_2$, 10 mM Tris-HCl pH 8.3, 0.45% Tween20, 0.45% Nonidet P-40 and freshly added 100

μg/ml Proteinase K in H_2O. Proteinase K was then inactivated by shaking at 94 °C and 450 rpm for 15 min.

2.4.2 Polymerase chain reaction (PCR)

For genotyping, 5 μl of previously extracted genomic DNA (2.4.1) were added to 20 μl of corresponding PCR master mix and polymerase chain reaction (PCR) was performed using the primers listed in Table 2.1. PCR master mix contained approximately 25 pMol of each primer, 25 μM dNTP mix, 1% Dream Taq Green Buffer (Thermo Fisher Scientific) and 1 unit Dream Taq DNA polymerase (Thermo Fisher Scientific) per 25 μl reaction. PCRs were performed using the following programs:

Ucp1-Cre

Temperature [°C]	Time [m:s]	
95.0	5:00	
95.0	0:30	39 x
61.0	0:45	
72.0	1:00	
72.0	10:00	
4.0	∞	

Dicer1-flox

Temperature [°C]	Time [m:s]	
95.0	3:00	
60.0	1:00	
72.0	2:00	
95.0	0:30	34 x
60.0	0:40	
72.0	0:30	
72.0	3:00	
4.0	∞	

2.4.3 Agarose gel electrophoresis

PCR products from genotyping were visualised in 2% agarose gels containing 5% Midori Green Advance DNA stain (Nippon Genetics Europe). DNA fragments were separated at 120 V and visualised under UV light. Expected products size are indicated below:

Expected products for *Ucp1*-Cre:

WT:	554 bp
WT / Tg:	554 bp and 336 bp

Expected products for *Dicer1*-flox:

WT:	254 bp
WT / flox:	254 bp and 384 bp
fox / flox:	384 bp

Table 2.1: List of primers for genotyping PCR.

PCR	Name	Sequence (5'-3')
Ucp1-Cre	Ucp1-Cre_F	CAAGGGGCTATATAGATCTCCC
	Ucp1-Cre_R1	ATCAGAGGTGGCATCCACAGGG
	Ucp1-Cre_R2	GTTCTTCAGCCAATCCAAGGG
Dicer1-flox	Dicer1-flox_F	GGTTACATGGCTAGACTCAAAGC
	Dicer1-flox_R	AGGTGCCTTTCGTTTAGGAAC
	Dicer1-flox_Fwt	AAAGCAGAACTCTAATGCCCC

2.5 Mice phenotyping

2.5.1 Body weight

Body weight of HFD ± RO5508887-fed mice was assessed weekly for each individual mouse for ages 4-19 weeks.

2.5.2 Food intake

Food intake of HFD ± RO5508887-fed mice was quantified using standardised racks with defined amounts of diet provided. The food pellets were exchanged every three days throughout the experiment (12 weeks), residual pellets weighed and food intake calculated per mouse and day.

2.5.3 Glucose tolerance test (GTT)

For glucose tolerance test, mice were fasted for 16 h overnight. Fasted blood glucose levels were measured using a glucometer (Contour, Bayer Diabetes Care). Following intraperitoneal administration of insulin 0.75 U per kg of body weight (Actrapid; Novo Nordisk), blood glucose levels were recorded after 15, 30 and 60 min.

2.5.4 Insulin tolerance test (ITT)

For insulin tolerance test, baseline blood glucose levels were measured using a glucometer. Following intraperitoneal administration of 2 g glucose per kg of body weight (20% glucose, Delta select), blood glucose levels were recorded after 15, 30, 60 and 120 min. For determination of insulin tolerance, 15, 30 and 60 min values were calculated relative to baseline blood glucose levels for each individual mouse.

2.5.5 Insulin and leptin serum analysis

Serum levels of insulin and leptin were measured by enzyme-linked immunosorbent assay (ELISA) according to manufacturer's instructions (mouse-rat insulin ELISA, mouse leptin ELISA, Crystal Chem) in fasted animals at 8-9 weeks of age.

2.5.6 Metabolic cages

Metabolic measurements were obtained using a PhenoMaster System (TSE systems). Animals were allowed to adapt to the single housing in metabolic cages (7.1 liter) for a training phase of five days. Food and water were provided *ad libitum* in the appropriate devices and measured by the built-in automated instruments. Parameters of indirect calorimetry were measured for 72 h.

2.5.7 Body mass composition

Lean and fat mass of HFD ± RO5508887-fed mice were determined using nuclear magnetic resonance (NMR Analyzer minispeq mq7.5, Bruker Optik) in live mice at 19 weeks of age.

2.6 Thin-layer chromatography-mediated quantification of lipids

Thin-layer chromatography (TLC) was performed at the CECAD lipidomic facility (Cologne, Germany) headed by Dr. Susanne Brodesser. Frozen skeletal muscle and liver samples were homogenized in H_2O (100 mg of tissue per 1 ml) using the Precellys 24 Homogenisator (Peqlab) at 6,500 rpm for 30 s. The protein content of the homogenate was routinely determined using bicinchoninic acid and lipids were extracted as described in [172]. The lipid extract was applied to 20×10 cm high-performance thin-layer chromatography (HPTLC) Silica Gel 60 plates (Merck), which were pre-washed twice with chloroform/methanol 1:1 (v/v) and air-dried for 30 min. For quantification of triacylglycerols, each lane of the TLC plate was loaded with the equivalent of 5 μg (liver) or 9 μg (skeletal muscle) of protein. The TLC solvent system used for detection of triacylglycerols was hexane/toluene 1:1 (v/v), followed by hexane/diethyl ether/glacial acetic acid 80:20:1 (v/v/v). For quantification of cholesterol and free fatty acids, the equivalent of 150 μg (liver) and 700 μg (skeletal muscle) of protein was applied to 20×20 cm TLC plates, which were developed in hexane/diethyl ether/formic acid 30:50:1 (v/v/v). Quantitative analytical TLC determination was performed as described in [172].

2.7 Cell culture

2.7.1 Mycoplasma test

Prior to usage cells were tested for mycoplasma contamination using the PCR Mycoplasma Test Kit (AppliChem) according to manufacturer's protocol.

2.7.2 Growth medium

All cell lines were maintained in growth medium composed of Dulbecco's modified Eagle's medium (DMEM, Thermo Fisher Scientific) containing 4.5 g l^{-1} glucose supplemented with 10% fetal bovine serum (FCS, Biochrom AG), 1% L- glutamine (Thermo Fisher Scientific), 1% penicillin/streptomycin (P/S, Thermo Fisher Scientific), 1% minimum essential medium non-essential amino acids (MEM NEAA, Thermo Fisher Scientific,) and 1% sodium pyruvate (Thermo Fisher Scientific).

2.7.3 HEK293

HEK293 cells were obtained from Leibniz-Institut DSMZ (Deutsche Sammlung von Mikroorganismen und Zellkulturen).

2.7.3.1 Transfection of HEK293

For transfection, 1×10^5 cells were seeded per well in 24-well plates and grown to confluence in growth medium. One hour before transfection, the medium was changed to growth medium without antibiotics. 400 ng DNA of reporter construct together with 100 nM miRIDIAN microRNA mimic (Thermo Scientific, Dharmacon) were transfected using Lipofectamine® 2000 Reagent (1 mg/ml, Thermo Fisher Scientific, 52758) according to the manufacturer's protocols. Sequences of the utilised miRIDIAN microRNA mimics are indicated in Table 2.2.

Table 2.2: List of sequences for *in vitro* loss- or gain-of function experiments.

Experiment	Name	Sequence (5'-3')	Concentration
miRCURY LNA™ Power Inhibitor	Negative Control A	GTGTAACACGTCTATACGCCCA	100 nM
	mmu-miR-193b	CGGGACTTTGTGGGCCAGT	100 nM
	hsa-miR-328	GGAAGGGCAGAGAGGGCCA	100 nM
miRIDIAN microRNA mimic	Negative Control #1	Catalog Item (CN-001000-01-05)	100 nM
	mmu-miR-193b-3p	AACUGGCCCACAAAGUCCCGCU	100 nM
	mmu-miR-328-3p	CUGGCCCUCUCUGCCCUUCCGU	100 nM
Antisense LNA™ GapmeR	Scrambled GapmeR	GACGGTAACTAGGCGA	80 nM
	mmu-Bace1_1	ATTCGCATCGCATAG	80 nM
	mmu-Gprc5b_1	AGTGTCGAAGTAGTT	80 nM

2.7.4 Immortalised brown pre-adipocytes (PIBA)

PIBA cells were generated in-house using standard protocols. [173]

2.7.4.1 Transfection of PIBA

For transfection, 5×10^4 cells were seeded per well in 6-well plates and grown to confluence in adipogenic differentiation medium (2.7.4.2). One hour before transfection, the medium was changed to differentiation medium without antibiotics. For transfection, miRCURY LNA™ Power Inhibitors (Exiqon), miRIDIAN microRNA mimic (Thermo

Fisher Scientific, Dharmacon) or Antisense LNA™ GapmeRs (Exiqon) were diluted to the desired concentration and transfected using Lipofectamine® 2000 according to the manufacturer's protocols. Sequences and concentrations of utilised miRCURY LNA™ Power Inhibitors, miRIDIAN microRNA mimics or Antisense LNA™ GapmeRs are indicated in Table 2.2.

2.7.4.2 Induction and differentiation

For adipogenic differentiation, cells were seeded in growth medium supplemented with 20 nM human insulin solution (Sigma-Aldrich, I9278-5ML) and 1 nM 3,3',5-Triiodo-L-thyronine (T_3, Sigma Aldrich, T2877) (differentiation medium). Once 100% confluent, the medium was switched to differentiation medium supplemented with 125 nM indomethacin (Sigma-Aldrich, I7378), 0.5 mM isobutylmethylxanthine (IBMX, Sigma Aldrich, I5879-5G) and 0.5 μM dexamethasone (Sigma-Aldrich, D1756) for 24 h. The medium was then switched to differentiation medium for the next two days before samples collection.

2.7.5 3T3-L1

3T3-L1 cells were acquired from American Type Culture Collection (ATCC).

2.7.5.1 Transfection of 3T3-L1

For transfection, 5×10^4 cells were seeded per well in 6-well plates and grown to confluence in growth medium. One hour before transfection, the medium was changed to growth medium without antibiotics. Lipofection was carried out as described for PIBA cells (2.7.4.1) using a concentration of 50 nM. Sequences of utilised miRCURY LNA™ Power Inhibitors, miRIDIAN microRNA mimics or Antisense LNA™ GapmeRs are indicated in Table 2.2.

2.7.5.2 Induction and differentiation

For adipogenic differentiation, cells were seeded in growth medium and when 100% confluent the medium was switched to growth medium supplemented with 20 nM human insulin solution, 0.5 mM IBMX and 0.5 μM dexamethasone for 24 h. The medium was then switched to growth medium supplemented with 20 nM human insulin solution for the next four days before samples collection. The medium was changed every two days.

2.7.6 C2C12

C2C12 myoblast cells were acquired from American Type Culture Collection (ATCC). C2C12$^{\Delta Bace1}$ cells were generated as described in 2.8.

2.7.6.1 Transfection of C2C12

For transfection, 1×10^5 cells were seeded per well in 6-well plates and grown to confluence in growth medium. One hour before transfection, the medium was changed to myogenic differentiation medium (2.7.5.2) without antibiotics. Lipofection was carried out as described for PIBA cells (2.7.4.1). Sequences of utilised miRCURY LNA™ Power Inhibitors, miRIDIAN microRNA mimics or Antisense LNA™ GapmeRs are indicated in Table 2.2.

2.7.6.2 Myogenic differentiation

For myogenic differentiation, growth medium was switched to DMEM supplemented with 1.5% Hi Horse Serum (Thermo Fisher Scientific, 26050-088), 1% L- glutamine and 1% P/S (myogenic differentiation medium) at 100% confluence. Medium was changed every two days for the subsequent five days before sample collection.

2.7.6.3 Adipogenic differentiation

For forced adipogenic differentiation of C2C12, when cells were 100% confluent growth medium was switched to growth medium supplemented with 850 nM human insulin solution, 1 μM rosiglitazone (Sigma-Aldrich, R2408-10MG), 1 nM T_3, 0.5 μM dexamethasone, 0.25 mM IBMX and 125 nM indomethacin (adipogenic induction medium) for 48 h. The medium was then switched to growth medium supplemented with 160 nM human insulin solution and 1 μM rosiglitazone (adipogenic differentiation medium) for three days before sample collection.

2.7.6.4 Conditioned media adipogenic differentiation

C2C12 and C2C12$^{\Delta Bace1}$ seeder cells were plated in a 15 cm dish and once 100% confluent, medium was replaced with 13 mL of growth medium. After 24 h the medium was collected (conditioned medium) and replaced with 13 mL of fresh growth medium. The conditioned medium was collected daily. 1×10^4 wild-type C2C12 were seeded in 6-well plates in conditioned medium from both cell lines supplemented with 10% FCS, 1% L- glutamine

1% P/S, 1% MEM NEAA and 1% sodium pyruvate (conditioned growth medium). After three days of conditioned growth medium, when C2C12 cells were 100% confluent the medium was switched to conditioned growth medium supplemented as the adipogenic induction medium in 2.7.6.3. The medium was changed daily for 2 days. Subsequently the medium was switched to adipogenic differentiation medium (2.7.6.3) for three days. C2C12 cells were then collected for RNA or protein isolation.

2.8 CRISPR/Cas9 generation of C2C12$^{\Delta Bace1}$

For generation of a stable *Bace1* knock-out in C2C12 cells using CRISPR/Cas9 technology, a modified pX330 vector [174] [175] containing two gRNAs and carrying a GFP-puromycin selection cassette was used. The plasmid was provided by Dr. Stefan Frank and generated at the Max-Planck Institute for Molecular Biomedicine (Münster, Germany).
The knock-out strategy was based on [32]. In brief, deletion of exon 2 (89 bp) from *Bace1* genomic DNA results in loss of function of *Bace1* translation by generating a frameshift (premature STOP codon in exon 3).

2.8.1 GuideRNA generation

A template DNA sequence for the gRNA was prepared as annealed oligonucleotides and inserted into the BbsI-digested vector using the primers listed below. The second gRNA was inserted using a SapI-mediated Golden Gate assembly method for the concatemerization of gRNA cassettes using the primers listed below. gRNAs sequences were generated using the CRISPR Design online tool (http://crispr.mit.edu/). Quality score represent the faithfullness of on-target activity computed as 100% minus a weighted sum of off-target hit-scores in the target genome. No high-scoring off-targets fell in marked gene regions.

GuideRNAs BbsI (Quality score 86)
Forward: 5'- CACCGCTGCTCTTATTCCGTGGAC - 3'
Reverse: 5'- AAACGTCCACGGAATAAGAGCAGC - 3'

GuideRNAs SapI (Quality score 78)
Forward: 5' - ACCGAGCCTTTCTTCTACTAGGG - 3'
Reverse: 5' - AACCCCTAGTAGAAGAAAGGCTC - 3'

2.8.2 Vector generation

For CRISPR/Cas9 vector generation, restriction digestion of 1 μg of vector with FastDigest BbsI (Thermo Fisher Scientific) was performed for 30 min at 37 °C. The obtained vector was purified using the MinElute PCR Purification kit (Qiagen) following manufacturer's instructions.
1 μl of 100 μM solution of forward and reverse primers (2.8.1) was phosphorylated by T4 polynucleotide kinase (New England Biolabs) for 30 min at 37 °C. Annealing took place at 95 °C for 5 min and subsequent cooling to 25 °C at a cooling rate of 5 °C/min.
Ligation of 1 μl of oligo reaction (1:200 dilution in H_2O) with 50 ng of digested vector was assessed using the QuickLigase kit (New England Biolabs) for 20 min at room temperature according to manufacture's instructions.
Degradation of unspecific recombination products was performed with the PlasmidSafe DNase kit (EpiCentre) for 30 min at 37 °C following manufacturer's protocol.

2.8.3 Cell transformation and clone selection

2.5 μl of the obtained vector (2.8.2) were transformed into XL10-Gold Ultracompetent Cells (Agilent) and plated overnight on LB-ampicillin plates. Bacterial colonies were resuspended in 30 μl H_2O and lysed at 95 °C for 5 min. 3 μl of the lysate were used to identify positive clones by colony PCR (annealing at 64 °C) using the respective forward primer (2.8.1) and as reverse primer 5' - GGAAAGTCCCTATTGGCGTT - 3'. PCR products were run on a 2% agarose gel for 20 min at 120 V and positive clones were further verified by sequencing (2.10).
After correct insertion of the first gRNA, the procedure was repeated on the BbsI-digested plasmid, this time using FastDigest SapI (Thermo Fisher Scientific).

2.8.4 Cell transfection and selection

C2C12 cells were transfected with 3 μg of CRISPR/Cas9 plasmid using FuGENE® Transfection Reagent (Promega) according to the manufacturer's protocol.
After 24 h of transfection efficiency was visually verified via GFP expression and puromycin selection (5 μg/ml, Thermo Fisher Scientific) was performed for 72 h. Puromycin-resistant cells were trypsinised and plated as single cells on a 96-well plate. For PCR screening of positive cells, DNA was isolated using the QuickExtract™DNA Extraction Solution (Epicentre) and samples were incubated at 68 °C for 15 min followed by 95 °C for 8 min. PCR was performed using the primers listed in Table 2.3 following the strategy

shown in Figure 4.7 c. The PCR program used was as follows:

Temperature [°C]	Time [m:s]	
95.0	3:00	
95.0	0:30	34 x
59.0	0:30	
72.0	1:00	
72.0	3:00	
4.0	∞	

Further validation was performed via DNA sequencing (2.10).

Table 2.3: List of primer sequences for clone selection.

Name	Method of validation	Sequence (5'-3')
Bace1_ex2_in_F	PCR IN	GGTCCAGAGCCGTCTGTCT
Bace1_ex2_in_R	PCR IN	ACCCCTCCCCAGGACTTAC
Bace1_ex2_out_F	PCR OUT	TTTCTGACGATGGCACACAT
Bace1_ex2_out_R	PCR OUT	CACCCTTTCCCACACTGTCT

2.9 Oxygen consumption rate (OCR) analysis

For OCR quantification, 5,000 or 10,000 PIBA and C2C12 cells respectively were seeded into Seahorse XFe96 (Seahorse Bioscience, Agilent) cell culture plates and transfected/ differentiated as described in 2.7. One hour prior to the assay both PIBA and C2C12 cells were given XF Base medium (Seahorse Bioscience, Agilent) supplemented with 1 mM sodium pyruvate, 2 mM L-glutamine, and 10 mM glucose (pH 7.4).
The assay was set as follows: 3 measurements (3 min mixing plus 3 min measuring each) for basal respiration, 3 measurements after oligomycin (1 μM) injection, 3 measurements after FCCP (1 μM) injection and 3 measurements after rotenone/antimycin A (0.5 μM) injection. Oligomycin treatment allowed quantification of ATP production via inhibiting ATP synthase (complex V), FCCP (Carbonyl cyanide-4 (trifluoromethoxy) phenylhydrazone) uncoupler caused maximal cellular respiration and rotenone/antimycin A treatment revealed the amount of non-mitochondrial respiration via inhibiting complex I/III of the mitochondrial electron transport chain.

2.10 Extraction and sequencing of DNA fragments

For purification of DNA fragments from an agarose gel the QIAEXII Gel Extraction Kit (Qiagen) was used following manufacturer's instruction and eluted in 20 μl H_2O. 3 μl of purified DNA fragments were ligated into pGEM®-T Easy Vector (Promega) according to manufacturer's protocol for 4 h at room temperature.
2 μl of ligated vector were transformed into XL10-Gold Ultracompetent Cells (Agilent) and plated overnight on LB-ampicillin plates. Subsequent positive colonies were expanded overnight in 5 ml LB-ampicillin medium and DNA isolated using the Plasmid Miniprep Kit I, peqGOLD (Peqlab). 30 μl of 50 ng/μl isolated DNA were sent to GATC Biotech for DNA Sanger sequencing.

2.11 Dual luciferase reporter assays

For the generation of reporter constructs, fragments containing either the wild-type or mutated *miR-193b*/*miR-328*-binding sites of the 3'-UTR of potential miRNA target genes were cloned behind the STOP codon of the firefly luciferase open reading frame

Table 2.4: List of 3'-UTR primer sequences.

3'-UTR	Forward sequence (5'-3')	Reverse sequence (5'-3')
Bace1	GCTAGCGGCTAATAAGCCCTTTTTCCCC	GCTAGCGGCTAATAAGCCCTTTTTCCCC
Gprc5b	GAGCTCAAAGAAAGCTAGGGCTGTGTGGG	GCTAGCCTCTCATCAGCTCACATGGTCGC
Gprc5c	GAGCTCGGAAGCAGGTTGATTTAGAGAGGG	GCTAGCTCCTCACAGAGGAGCAGGATCC
Gpsm1	GAGCTCAGTCTTTTCCCTCAAGCCCTGCC	GCTAGCTACCTCTCGGGTCAGAAAGGACCC
Lmod1	GAGCTCAAGCACGTCACAGAGAAGATGGC	GCTAGCAAAACAGGGCCTCTGTGCTGGG
Myod1	GAGCTCGAGATCGACTGCAGCAGCAGAGG	GCTAGCTATTTCCAACACCTGAGCGAGCG
Pax7	GAGCTCGGAAACCTGGTTCCCTGAAAGGG	GCTAGCCAAAAGGAGAACCTGGGTTCCC
Pbx2	GAGCTCACAACATGGCAGGGAGAGTGGG	GCTAGCCAGGGGAAAAAGAAATATCTTTAT
Six4	GAGCTCTGCCTCTGCCTTCCAAGTACCG	GCTAGCGATATTCTGCCACGTGAACTCC

of the pmiRGLO dual luciferase vector (Promega). The primers used are listed in Table 2.4. The integrity of all constructs was verified by Sanger sequencing. Dual luciferase reporter assays were performed 48 h after transfection of HEK293 (see 2.7.3.1) following the manufacturer's protocol and values for firefly luciferase were normalized to Renilla luciferase and set to unity compared with scr mimics.

2.12 Total RNA isolation

2.12.1 Trizol based method

Total RNA was isolated from tissues or cells using peqGOLD TriFast™ (Peqlab) according to manufacturer's protocol. RNA was resuspended in 50 μl DEPC-H_2O (0.1% DEPC) and concentrations measured via a Nanodrop Spectrophotometer ND-1000 (Thermo Fisher Scientific).

2.12.2 miRVANA kit isolation

RNA samples for RNA sequencing were isolated using the miRVana Isolation Kit (Ambion, Life Technologies) following the protocol for total RNA isolation. RNA integrity and concentration was assessed using the Experion Bioanalyzer system (Bio-Rad) according to the manufacturer's instructions. Contaminating DNA was removed using the TURBO DNA-free™ Kit (Ambion, Life Technologies) following manufacturer's protocol.

2.13 Real-time quantitative RT-PCR (qPCR)

2.13.1 Reverse transcription and qPCR

1 μg of total RNA was reversely transcribed with High-Capacity cDNA RT kit (Thermo Fisher Scientific) and amplified using TaqMan® Universal PCR-Master Mix (Thermo Fisher Scientific) according to manufacturer's instructions. Relative expression of target mRNAs was adjusted for total RNA content by Hprt. TaqMan® probes used for gene expression analysis are listed in Table 2.5. Calculations were performed by comparative method ($2^{-\Delta\Delta CT}$).

2.13.2 MicroRNA reverse transcription and qPCR

For reverse transcription of particular miRNAs, 10 ng total RNA were reversely transcribed using TaqMan® microRNA reverse-transcription (RT) kit (Thermo Fisher Scientific) and TaqMan® primary and mature microRNA assays (Thermo Fisher Scientific) according to the manufacturer's instruction. Relative expression of target miRNAs was adjusted for total RNA content by *sno-429* expression. TaqMan® assays used for miRNA expression analysis are listed in Table 2.5. Calculations were performed by comparative method ($2^{-\Delta\Delta CT}$).

Table 2.5: List of TaqMan® assays.

TaqMan® assay	Gene name	TaqMan® ID
miR-193b	mmu-miR-193b	002467
miR-328	hsa-miR-328	000543
miR-365	hsa-miR-365	001020
pri-miR-193b	primary mmu-miR-193b	Mm03308440_pri
pri-miR-365	primary hsa-miR-365	Mm03307334_pri
sno-429	snoRNA429	001240
Adam12	a disintegrin and metallopeptidase domain 12 (meltrin alpha)	Mm00475719_m1
Adam17	a disintegrin and metallopeptidase domain 17	Mm00456428_m1
Adamts1	a disintegrin-like and metallopeptidase (reprolysin type) with thrombospondin type 1 motif, 1	Mm00477355_m1
Adamts9	a disintegrin-like and metallopeptidase (reprolysin type) with thrombospondin type 1 motif, 9	Mm00614433_m1
Adipoq	adiponectin, C1Q and collagen domain containing	Mm00456425_m1
Aoc2	amine oxidase, copper containing 2	Mm00841716_m1
Aoc3	amine oxidase, copper containing 3	Mm00839624_m1
Bace1 exons 1-2	beta-site APP cleaving enzyme 1	Mm00478664_m1
Bace1 exons 3-4	beta-site APP cleaving enzyme 1	Mm01146407_m1
Bace1 exons 4-5	beta-site APP cleaving enzyme 1	Mm01146408_m1
Bace1 exons 8-9	beta-site APP cleaving enzyme 1	Mm00478671_m1
Cebpa	CCAAT/enhancer binding protein (C/EBP), alpha	Mm00514283_s1
Cebpb	CCAAT/enhancer binding protein (C/EBP), beta	Mm00843434_s1
Cidea	cell death-inducing DNA fragmentation factor, alpha subunit-like effector A	Mm00432554_m1

TaqMan® assay	Gene name	TaqMan® ID
Ckm	creatine kinase, muscle	Mm01321487_m1
Dio2	deiodinase, iodothyronine, type II	Mm00515664_m1
Elovl3	elovl family member 3	Mm01194164_m1
Fabp4	fatty acid binding protein 4, adipocyte (AP2)	Mm00445878_m1
Gprc5b	G protein-coupled receptor, family C, group 5, member B	Mm00458150_m1
Hprt	hypoxanthine guanine phosphoribosyl transferase 1	Mm00446968_m1
Igfbp5	insulin-like growth factor binding protein 5	Mm00516037_m1
Myf5	myogenic factor 5	Mm00435125_m1
Myf6	myogenic factor 6	Mm00435127_g1
Myod1	myogenic differentiation 1	Mm00440387_m1
Myog	myogenin	Mm00446195_g1
Pax3	paired box 3	Mm00435491_m1
Ppara	peroxisome proliferator activated receptor alpha	Mm00440939_m1
Pparg	peroxisome proliferator activated receptor gamma	Mm01184322_m1
Ppargc1a	peroxisome proliferative activated receptor, gamma, coactivator 1 alpha	Mm01208835_m1
Runx1t1	runt-related transcription factor 1; translocated to, 1 (cyclin D-related)	Mm00486771_m1
Tnnt3	troponin T3, skeletal, fast	Mm01268863_m1
Ucp1	uncoupling protein 1	Mm01244861_m1

2.14 RNA sequencing

RNA sequencing was performed at the Cologne Center for Genomics (CCG, Cologne, Germany) headed by Prof. Peter Nürnberg. 1 μg of total RNA (2.12) was used. cDNA libraries were prepared from poly-A-selected RNA applying the Illumina TruSeq protocol for mRNA. Libraries were amplified with 14 cycles of PCR, pooled, quantified through qPCR and sequenced with a 2×100 bp paired-end protocol, resulting in 30-43 million paired reads per sample. Details on RNA QC, library preparation and data analysis were described in [176]. Raw data for the RNA sequencing were deposited within GEO under accession no. GSE69913.

2.15 Protein biochemistry

2.15.1 Protein isolation

Indicated tissues or pelleted cells were lysed in RIPA buffer. For tissues an Ultra-Turrax homogenizer (IKA Werke) was used. RIPA buffer was composed of 50 mM Tris-HCl pH 7.5, 150 mM NaCl, 1% Nonidet P-40, 500 mM EDTA, 0.1% sodium deoxycholate, 0.2 M β-glycerol phosphate and 1 protease inhibitor tablet (cOmplete, Roche Diagnostics) for 10 ml of buffer. The samples were then snap-frozen in liquid nitrogen and thawed on ice for three repeated cycles. After 10 min of centrifugation at 13,000 rpm supernatant was transferred to fresh tubes and kept at -80 °C for long term storage.

2.15.2 Western blot (WB) analysis

Samples were separated by SDS-PAGE after being mixed 1:4 with 4× Laemmli Sample Buffer (Bio-Rad) containing 10% β-mercaptoethanol and heated to 95 °C for 5 min. PageRuler™ Prestained Protein Ladder (ThermoScientific) was used as standard.

Table 2.6: List of antibodies.

Protein target	Product no.	Supplier	Dilution
Aoc3 C-term	ab181168	AbCam	1:1000
Aoc3 N-term	ab187202	AbCam	1:1000
Bace1	ab2077	AbCam	1:1000
Bace1	SAB 2106747	Sigma	1:1000
Bace1	B0681	Sigma	1:1000
Cebpa	sc 61	Santa Cruz	1:200
Egfr	sc 03	Santa Cruz	1:200
Hsc70	sc 7298	Santa Cruz	1:10000
Pdgrfb	ab 32570	AbCam	1:5000
Pparg	07 7466	Millipore	1:1000
Ucp1	sc 6528	Santa Cruz	1:200

2.16 Southern blot (SB) analysis

2.16.1 Gel electrophoresis and blotting

Bruce 4 (Br4) ES cells transfected with LSL-Bace1 and Bace1-flox plasmids were generated in-house by the laboratory headed by Dr. Thomas Wunderlich.

Genomic DNA (5-10 μg) derived from transfected ES cells was digested with high concentrated EcoRI-HF (NEB) for LSL-Bace1 or high concentrated NheI-HF (NEB) for Bace1-flox. Br4 ES cell DNA served as a wild-type control. Digested DNA was loaded with loading dye onto a 0.8% agarose gel and separated at 30 V over night. The DNA was then depurinated by incubating the gel in 0.25 M HCl for 20 min while shaking. The DNA was then transferred onto a charged Amersham Hybond-XL nylon membrane by alkaline capillary transfer over night using a sodium hydroxide solution (0.4 M NaOH) to transfer the DNA from the gel to the membrane. The membrane was then incubated in 2× SSC for 20 min and dried at 80 °C for 45 min to fix the DNA.

2.16.2 Probe labeling and hybridization

For SB of LSL-Bace1, a 1.2 kb ROSA26 probe was amplified from the Orkin-plasmid [177] by EcoRI/ BamHI (NEB) restriction. For SB of Bace1-flox, a 636 bp probe was amplified from Br4 ES cells DNA using the primers 5' - tcatctccaccctctctcca - 3' and 5' - tagcctgagtatgacgccag - 3'. Subsequently DNA gel extraction was performed as described in 2.10. The generated probes were radioactively labeled with 2.5 μCi[α32P]dCTP (Amersham) using the Ladderman™ Labeling Kit (Takara). After addition of 10 mM TE buffer (pH 8.5), the probe was further purified by spin-column chromatography using illustra MicroSpin S-200 HR columns. After moistening in 2× SSC, the membrane was pre-hybridized with sperm DNA in Southern blot pre-hybridization buffer at 65 °C for at least 4 h, to prevent binding of the Southern blot probe to areas with no DNA. Radioactive probes in pre-hybridization buffer were incubated overnight at 65 °C. After washing steps, the membrane was placed on Kodak MS hypersensitive films in film cassettes containing an intensifying screen over night to detect the radioactive signal. Expected DNA products were as follows:

LSL-Bace1
WT: ~15.6 kb
Tg: ~7.1 kb

Bace1-flox
WT: ~12.6 kb
flox: ~16.8 kb

2.17 Immunohistochemistry

Immunohistochemistry was performed by the facility within our institute (Max-Planck Institute for metabolism research). Indicated tissue samples were incubated at 4 °C overnight in 4% paraformaldehyde, embedded in paraffin (FFPE) and sliced according to standard protocols. Haematoxylin and eosin (H&E) staining and insulin immunohistochemistry were carried out after deparaffination as previously described in [176]. A Zeiss Axioskop 40microscope (Carl Zeiss MicroImaging) and Zeiss AxioVision 4.2 software (Carl Zeiss MicroImaging) were used for imaging and quantification of slides.

2.18 Cell surface capturing (CSC) analysis

CSC was performed in collaboration with the ETH proteomics facility (Zürich, Switzerland) headed by Prof. Bernd Wollscheid.

2.18.1 Capture of cell surface glycoproteins

For each of the three replicates, C2C12 or C2C12$^{\Delta Bace1}$ cells of three fully confluent 15 cm dishes were washed two times with cold labelling buffer (LB; PBS pH 6.5). Cells were mildly oxidized with 2.5 mM sodium periodate in 5 ml LB for 15 min at 4 °C in the dark. Oxidized cells were washed with 10 ml LB and incubated in 5 ml LB containing 5 mM biocytin-hydrazide and 5 mM 2-Amino-5-methoxybenzoic acid for 20 min at 4 °C in the dark to biotinylate cell surface glycoproteins. Labelled cells were washed two times with cold PBS and harvested by scraping. After centrifugation at 300 g for 5 min, supernatant was removed and cell pellet resuspended in 800 μl lysis buffer (50 mM AmBic, 0.05% RapiGest, 2 mM TCEP). Cells were lysed by sonication in a VialTweeter (Hielscher Ultrasonics GmbH) 3 × 30 sec (0.8 s cycle time and 100% amplitude) with intermitted vortexing and cooling on ice. Cell debris were settled down by centrifugation at 10'000 g for 10 min, supernatant collected and protein concentration determined using Pierce 660 nm protein assay (Thermo Fisher Scientific). Iodoacetamide was added to a final concentration of 10 mM and lysate incubated in the dark for 30 min at room temperature. Calcium chloride was added to a final concentration of 1 mM and proteins digested into peptides overnight at 37 °C by adding trypsin in an enzyme:protein mass ratio of 1:200. Trypsin was inactivated by adding PMSF to 2 mM final concentration and acidification to pH < 3 with 10% formic acid. Digested protein lysate was centrifuged at max. speed for 15 min and peptide concentration of supernatant measured with

a NanoDrop 2000 spectrophotometer (Thermo Fisher Scientific). Per replicate, 15 mg peptide were subjected to automated purification of cell surface biotinylated glycopeptides. For this, in-house packed tips containing 80 μl streptavidin resin were hooked to a Versette liquid handling robotic system (Thermo Fisher Scientific) and incubated with the digested cell lysate for 1 h at room temperature with up-and-down pipetting. In an automated fashion, bead-bound peptides were subsequently washed with 5 M NaCl, StimLys Buffer (50 mM Tris pH 7.8, 137 mM NaCl, 150 mM Glycerol, 0.5 mM EDTA, 0,1% Triton X-100), 100 mM $NaHCO_3$ and 50 mM NH_4HCO_3 (AmBic). Beads were further incubated overnight at 37 °C with 600 μl AmBic containing 1000 units PNGase F to specifically release formerly N-glycosylated peptides. Eluted peptides were acidified to pH < 3 by formic acid and subjected to C18 purification using 3-30 μg UltraMicroSpin Columns (The Nest Group) according to manufacturer's instructions.

2.18.2 LC-MS and data analysis

Peptides were reconstituted in 3% acetonitrile (ACN) with 0.1% formic acid (FA) and separated by reversed-phase chromatography on a high-performance liquid chromatography (HPLC) column (75-μm inner diameter, New Objective) that was packed in-house with a 15-cm stationary phase (ReproSil-Pur C18-AQ, 1.9 μm) and connected to a nano-flow HPLC combined with an autosampler (EASY-nLC 1000, Thermo Fisher Scientific). The HPLC was coupled to a Q-Exactive plus mass spectrometer (Thermo Fisher Scientific) equipped with a nano electrospray ion source (Thermo Fisher Scientific). Peptides were loaded onto the column with 100% buffer A (99.9% H2O, 0.1% FA) and eluted at a constant flow rate of 300 nl/min with a 70-min linear gradient from 6-28% buffer B (99.9% ACN, 0.1% FA) followed by a 4-min transition from 28 to 50% buffer B. After the gradient, the column was cleaned for 18 min with two steep consecutive gradients of ACN (10%-98%). Electrospray voltage was set to 2 kV, sheath and auxiliary gas flow to zero and capillary temperature to 250 °C. Following a high-resolution survey mass spectrum (from 300 to 1,700 m/z) acquired in the Orbitrap with resolution R = 70,000 at m/z 200 (automatic gain control target value 3×106), the 15 most abundant peptide ions with a minimum intensity of 2.5×104 were selected for subsequent HCD fragmentation with an isolation window of 1.4 Da and fragments were detected in the Orbitrap at resolution R = 35,000 (automatic gain control target value 1×106). Targeted ion masses already selected for fragmentation were dynamically excluded for 30 seconds. Acquired raw files were subjected to peptide and protein identification using the Trans Proteomic Pipeline v.4.7 [178]. First, fragment ion spectra were matched

against a database of SwissProt (UniProt consortium) reviewed mouse protein sequences (downloaded April 2014) and common contaminants. Peptides were required to have one tryptic cleavage terminus (semitryptic) with a maximum of 2 missed cleavage sites and carbamidomethylation as a fixed modification. Methionine oxidation and PNGase F mediated asparagine deamidation were set as dynamic modifications. The precursor and fragment mass tolerance was set to 20 ppm and 0.02 Da, respectively. Identified proteins were quantified by integration of chromatographic traces of their corresponding peptides on MS1 level using Progenesis QI v.2.0 (Nonlinear Dynamics, UK). Contaminant hits were removed and proteins filtered to obtain a false discovery rate of < 1%. Raw protein abundances based on non-conflicting peptides were exported. Proteins with at least one transmembrane domain and an asparagine deamidation modification within the common N-X-S/T glycosylation motif were considered as bona fide cell surface glycoproteins and were subjected to differential abundance testing using R-package MSstats v3.2.2 [179]. Proteins with an abundance fold change of ± 1.5 and adjusted p-value < 0.05 indicate significantly regulated proteins upon perturbation.

2.19 Improved secretome protein enrichment with click sugars (iSPECS)

iSPECS was performed in collaboration with the laboratory of neuroproteomics at the German Center for Neurodegenerative Diseases (DZNE, Munich, Germany) headed by Prof. Stefan Lichtenthaler.
For each of the six replicates, C2C12 or C2C12$^{\Delta Bace1}$ cells were seeded in 6-well plates. When fully confluent (~ 1.5 million cells), cells were first washed with PBS and then maintained in growth medium supplemented with 50 μM ManNAz sugar dissolved in DMSO. After 48 h supernatants were filtered through 0.2 μM filters, stored at -20 °C and later sent to our collaborators on dry ice. iSPECS proteomic analysis was performed using an unpublished protocol based on the SPECS technique described in [180] [181].

2.20 MicroRNA gene target overlap

Overlap between target genes of each pair of mouse microRNAs was calculated using the Targetscan algorithm (http://www.targetscan.org). Applying this procedure to all possible pairs, resulted in a representation of the probability density function of the overlap size.

Finally, p value for a particular pair of microRNAs was computed by comparing the size of their target overlap with this distribution.

2.21 Ingenuity pathway analysis (IPA)

For pathway analysis of RNA sequencing (2.14) results, the 2,000 most changed genes were shortlisted using the Ingenuity Pathway Analysis software (IPA, Ingenuity Systems). Overrepresented gene ontology (GO) pathways were visualised using the IPA suite.

2.22 Graphical representation of data and statistical analysis

All graphs were created using GraphPad Prism 6.0 (GraphPad Software). Floating bars indicate minimum, maximum and mean values. GraphPad Prism 6.0 software was used to perform statistical calculations. When two groups were analysed, significance was determined using an unpaired or paired Student's t-test. One-way ANOVA followed by Bonferroni correction was used when three groups were analysed. Two-way ANOVA for repeated measures (2WA-RM) followed by Bonferroni post-hoc test was used to judge the effect of two independent variables. Statistical details are given in the figure legends. A p value < 0.05 is considered statistically significant.

n.s.	p >0.05
*	p <0.05
**	p <0.01
***	p <0.001
****	p <0.0001

2.23 Utilised chemicals

Table 2.7: Chemicals

Chemical	Supplier
0.9% Saline (sterile)	AlleMan Pharma GmbH
3-Isobutyl-1-methylxanthin (IBMX)	Sigma-Aldrich
3,3',5-Triiodo-L-thyronine (T_3)	Sigma-Aldrich
Acrylamide	Roth
Agarose	Peqlab
Agarose (Ultra Pure)	Invitrogen
Ammoniumpersulfat (APS)	Sigma-Aldrich
Ampicillin	Sigma-Aldrich
Bacillol	Bode Chemie
Biocytin-hydrazide	Pitsch NucleicAcids
Bovine serum albumin (BSA)	Sigma-Aldrich
Chloroform	Merck
D(+)-Glucose-Monohydrat	AppliChem
DEPC	AppliChem
Developer G153	AGFA
Dexamethasone	Sigma-Aldrich
Dimethylsulfoxide (DMSO)	Merck
dNTPs Set, 100 mM Solutions	Thermo Fisher Scientific
Dulbecco's Phosphate Buffered Saline (DPBS)	Thermo Fisher Scientific
Enhanced chemiluminescence (ECL)	Kit Perbio Science
Ethanol, absolute	AppliChem
Ethidium bromide	Sigma-Aldrich
Ethylendiamine tetraacetate (EDTA)	AppliChem
Fixer G354	AGFA
Formamide	AppliChem
GeneRuler DNA Ladder Mix	Thermo Fisher Scientific
Glucose 20%	DeltaSelect
Glycerol-free PNGase F	New England Biolabs
Hydrochloric acid (37%)	KMF Laborchemie
Indomethacin	Sigma-Aldrich
Insulin	Novo Nordisk
Isopropanol (2-propanol)	Roth
Click-IT™ ManNAz	Thermo Fisher Scientific
Methanol	Roth
Nitrogen (liquid)	Linde
Nonidet P-40	Roche Diagnostics
OPTI-MEM (1×)	Thermo Fisher Scientific

Chemical	Supplier
Paraformaldehyde (PFA)	Sigma-Aldrich
Quick Start™ Bradford dye reagent	Bio-Rad
RapiGest SF Surfactant	Waters
Rosiglitazone	Sigma-Aldrich
Rotiphorese® Gel 30 (37,5:1)	Roth
Sequencing Grade Modified Trypsin	Promega
Sodium chloride (NaCl)	AppliChem
Sodium deoxycholate	Sigma-Aldrich
Sodium dodecyl sulfate	AppliChem
Streptavidin Plus UltraLink Resin	Thermo Fisher Scientific
Tetramethylethylenediamine (TEMED)	Sigma-Aldrich
Tissue Freezing Medium	Jung
Trishydroxymethylaminomethane (Tris)	AppliChem
Trypsin-EDTA (10×)	Thermo Fisher Scientific
Tween 20	AppliChem
Western Blocking Reagent	Roche Diagnostics
β-glycerophosphate disodium salt hydrate	Sigma-Aldrich
β-mercaptoethanol	AppliChem

CHAPTER 3

PRELIMINARY DATA

Our group could show that brown fat-specific heterozygous knock-out of *Dicer* in mice was associated with deterioration of glucose metabolism [170]. This was aggravated under obese condition and was likely dependent on decreased EE due to reduced BAT activity and function [170]. In light of these findings, we investigated which specific miRNAs were involved in the regulation of brown adipocyte homeostasis. Using microarray analysis, we quantified the expression of miRNAs during adipogenic differentiation of primary immortalised brown adipocytes (PIBAs), a stable cell line of brown-programmed pre-adipocytes (Figure 3.1 a). To examine both *in vitro* and *in vivo* miRNA regulation, we also investigated the expression of these noncoding RNAs in mouse models of altered BAT function. For this purpose we analysed BAT samples from mouse models of diet-induced obesity (DIO) via high-fat diet (HFD) feeding, premature ageing in progeroid *Ercc1*$^{-/-}$ mice and long-lived homozygous Ames dwarf mutants (Ames^{df}). The first two conditions are known to have detrimental effects on BAT [182] [183], while the latter is known to enhance BAT function [184]. We selected miRNAs up-regulated during PIBA commitment and in BAT of Ames^{df} mice and decreased in brown fat of DIO and progeroid mice, finding 23 miRNAs fulfilling these criteria (Figure 3.1 b). Of these we selected eight for further *in vitro* characterisation, namely *miR-96*, *miR-210*, *miR-328* and all five *miR-30* family members (*miR-30a-e*), some of which have already been shown to play a role in BAT homeostasis (1.5.4.1). We could validate the microarray results on qPCR level showing an increased expression during PIBA differentiation and a down-regulation upon HFD feeding for all the miRNA candidates (Figure 3.1 c). We then

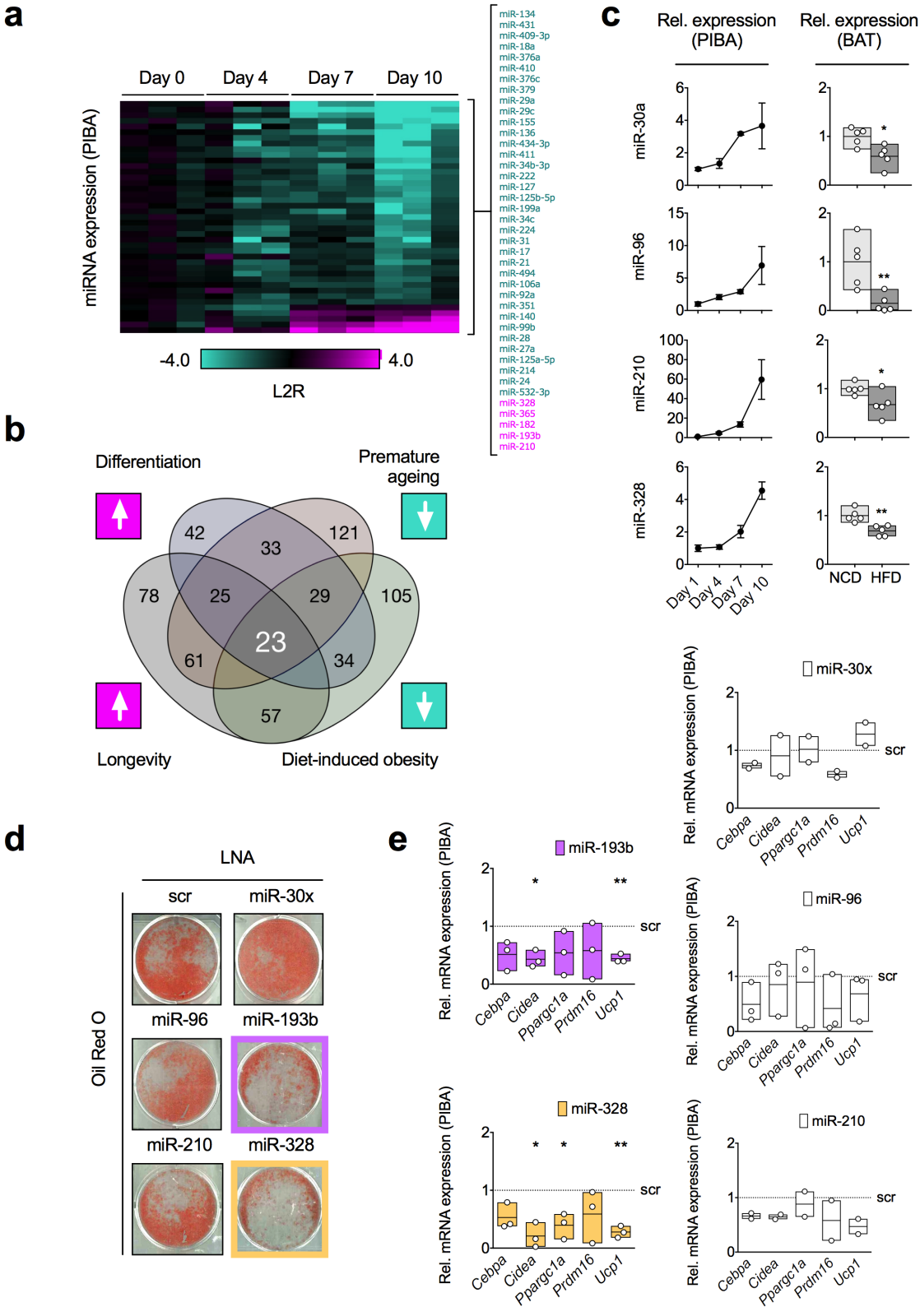
a
Day 0
Day 4
Day 7
Day 10
miRNA expression (PIBA)
-4.0
4.0
L2R
miR-134
miR-431
miR-409-3p
miR-18a
miR-376a
miR-410
miR-376c
miR-379
miR-29a
miR-29c
miR-155
miR-136
miR-434-3p
miR-411
miR-34b-3p
miR-222
miR-127
miR-125b-5p
miR-199a
miR-34c
miR-224
miR-31
miR-17
miR-21
miR-494
miR-106a
miR-92a
miR-351
miR-140
miR-99b
miR-28
miR-27a
miR-125a-5p
miR-214
miR-24
miR-532-3p
miR-328
miR-365
miR-182
miR-193b
miR-210
b
Differentiation
Premature ageing
42
33
121
78
25
29
105
23
61
34
57
Longevity
Diet-induced obesity
c
Rel. expression (PIBA)
Rel. expression (BAT)
miR-30a
miR-96
miR-210
miR-328
Day 1
Day 4
Day 7
Day 10
NCD
HFD
d
LNA
scr
miR-30x
miR-96
miR-193b
miR-210
miR-328
Oil Red O
e
miR-30x
miR-193b
miR-96
miR-328
miR-210
Rel. mRNA expression (PIBA)
scr
Cebpa
Cidea
Ppargc1a
Prdm16
Ucp1

FIGURE 3.1. ***MiR-328* regulates brown adipose tissue differentiation *in vitro*.** **a** Heatmap diagram illustrating expression of miRNAs in differentiating PIBA cells at indicated time points. For each time-point, miRNA expression levels in three PIBA samples were quantified using an independent qPCR array each. **b** Venn diagram depicting overlap of miRNA expression in the four indicated conditions. **c** Relative expression of indicated miRNAs during PIBA differentiation (left) or in BAT from HFD-fed (n=6) versus NCD-fed (n=6) mice (right). **d** Representative Oil Red O staining of differentiated PIBAs seven days after transfection with LNAs against indicated miRNAs versus scramble (scr) controls. Image is representative of three independent experiments. **e** Expression of indicated genes in differentiated PIBA cells seven days after transfection with LNAs against indicated miRNAs versus scr controls. Experiments were performed in triplicate and represent the average of two/three independent experiments. *p<0.05, **p<0.01.

assessed the effects of inhibition of these miRNAs on the adipogenic differentiation of PIBA cells. For this purpose we utilised miRCURY LNA™ Power Inhibitors and selected *miR-193b*, previously shown to regulate brown adipocyte fate [168] and present in our list of differentially expressed miRNAs (Figure 3.1 a), as internal control. We could observe an impairment in the differentiation of PIBA cells upon *miR-193b* and *miR-328* inhibition, as shown by decreased lipid accumulation (Figure 3.1 d). These results were supported by decreased expression of BAT-specific genes in PIBAs treated with LNAs against *miR-193b* and *miR-328* (Figure 3.1 e).

Taken together our results identified *miR-328* as a novel regulator of brown fat commitment *in vitro* and confirmed previous reports on the *in vitro* regulation of brown adipocytes by *miR-193b*.

CHAPTER 4

RESULTS

4.1 *Dicer1* regulation of brown adipose tissue

4.1.1 Metabolic analysis of *Dicer1*$^{\Delta BAT/+}$ mice

Hormone level analysis

Dicer1$^{\Delta BAT/+}$ mice showed decreased glucose tolerance in both males and females already under NCD condition [170]. When fed a HFD, this defect in glucose homeostasis was even more pronounced and was associated with decreased insulin sensitivity. In order to understand if this decline in glucose metabolism was due to hormone impairment we analysed the plasma levels of the adipocyte hormone leptin and of the pancreatic hormone insulin in both sexes and diet conditions. ELISA analysis showed no difference in hormone levels in the plasma of *Dicer1*$^{\Delta BAT/+}$ mice compared to control littermates (Figure 4.1 a and b).

Adiposity analysis

Although HFD-fed *Dicer1*$^{\Delta BAT/+}$ mice showed an increase in adiposity [170], we could not observe any macroscopical sign of body fat redistribution as published for pan-adipose *Dicer1*-null mice by Mori *et al.* [151]. To assess whether the fat redistribution occurred merely on a microscopical level we performed plasma lipid and immunohistochemical analyses in *Dicer1*$^{\Delta BAT/+}$ mice fed a HFD diet. However, thin-layer chromatography (TLC)-mediated quantification of cholesterol, free fatty acids and triglycerides in liver and muscle (Figure 4.1 c) revealed no alteration in lipid concentrations in knock-out mice.

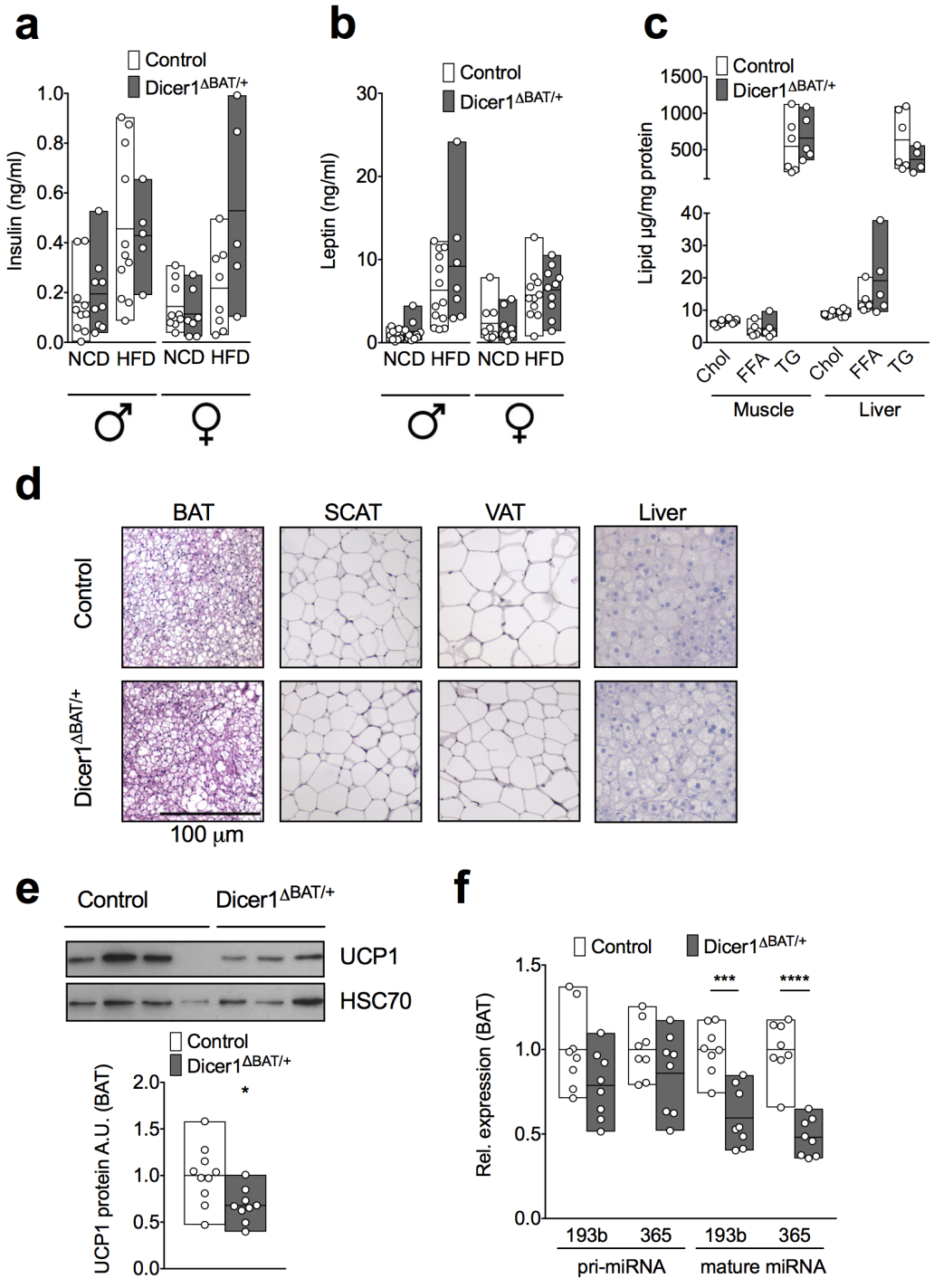

FIGURE 4.1. ***Dicer1* regulation of brown adipose tissue. a** Serum insulin level of NCD-fed, male *Dicer1*$^{\Delta BAT/+}$ (n=9) versus control mice (n=10) and HFD-fed, male *Dicer1*$^{\Delta BAT/+}$ (n=5) versus control mice (n=8, *left*) or NCD-fed, female *Dicer1*$^{\Delta BAT/+}$ (n=8) versus control mice (n=9) and HFD-fed, female *Dicer1*$^{\Delta BAT/+}$ (n=5) versus control mice (n=12, *right*). **b** Se-

rum leptin level of NCD-fed, male *Dicer1*$^{\Delta BAT/+}$ (n=10) versus control mice (n=9) and HFD-fed, male *Dicer1*$^{\Delta BAT/+}$ (n=7) versus control mice (n=13, *left*) or NCD-fed, female *Dicer1*$^{\Delta BAT/+}$ (n=9) versus control mice (n=9) and HFD-fed, female *Dicer1*$^{\Delta BAT/+}$ (n=10) versus control mice (n=11, *right*). **c** Thin-layer chromatography-mediated quantification of lipid species (Chol, cholesterole; FFA, free fatty acids; TG, triglycerides) in indicated tissues of HFD-fed *Dicer1*$^{\Delta BAT/+}$ (n=5) versus control (n=6) mice. **d** Photomicrograph of indicated tissues in HFD-fed *Dicer1*$^{\Delta BAT/+}$ and control mice. A representative image is shown. **e** Immunoblot of UCP1 expression in BAT of *Dicer1*$^{\Delta BAT/+}$ (n=9) versus control (n=10) mice. Image is representative of two independent experiments (*top*). Densitometric quantification of protein levels in *Dicer1*$^{\Delta BAT/+}$ mice (n=9) versus controls (n=10). Relative levels for control mice were set to unity=1 (*bottom*) **f** Relative expression of indicated primary (pri-) and mature microRNAs in BAT of male *Dicer1*$^{\Delta BAT/+}$ (n=8) versus control (n=8) mice. *p<0.05, ***p<0.001, ****p<0.0001.

Furthermore, comparison of H&E stainings of the three main adipose depots and liver of *Dicer1*$^{\Delta BAT/+}$ mice with littermate controls indicated no redistribution of body fat (Figure 4.1 d).

Moreover, we examined whether the inability of lean *Dicer1*$^{\Delta BAT/+}$ mice to maintain core body temperatures under thermal stress (4 °C) was correlated with molecular defects in thermogenic markers. For this purpose we analysed the protein levels of uncoupling protein 1 (*Ucp1*) in BAT of *Dicer1* deficient mice. Our results showed a decrease in UCP1 protein in *Dicer1*$^{\Delta BAT/+}$ mice compared to controls (Figure 4.1 e), further supporting a thermogenic impairment in these mice.

These experiments suggest that *Dicer1* deficiency specifically in BAT does lead to an obesity-associated impairment in both glucose homeostasis and thermogenesis without causing ectopic fat deposition or lipodystrophy [151].

4.1.2 MicroRNA processing is impaired in brown fat of *Dicer1*$^{\Delta BAT/+}$ mice

DICER1 is one of the key regulators of miRNA processing, generating miRNA duplexes through cleaving of pre-miRNAs in the cytoplasm prior to mature miRNAs generation (1.5.2). *Dicer1*$^{\Delta BAT/+}$ mice were generated by depletion of the gene from one of the two DNA alleles [170]. Since the heterozygous *Dicer1* knock-out in BAT resulted in a mere 25% decrease of *Dicer1* mRNA, we investigated whether the ratio of mature miRNAs over pri-miRNAs was affected. We selected two miRNAs (*miR-193b* and *miR-365*) for expression analysis of both primary and mature sequences. As seen in Figure 4.1 f only mature forms of *miR-193b* and *miR-365* were decreased, indicating a specific effect of *Dicer1* knock-out on mature miRNAs only.

We could hereby confirm a successfully established defect in miRNA maturation that might account for the thermogenic phenotype we observed in *Dicer1*$^{\Delta BAT/+}$ mice.

4.2 *MiR-328* regulates the switch between brown adipose tissue and muscle

4.2.1 Localisation analysis of miRNA candidates

As shown in chapter 3 our laboratory discovered *miR-328* as BAT-related miRNA whose expression is regulated in mouse models of obesity and ageing. In addition *miR-328* was shown to affect differentiation of brown preadipocytes (Figures 3 d and e). For an overview of the tissue distribution of *miR-193b* and *miR-328*, expression of the two miRNAs was analysed on a transcript level in metabolic-related tissues (brown and white adipose tissue, skeletal and cardiac muscle and liver, Figure 4.2 a). qPCR analysis revealed an enrichment of *miR-193b* and *miR-328* in BAT and WAT, supporting a potential role of these in adipose tissue regulation. These results are in line with previous studies depicting these miRNAs as highly enriched in murine and human BAT [163].
Given the enrichment of *miR-193b* and *miR-328* brown adipose tissue and the regulation of *miR-328* specifically on brown adipogenesis *in vitro*, we decided to determine the expression levels of *miR-193b* and *miR-328* in our *in vivo* model for BAT-specific *Dicer1* deficiency. As expected the miRNA candidates showed a decreased expression in *Dicer1*$^{\Delta BAT/+}$ mice compared to littermate controls (Figure 4.2 b).
The defect in thermogenesis and glucose homeostasis observed in *Dicer1*$^{\Delta BAT/+}$ mice could hence also be linked to the reduction of *miR-193b* and *miR-328*.

4.2.2 *MiR-193b*/*miR-328* deficiency stimulates myogenic marker expression

Skeletal myoblasts and brown adipocytes derive from a common cell lineage (1.3.2) and modulation of transcriptional factors like PRDM16 [70] can control a bidirectional cell fate switch between the two tissues. We therefore investigated the expression of myogenic markers in PIBA cells and in the mouse myoblast C2C12 cell line upon *miR-193b* and *miR-328* knock-down. Deficiency of both miRNAs showed an increase in the expression of paired box 3 (*Pax3*) and RUNX1 translocation partner 1 (*Runx1t1*) in PIBA cells and the same expression pattern could be observed in C2C12 cells exclusively upon knock-down of *miR-328* (Figure 4.2 c).
As *miR-193b* and - even more potently - *miR-328* knock-down could enhance a myogenic phenotype in both skeletal myoblasts and brown adipocytes, we examined whether the

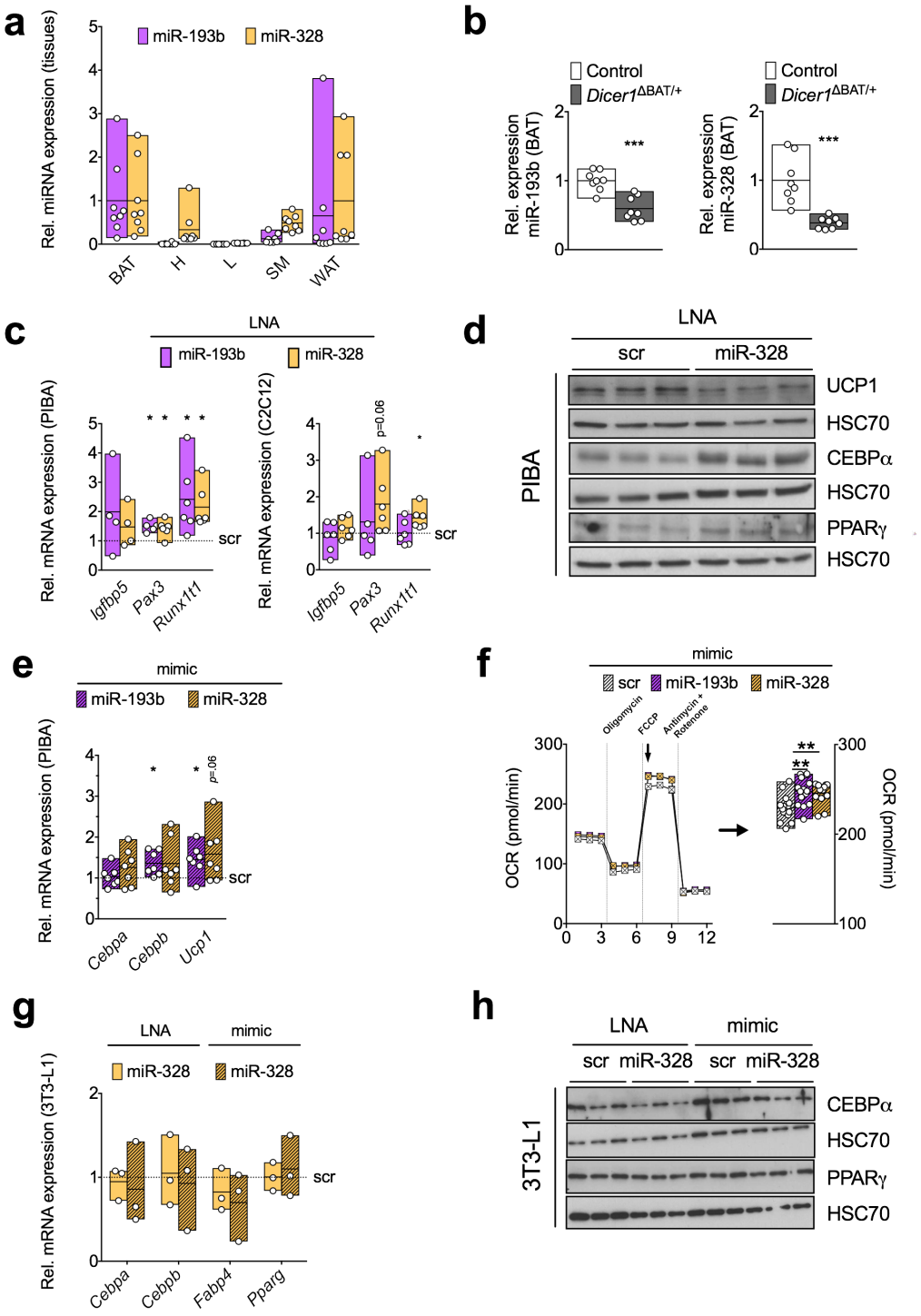

FIGURE 4.2. ***MiR-328* regulates the switch between brown fat and muscle. a** Relative expression of *miR-193b* and *miR-328* in n=8 indicated tissues (BAT, brown adipose tissue;

H, heart; L, liver; SM, skeletal muscle; WAT, white adipose tissue). Expression levels in BAT were set to unity=1. **b** Relative expression of indicated microRNAs in BAT of male *Dicer1*$^{\Delta BAT/+}$ (n=8) versus control (n=8) mice. **c** Relative expression of indicated genes in PIBA (*left*) or C2C12 (*right*) cells transfected with scr, *miR-193b* or *miR-328* LNAs. **d** Immunoblots against indicated proteins after transfection of PIBA cells with LNAs against *miR-328* versus scr. Image is representative of three (UCP1) or two (others) independent experiments. **e** Relative expression of indicated genes in PIBA cells transfected with scr, *miR-193b* or *miR-328* mimics. **f** Oxygen consumption rates (OCR) of PIBA cells transfected with scr, *miR-193b* or *miR-328* mimics (*left*). Illustration of maximal OCR at measurement 7 (arrow, *right*). The data shown are from measurements in at least 14 wells for each condition. **g** Relative expression of indicated genes in 3T3-L1 cells after transfection with LNAs against indicated miRNAs versus scr controls or miRNA mimics versus scr. Experiments were performed in triplicate and represent the average of three independent experiments. **h** Immunoblots against indicated proteins after transfection of 3T3-L1 cells with miRNA LNAs versus scr or miRNA mimics versus scr. Image is representative of two independent experiments. *p<0.05, **p<0.01, ***p<0.001.

knock-down would likewise cause a reduced adipogenic phenotype. We could indeed show a decrease in protein expression of BAT-specific UCP1 together with increased expression of WAT markers like CCAAT/enhancer binding protein (C/EBP) alpha (CEBPα) and peroxisome proliferator activated receptor gamma (PPARγ) after *miR-328* silencing in PIBA cells (Figure 4.2 d).
These results point to a decrease in BAT activity upon miRNA candidates depletion, possibly due to increased myogenic potential or whitening (1.3.1) of brown fat.

4.2.3 MicroRNA over-expression in PIBAs stimulates adipogenic features

Given the reduced thermogenic activity of brown adipocytes upon LNA-based knock-down of *miR-193b* and *miR-328*, we hypothesized that an over-expression of these miRNAs could potentially trigger a therapeutically desirable increase in BAT activity. For this purpose we transfected miRIDIAN microRNA mimics, which supplement endogenous miRNA activity, in PIBA cells. Notably, both *miR-193b* and *miR-328* over-expression increased gene expression of *Cebpb* and *Ucp1* (Figure 4.2 e). On a functional level, both over-expression models caused elevated oxygen consumption rates (OCRs), a metabolic hallmark of activated brown fat cells (Figure 4.2 f).
We could hereby prove, that *miR-193b* and *miR-328* over-expression is positively correlated with thermogenic activity.

4.2.4 White adipose tissue cell line is not affected by *miR-328* expression

As we hypothesized that *miR-328* activity on cell fate decision is specific for the cell lineage which gives rise to myocytes and brown - but not white - adipocytes, we decided to test the effects of our gain- and loss-of-function models in the white adipogenic 3T3-L1 cell line (Details in 2.7.5). Both mRNA (Figure 4.2 g) and protein expression (Figure 4.2 h) of adipogenic markers like *Cebpa* and *Pparg* were unaltered in LNA knock-down and mimic over-expression experiments, supporting a BAT-specific effect of *miR-328*.
We thus confirmed *miR-328* to have a role in the regulation of myogenic and brown - but not white - adipogenic homeostasis.

4.3 *Bace1* and *Gprc5b* as novel targets of *miR-328*

4.3.1 *MiR-193b* and *miR-328* share common target genes

MicroRNAs are key regulatory RNAs known to repress mRNA translation via base-pairing of their seed sequence with complementary sequences present mainly in the 3'-UTR of targeted mRNA molecules (1.5.2). As shown in 3.1 our group confirmed *miR-193b* and newly discovered *miR-328* to support brown preadipocyte differentiation and skew muscle progenitor cells towards a brown fat transcriptional profile. Considering the inhibitory role of miRNAs we decided to look for potential targets of these two miRNAs that could have an effect on peripheral tissue metabolism. Strikingly, we observed notable sequence similarities between the seed regions of *miR-193b* and *miR-328*, thus resulting in a significant overlap of common predicted target genes (Figure 4.3 a). This consequently suggests that the two miRNAs might control brown adipogenesis by regulating the same pool of mRNAs via expression silencing. Using in silico prediction (www.microRNA.org), we selected nine predicted common target genes between *miR-193b* and *miR-328*. The criteria used for this selection included genes harbouring binding sites for both miRNAs in their 3'-UTR and genes enriched in muscle as shown through publicly available expression profiles (www.biogps.org). The nine selected target genes were then validated by luciferase reporter assay. For this, the firefly luciferase open reading frame was cloned upstream of the 3'-UTRs of putative target genes. HEK293 transfection of the generated vectors revealed that over-expression of *miR-193b* and *miR-328* down-regulated the luciferase activity of two transcripts (Figure 4.3 b): β-site amyloid precursor protein cleaving enzyme 1 (*Bace1*), known for its role in the development of Alzheimer's disease (AD), and G-protein coupled receptor family C group 5 member B (*Gprc5b*). *Bace1* was reported to be potentially targeted by *miR-328* in neuronal cells [185].

4.3.2 *Bace1* and *Gprc5b* are direct targets of *miR-193b* and *miR-328*

To asses if the aforementioned decrease in luciferase activity seen for *Bace1* and *Gprc5b* occurred exclusively due to base-pairing of *miR-193b* and *miR-328* to the 3'-UTR of the two genes, we mutated the predicted miRNA seed sequences. The seed mutation did indeed abrogate the effect of microRNA over-expression on *Bace1* and *Gprc5b* in the luciferase reporter assay (Figure 4.3 c). Furthermore, LNA-mediated down-regulation and mimic-mediated over-expression of *miR-193b* and *miR-328* in PIBA cells correlated

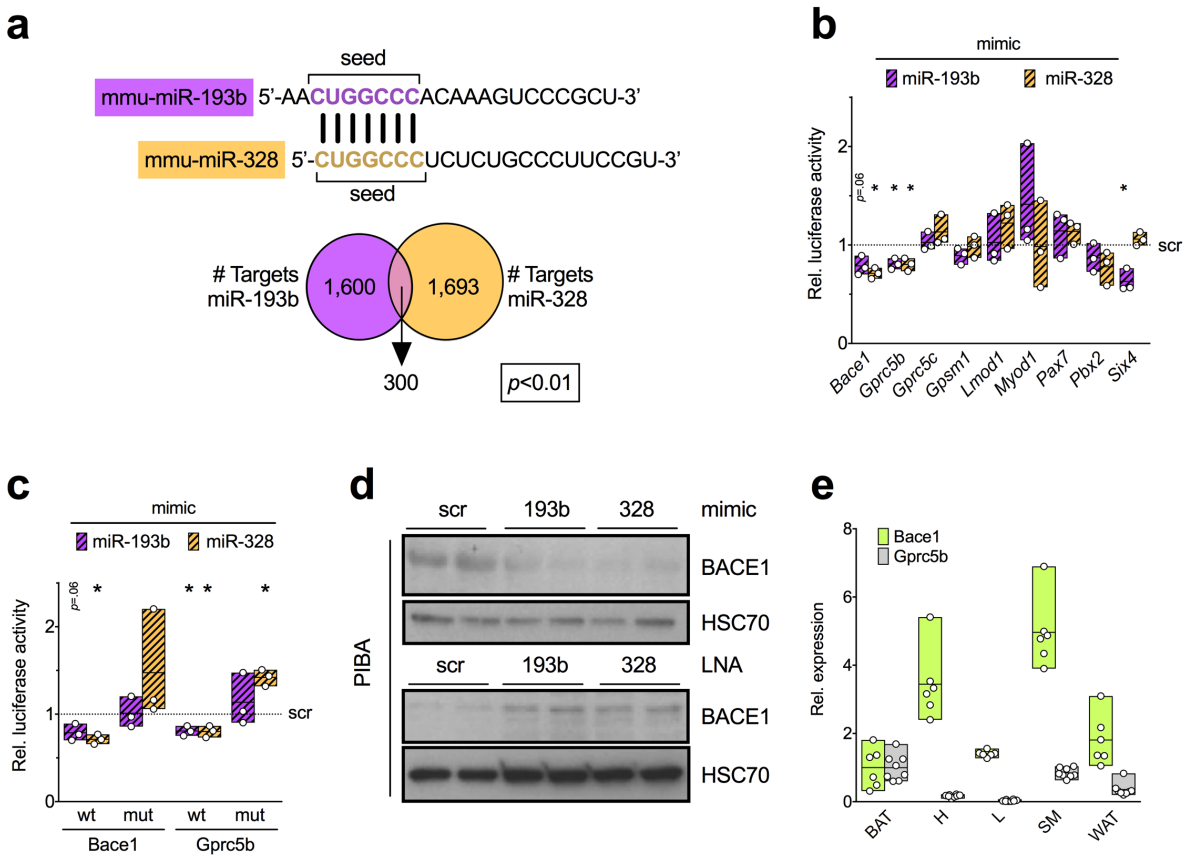

FIGURE 4.3. ***Bace1* and *Gprc5b* as novel targets of *miR-328*.** **a** Comparison of *miR-193b* versus *miR-328* seed sequences (*top*) and overlap of in silico predicted *miR-193b* and *miR-328* mRNA targets (*bottom*). **b** Relative luciferase activity in HEK293 cells after co-transfection of pmiRGlo reporter constructs harbouring wild-type 3'UTR fragments of indicated genes together with scr, *miR-193b* or *miR-328* mimics. **c** Relative luciferase activity in HEK293 cells after co-transfection of pmiRGlo reporter constructs harbouring wild-type (wt) or mutated (mut) 3'UTR fragments of indicated genes together with scr, *miR-193b* or *miR-328* mimics. **d** Immunoblot analysis of BACE1 in PIBA cells transfected with scr, *miR-193b* or *miR-328* mimics (*top*) or LNAs (*bottom*). Image is representative of two (mimics) or three (LNAs) independent experiments. **e** Relative expression of *Bace1* (n=6) and *Gprc5b* (n=8) in indicated tissues (BAT, brown adipose tissue; H, heart; L, liver; SM, skeletal muscle; WAT, white adipose tissue). Expression levels in BAT were set to unity=1. *p<0.05.

with protein expression of *Bace1* (Figure 4.3 d). To analyse tissue distribution of *Bace1* and *Gprc5b* we performed qPCR analysis in BAT, heart, liver, SM and WAT. We found *Bace1* to be enriched in the two muscle tissues while *Gprc5b* is enriched in BAT and SM (Figure 4.3 e).

These results indicate *Bace1* and *Gprc5b* as direct targets of *miR-193b* and *miR-328* that could potentially regulate adipose tissue and muscle metabolism.

4.4 *Bace1* deficiency *in vitro* promotes brown adipogenesis while inhibiting myogenesis

4.4.1 *Bace1* but not *Gprc5b* knock-down inhibits late myogenesis of C2C12 cells

Depletion of *miR-193b* and *miR-328* in vitro attenuated myogenic potential. To asses whether *Bace1* and *Gprc5b* act downstream of *miR-193b* and *miR-328* in regulating myogenesis and brown adipogenesis *in vitro*, we examined the effects of the inhibition of these genes in C2C12 cells. *Bace1* and *Gprc5b* inhibition was obtained using Antisense LNA™ GapmeRs (Exiqon) and validated via qPCR (Figure 4.4 a and d).
Gprc5b silencing in C2C12 cells during the course of myogenic differentiation showed no effect on cell morphology or myogenic marker expression (Figure 4.4 b and c). Knock-down of *Bace1* transcript levels on the other hand caused morphological defects in myogenesis (Figure 4.4 b) and a concomitant reduction in late - but not early - myogenic marker expression, such as creatine muscle kinase (*Ckm*), myogenin (*Myog*) and troponin T type 3 (*Tnnt3*) (Figure 4.4 c).
Thus we concluded that the enhanced myogenic phenotype upon silencing of *miR-193b* and *miR-328* is likely to occur due to direct inhibition of *Bace1* but not *Gprc5b* mRNA.

4.4.2 *Bace1* down-regulation promotes brown adipocyte differentiation and activity *in vitro*

Silencing of *miR-193b* and *miR-328* did not only result in increased myogenic potential in myoblasts and brown adipocytes, but also in a reduction of thermogenesis in PIBA cells. We hence hypothesized that *Bace1* as direct target of *miR-193b* and *miR-328* may not only affect myogenesis but also brown adipogenesis. In fact, *Bace1* knock-down in PIBA cells accelerated lipid accumulation (Figure 4.4 e) and augmented the expression of brown fat-specific markers as elongation of very long chain fatty acids-like 3 (*Elovl3*), peroxisome proliferator activated receptor alfa (*Ppara*), *Pparg* and *Ucp1* (Figure 4.4 f). This effect was not observed in the white adipocyte cell model 3T3-L1 (Figure 4.4 g). Furthermore, *Bace1* inhibition in PIBA cells increased oxidative metabolism as indicated by higher OCRs detected for maximal cellular respiration (Figure 4.4 h).
Taken together our results indicate a role for *Bace1* inhibition by *miR-193b* and *miR-328* in supporting brown - but not white - adipogenesis to the detriment of myogenesis.

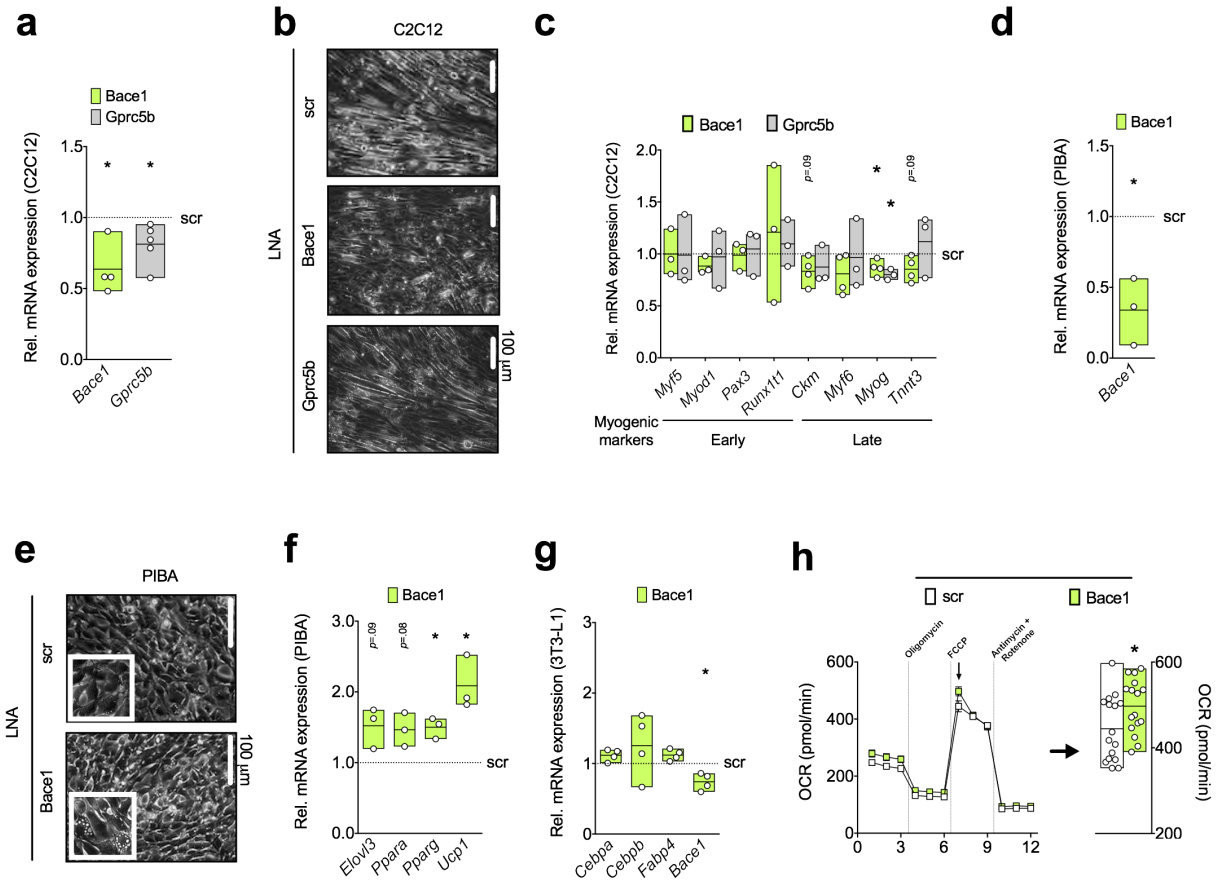

FIGURE 4.4. ***Bace1* deficiency *in vitro* promotes brown adipogenesis while inhibiting myogenesis. a** Relative expression of *Bace1* and *Gprc5b* in C2C12 cells 2 days after transfection with indicated LNA GapmeRs. **b** Photomicrograph of C2C12 cells after transfection with indicated LNA Gapmers. Image is representative of three independent experiments. **c** Relative expression of indicated genes in C2C12 cells transfected with indicated LNA GapmeRs. **d** Relative expression of *Bace1* in PIBA cells 2 days after transfection with indicated LNA GapmeRs. Experiments were performed in triplicate and represent the average of three independent experiments. **e** Photomicrograph of PIBA cells after transfection with *Bace1* LNA Gapmers. Image is representative of three independent experiments. **f** Relative expression of indicated genes in PIBA cells transfected with *Bace1* LNA GapmeRs. **g** Relative expression of indicated genes in 3T3-L1 cells transfected with *Bace1* LNA GapmeRs. **h** Oxygen consumption rates (OCR) of PIBA cells transfected with Bace1 LNA GapmeRs (*left*). Illustration of maximal OCR at measurement 7 (arrow, *right*). The data shown are from measurements in at least 16 wells for each condition. All qPCR experiments were performed in triplicate and represent the average of at least three independent experiments. *p<0.05.

4.5 BACE1 is differentially expressed in *in vivo* models of induced and impaired thermogenesis

To investigate whether the effects seen on brown adipocyte differentiation *in vitro* reflect a role for BACE1 on BAT also *in vivo*, we analysed the expression of *Bace1* in mouse models of challenged brown fat function. We quantified the mRNA levels of *Bace1* in mice exposed to 4 °C for one or seven days, as a model for thermogenic activity, proven by a drastic increase in BAT-specific markers *Elovl3* and *Ucp1* in BAT and SCAT. Results demonstrated that upon of both BAT activation and SCAT browning, *Bace1* mRNA levels were significantly decreased (Figure 4.5 a). As a model for inactivated BAT, progeroid (*Ercc1*$^{-/-}$) and obese (HFD) mice were examined. Protein analysis revealed an increase in BACE1 protein expression in BAT of both *in vivo* models compared to their control littermates (Figure 4.5 b).
These results suggest that *Bace1* expression is associated with the activity of BAT not only *in vitro* but also *in vivo*.

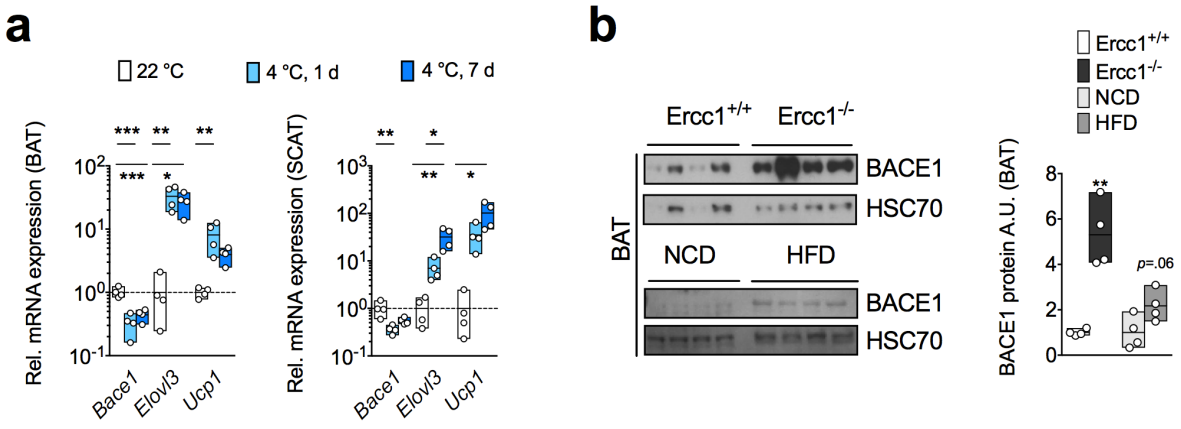

FIGURE 4.5. **BACE1 is altered in *in vivo* models of thermogenesis impairment. a** Relative expression of indicated genes in BAT and SCAT at ambient temperatures (22 °C) or under thermal stress (4 °C) for indicated time periods. Four tissue samples were used per time point/gene. **b** *left*: Immunoblot analysis of BACE1 in Ercc1$^{-/-}$ (n=4) mice versus Ercc1$^{+/+}$ (n=4) controls (*top*) or in NCD-fed (n=4) versus HFD-fed (n=4) mice (*bottom*). Image is representative of two (*top*) or three (*bottom*) independent experiments. **b** *right*: Densitometric quantification of protein levels. Relative protein levels for NCD-fed and Ercc1$^{+/+}$ control mice were set to unity=1. *p<0.05, **p<0.01, ***p<0.001.

4.6 BACE1 inhibition *in vivo* ameliorates energy homeostasis

4.6.1 Specific BACE1 inhibitor protects mice from diet-induced obesity

To support a BAT inactivating function of BACE1 *in vivo* and to investigate the therapeutic applicability of a BACE1 treatment, we decided to study the effects of BACE1 inhibition in obese mice with defective BAT functionality.
As described in 1.2.4, BACE1 inhibitors have been widely studied and tested in both mice and humans given the central role of the protease in AD development. For our *in vivo* studies we utilised the BACE1 inhibitor RO5508887, a small molecule generated by Roche [43], which is able to suppress BACE1 activity of more than 85% in rodent models and which has already been tested for potential toxicity.
We compared mice fed a HFD for 15 weeks (starting at 4 weeks of age) with mice that after 3 weeks of HFD were fed with HFD+RO5508887. Interestingly, after only one week mice fed with BACE1 inhibitor already gained less body weight than control mice (Figure 4.6 a) and maintained a lower body weight throughout the experiment despite no observed differences in food intake (Figure 4.6 b).
These data indicate that inhibition of BACE1 *in vivo* protects from diet-induced obesity without reducing energy intake.

4.6.2 BACE1 inhibition enhances glucose metabolism in obese mice

We next questioned whether the protection from diet-induced obesity upon BACE1 inhibition was linked to improved glucose homeostasis. Indeed, the decrease in body weight gain in mice receiving RO550887-supplemented HFD was associated with an ameliorated regulation of glucose metabolism as shown by glucose and insulin tolerance tests (GTT and ITT in Figure 4.6 c and d respectively).
Given the high sequence homology of BACE1 and the protease BACE2 (~75% homologous, 45% identical) [186][187] and considering that BACE2 was shown to affect glucose metabolism *in vivo* through increased insulin secretory capacity and pancreatic β-cell mass [188], we investigated whether inhibition of BACE1 in our *in vivo* model affects in-

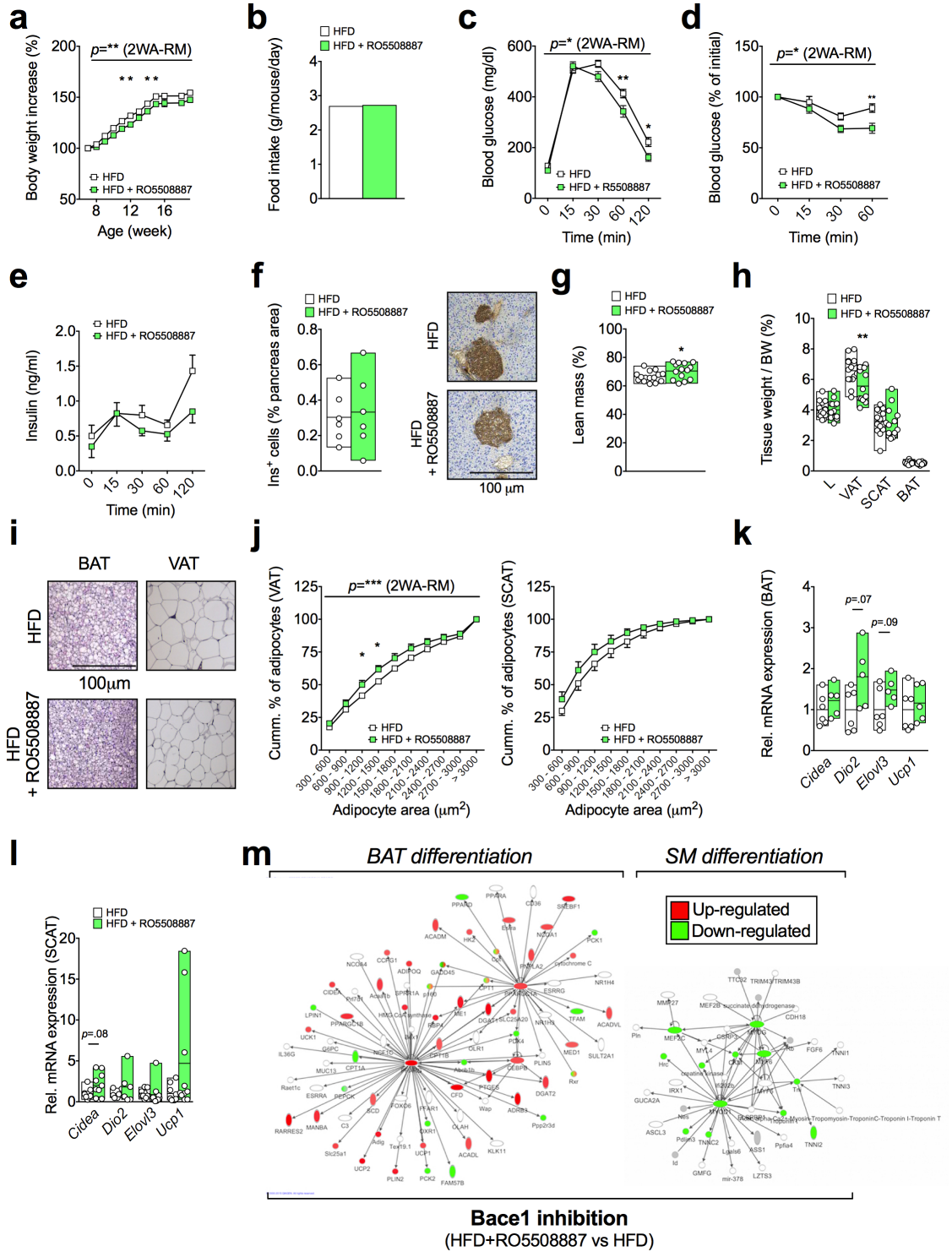

FIGURE 4.6. **BACE1 inhibition *in vivo* regulates glucose homeostasis.**
a Relative body weight gains in HFD-fed (n=15) versus HFD+RO550887-fed (n=15) male

C57BL/6 mice. **b** Average food intake quantified by manual recordings of HFD-fed (n=15) and HFD+RO550887-fed (n=15) mice during the course of the feeding experiment (12 weeks). **c** Glucose tolerance tests in HFD-fed (n=15) versus HFD+RO550887-fed (n=15) male C57BL/6 mice. **d** Insulin tolerance tests in HFD-fed (n=15) versus HFD+RO550887-fed (n=15) male C57BL/6 mice. **e** Glucose-stimulated insulin secretion of HFD-fed (n=7) versus HFD+RO550887-fed (n=7) mice. **f** Percentage of insulin-positive (ins+) cells in pancreatic sections from HFD-fed (n=6) and HFD+RO550887-fed (n=6) mice (*left*). Insulin staining and H&E counterstaining of pancreatic islets in HFD and HFD+RO550887-fed mice (*right*). A representative image is shown. **g** Body composition measured by nuclear magnetic resonance of HFD-fed control (n=15) versus HFD+RO550887-fed (n=14) male C57BL/6 mice. **h** Tissue weight/body weight (BW) ratio of indicated tissues in HFD-fed (n=15) versus HFD+RO550887-fed (n=14) male C57BL/6 mice. **i** Photomicrograph of BAT and VAT in HFD-fed and HFD+RO550887-fed male C57BL/6 mice. A representative image is shown. **j** H&E staining of VAT and SCAT sections from HFD-fed (n=5) and HFD+RO550887-fed (n=5) mice analyzed using Zeiss Axiovision 4.2 software and adipocyte area cummulatively plotted in 10 increments. **k** Relative expression of indicated genes in BAT of HFD (n=6) versus HFD+RO550887-fed (n=5) male C57BL/6 mice. **l** Relative expression of indicated genes in SCAT of HFD (n=9) versus HFD+RO550887-fed (n=10) male C57BL/6 mice. **m** Network illustration of changes in IPA pathways in HFD-fed (n=3) versus HFD+RO550887-treated (n=3) male C57BL/6 mice. *p<0.05, **p<0.01, ***p<0.001.

sulin regulation in a comparable manner as BACE2. However, we observed no differences in glucose-stimulated insulin secretion (Figure 4.6 e) or pancreatic islet morphology (Figure 4.6 f) between the two groups. Moreover, the improved insulin sensitivity upon BACE1 inhibition (Figure 4.6 d) does not hold true for Bace2$^{\Delta/\Delta}$ mice.
These findings lead to the conclusion that RO550887-mediated BACE1 inhibition improves glucose homeostasis in a BACE2-independent manner.

4.6.3 BACE1 regulates body fat composition

Having proven a beneficial effect of BACE1 inhibition on whole body metabolism, we assessed whether this phenotype may specifically be attributed to adipose tissue depots. Interestingly, RO5508887-feeding lead to an increase in lean mass (Figure 4.6 g) and a significant decrease of epididymal visceral adipose tissue weight (Figure 4.6 h). In order to analyse lipid distribution in fat depots, visual and automatic analysis of adipocyte size, for brown and white adipose tissue respectively, was performed (Figure 4.6 i and j). Immunohistochemical analyses revealed a decrease in lipid droplet size in BAT and VAT of RO5508887-treated mice compared to control littermates.
We could hereby show that suppression of BACE1 activity leads to smaller lipid burden in both thermogenically active and inactive adipose tissue.

4.6.4 RO5508887-treated mice show increased expression of BAT markers

Given the reduced energy storage at unaltered food intake rates, we addressed whether RO5508887-fed mice may show increased energy expenditure in form of thermogenesis. We therefore analysed brown fat marker expression in BAT and SCAT of obese BACE1 deficient mice. qPCR results revealed that *in vivo* BACE1 inhibition increased expression of those markers in the aforementioned tissues (Figure 4.6 k and l). Ingenuity pathway analyses on RNA sequencing data of BAT upon RO5508887 treatment not only confirmed a global up-regulation of transcriptional networks associated with BAT differentiation, but also revealed a down-regulation of skeletal muscle differentiation pathways (Figure 4.6 m).
These results support the idea that improvements in adiposity and glucose homeostasis due to BACE1 inhibition are related to an increased BAT activity.

4.7 Generation of stable *Bace1* knock-out C2C12 myoblasts

Our *in vitro* and *in vivo* results on BACE1 modus operandi suggest, that BACE1 regulates metabolism via tuning the switch between brown adipose tissue (activation) and skeletal muscle (inhibition). We thus decided to generate stable *Bace1* knock-out in C2C12 myoblasts to asses if *Bace1* deletion - rather than a mere knock-down - has an even more pronounced effect on the myogenic and adipogenic potential of these cells. Many *Bace1* knock-out mouse models have been generated during the years using different targeting strategies. The first BACE1 *in vivo* studies in 2001 used three main strategies: deletion of a 2 kb section of *Bace1* containing exon 1 [30], deletion of exon 4-8 that removes one of the two aspartate residues at the protease's active site [189] or deletion of exon 2 resulting in a shift of the open reading frame, hereby generating a STOP codon in exon 3 [32] (Figure 4.7 a). Considering that large genomic deletions can be problematic to obtain, we estimated the latter strategy to be the most promising for a successful knock-out, due to the small size of exon 2 (89 bp).

4.7.1 Generation of a knock-out cell line using CRISPR/Cas9 technology

The CRISPR/Cas9 system derives from the immune system of from *Streptococcus pyogenes* where it confers the bacteria the ability to recognise and degrade DNA from invading viruses. The system was first re-engineered by the group of Prof. Emmanuelle Charpentier by fusing the bacterial CRISPR RNA (crRNA) and trans-activating CRISPR RNA (tracrRNA) into a single-guide RNA (gRNA), which then directs a Cas9 endonuclease to introduce site-specific double-strand breaks in target DNA [190]. Given the simplicity and versatility of this system, many different methodologies and vector designs were generated in recent years (reviewed in [191]). For our purpose we decided to use a modified version of the pX330 CRISPR/Cas9 plasmid [174] containing two gRNAs and carrying a GFP-puromycin selection cassette [175] (Figure 4.7 b). The two gRNAs were designed to flank exon 2 of *Bace1* and positively transfected cells were identified via GFP and puromycin selection. C2C12 cells that survived puromycin selection were diluted to a ratio of 1 cell/well in a 96-well plate to obtain monoclonal cultures.

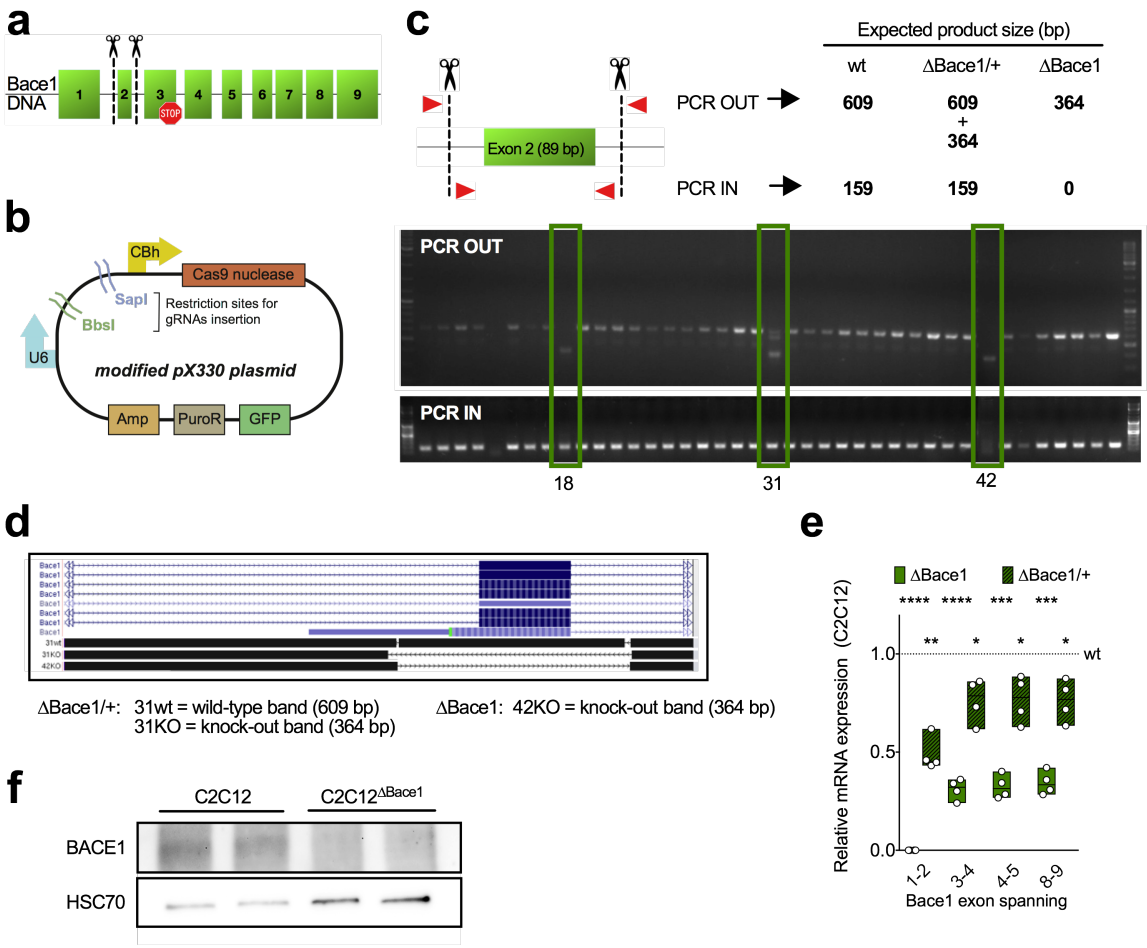

FIGURE 4.7. **Generation of a stable *Bace1* knock-out in C2C12 myoblasts.**
a Genomic sequences diagram of *Bace1*. *Bace1* exons are depicted as green boxes. Scissors indicate targeted knock-out cleaving sites, STOP sign indicates stop codon generated by frameshift due to exon 2 knock-out. **b** Schematic representation of modified pX330 CRISPR/Cas9 plasmid (Amp, ampicillin resistance cassette; CBh, chicken β-actin (CBA) promoter; GFP, green fluorescent protein; PuroR, puromycin resistance cassette; U6, U6 promoter). **c** Schematic representation of PCR-based screening method indicating expected DNA products (*top*). DNA products for PCR OUT and PCR IN (described above) detected by gel electrophoresis (*bottom*). **d** DNA sequencing results of indicated DNA products visualised in the UCSC Genome Browser (genome.ucsc.edu). **e** Relative expression of indicated exon spanning *Bace1* probes in C2C12$^{\Delta Bace1}$ cells. Experiments were performed in triplicate and represent the average of three independent experiments. **f** Immunoblot analysis of BACE1 in C2C12$^{\Delta Bace1}$ cells. Image is representative of two independent experiments. *p<0.05, **p<0.01, ***p<0.001, ****p<0.0001.

4.7.2 Validation of *Bace1* knock-out

PCR analysis

For evaluation of correct *Bace1* exon 2 deletion in selected C2C12 cell clones, we utilised a PCR-based screening method (summarised in Figure 4.7 c). For this we performed PCR analyses on DNA of putatively positive cells using two different sets of primers. The first set (PCR OUT) amplifies DNA outside the gRNAs-targeted region, giving rise to a bigger DNA product (609 bp) in case of unsuccessful *Bace1* exon 2 deletion, and a smaller one (364 bp) in case of effective exon 2 knock-out. Heterozygous cells would show both DNA products. The second set (PCR IN) is internal to the gRNAs-targeted region and a band of 159 bp would be detected on the agarose gel only for wild-type or heterozygous cell clones. Figure 4.7 c shows the PCR results obtained for both PCR OUT and PCR IN in 40 C2C12 cell clones. Some samples presented no bands in neither PCR, probably due to insufficient amounts of DNA obtained from these clones. One of the samples showed only the knock-out band in the PCR OUT, but a product was still detected in the PCR IN (18 in Figure 4.7 c). Surprisingly, all putatively heterozygous samples (31 is shown as an example in Figure 4.7 c) showed an additional third band just below the expected wild-type band. Only one cell clone (42) unequivocally showed the pattern expected from a complete knock-out of *Bace1* exon 2.

DNA sequencing analysis

PCR products from PCR OUT were extracted from the agarose gel and analysed by DNA sequencing (2.10). The sequencing was performed on each sample showing a KO band (Figure 4.7 c). In case of putative heterozygosity both wild-type bands were also analysed. DNA sequencing of selected cell clones revealed one homozygous and one heterozygous knock-out of *Bace1* exon 2 (42 and 31 respectively in Figure 4.7 d). The two distinct wild-type bands of the heterozygous samples were sequence-wise identical, but showed micro-indels around gRNAs binding sites (data not shown). Since this region is noncoding and contains no known noncoding RNAs or regulatory elements such as gene enhancers/silencers, those indels should not affect proper transcription of the *Bace1* gene. C2C12 cells obtained from clone 42 will be from now on named C2C12$^{\Delta Bace1}$, while heterozygous cells (clone 31) will be named C2C12$^{\Delta Bace1/+}$.

Messenger RNA analysis

To further validate whether deletion of *Bace1* exon 2 from one or two alleles was associated with a decrease in *Bace1* mRNA levels, we performed qPCR analysis of C2C12$^{\Delta Bace1}$

and C2C12$^{\Delta Bace1/+}$ cells. To asses if differential RNA splicing would occur upon exon 2 deletion, we used four different *Bace1* TaqMan™ probes, each targeting a different exon-exon junction (1-2, 3-4, 4-5, 8-9). Results confirmed a partial reduction of *Bace1* expression levels in C2C12$^{\Delta Bace1/+}$ cells in all tested probes (Figure 4.7 e). For C2C12$^{\Delta Bace1}$ we could detect a 100% decrease in *Bace1* mRNA only with the probe targeting exon 1 and 2, while residual splicing variants were detected for the remaining three probes (Figure 4.7 e). However, due to our *Bace1* targeting strategy (shown in Figure 4.7 a and explained in 4.7) these splicing variants should not affect the decrease in BACE1, especially considering that the mRNA levels detected for exon 3 (where the alternative STOP codon arises) are comparable with the ones of the other exons.

Protein analysis

In order to validate whether deletion of exon 2 leads to an abrogated *Bace1* translation despite the presence of alternative splicing isoforms we performed a western blot analysis of C2C12$^{\Delta Bace1}$ cells. The 70 kDa expected protein product present in C2C12 was undetectable in the knock-out cell line (Figure 4.7 f), giving final validation that a complete knock-out of BACE1 occurred in C2C12$^{\Delta Bace1}$. For further studies only the homozygous C2C12$^{\Delta Bace1}$ cell line was used.

4.8 *Bace1* knock-out in C2C12 blocks myogenesis while promoting adipogenesis

4.8.1 Myogenesis is halted in *Bace1*-null cells

Having successfully generated a *Bace1* knock-out model, we first determined the effect of *Bace1* deletion on C2C12 myogenesis. Already at confluence C2C12$^{\Delta Bace1}$ cells revealed a morphological phenotype, showing a distinctly rounder shape than the expected tapered shape of wild-type myoblasts. Knock-out cells maintained this shape throughout the entire myogenic differentiation protocol, while control C2C12 fused to form myocytes (Figure 4.8 a). This phenotype was associated with a complete down-regulation of myogenic markers like *Ckm*, *Myf6*, *Myog* and *Tnnt3* (Figure 4.8 b).
These data could confirm the anti-myogenic effect of *Bace1* deletion not only on qPCR but also on a morphological level.

4.8.2 Forced adipogenic differentiation of C2C12$^{\Delta Bace1}$ cells reveals increased adipogenic potential

As our *Bace1* knock-down experiments in PIBA cells (4.4.2) hinted towards increased adipogenesis and since confluent C2C12$^{\Delta Bace1}$ cells resembled a round, adipocyte-like phenotype, we decided to treat the myogenic C2C12$^{\Delta Bace1}$ cell line with a pro-adipogenic cocktail as described by Seale *et al.* [70]. Forced adipogenic differentiation of *Bace1* knock-out cells, but not wild-type controls, promoted lipid droplet formation and an adipocyte-like mRNA expression profile for adipogenic markers like adiponectin (*Adipoq*), fatty-acid binding protein 4 (*Fabp4*) and specific brown fat markers like cell death-inducing DNA fragmentation factor, alpha subunit-like effector A (*Cidea*), *Elovl3* and *Ucp1* (Figure 4.8 c). Upon prolonged exposition to the adipogenic cocktail, C2C12$^{\Delta Bace1}$ cells showed an even higher amount of lipid-laden adipocyte-like cells (Figure 4.8 d). Interestingly, only BAT-specific genes as *Cidea*, type II iodothyronine deiodinase (*Dio2*), *Elovl3* and *Ucp1*, but not pan-adipogenic genes, increased their expression compared to the shorter adipogenic procedure (Figure 4.8 e). Both adipogenic differentiation treatments showed a down-regulation of muscle markers like *Myf5* and *Pax3* in knock-out cells compared to wild-type C2C12 (Figure 4.8 d and e).
We could hereby show that to the detriment of myogenic potential, C2C12$^{\Delta Bace1}$ myoblasts could be forced into a specifically brown adipogenic expression profile and morphology.

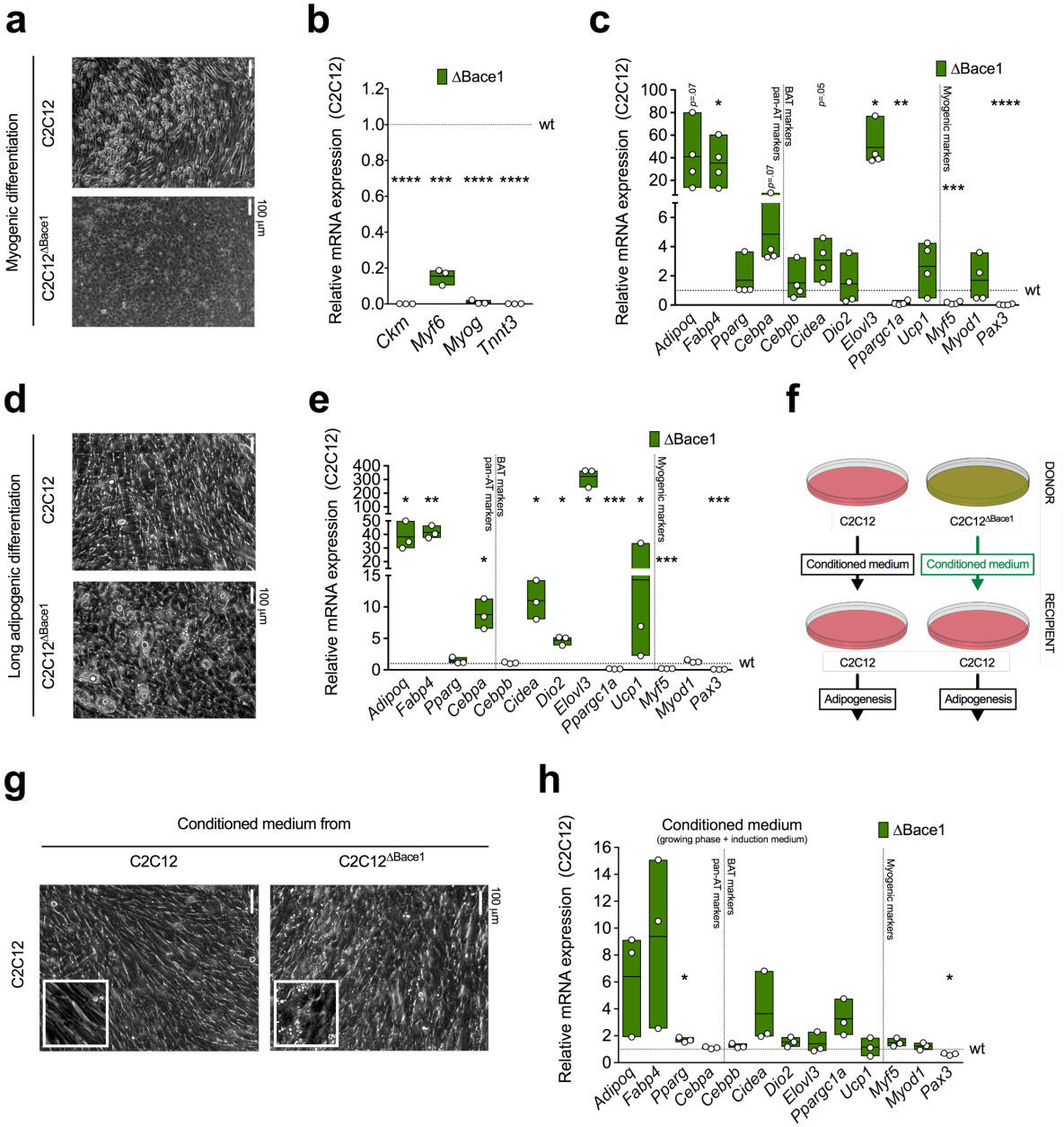

FIGURE 4.8. ***Bace1* knock-out in C2C12 blocks myogenesis while promoting adipogenesis.**

a Photomicrograph of C2C12 and C2C12$^{\Delta Bace1}$ cells after myogenic differentiation. Image is representative of three independent experiments. **b** Relative expression of indicated genes in C2C12 and C2C12$^{\Delta Bace1}$ cells after myogenic differentiation. **c** Relative expression of indicated genes in C2C12 and C2C12$^{\Delta Bace1}$ cells after adipogenic differentiation. **d** Photomicrograph of C2C12 and C2C12$^{\Delta Bace1}$ cells after long adipogenic differentiation. Image is representative of three independent experiments. **e** Relative expression of indicated genes in C2C12 and C2C12$^{\Delta Bace1}$ cells after long adipogenic differentiation. **f** Schematic

representation of conditioned media experiment (details in 2.7.6.4). **g** Photomicrograph of C2C12 and C2C12$^{\Delta Bace1}$ cells after adipogenic differentiation in conditioned medium. Image is representative of three independent experiments. **h** Relative expression of indicated genes in C2C12 and C2C12$^{\Delta Bace1}$ cells after adipogenic differentiation in conditioned medium. All experiments were performed in triplicate and represent the average of three independent experiments. *p<0.05, **p<0.01, ***p<0.001, ****p<0.0001.

4.8.3 C2C12$^{\Delta Bace1}$ conditioned medium promotes adipogenic differentiation of wild-type C2C12

As described in 1.2.2 the main enzymatic activity of BACE1 consists in the cleavage of transmembrane proteins. We thus hypothesised that the pro-adipogenic phenotype shown by C2C12$^{\Delta Bace1}$ cells could occur due to the lack of peptides in the medium, which physiologically would be cleaved by BACE1. Wild-type C2C12 cells were therefore given conditioned medium from either knock-out or wild-type cells during the initial phase of forced adipogenic differentiation (Figure 4.8 f, details in 2.7.6.4). To avoid a bias due to potentially alternating nutrient consumption rates by donor cells, we supplemented the conditioned medium with fresh nutrients prior to administration to wild-type C2C12. Although cells in both treatment conditions showed a tapered shape, the ones exposed to C2C12$^{\Delta Bace1}$ conditioned medium presented widespread lipid droplet formation (Figure 4.8 g). This phenotype was supported by an increased expression of adipose tissue-specific genes like *Adipoq*, *Fabp4*, *Pparg*, *Cidea* and peroxisome proliferative activated receptor, gamma, coactivator 1 alpha (*Ppargc1a*) (Figure 4.8 h).
Taken together, our results show that the C2C12$^{\Delta Bace1}$ secretome lacks un-identified BACE1-cleaved peptides, allowing the secretome to support (brown) adipogenesis.

4.9 Proteomic analysis of C2C12$^{\Delta Bace1}$ reveals potential BACE1 targets

We could show that the BACE1 sheddome in C2C12, consisting in the totality of protein peptides cleaved by the sheddase BACE1, affects the adipogenic potential of the myogenic cell line (4.8.3). We hence approached identification of proteins targeted by BACE1 enzymatic activity, which could account for this phenotype.
Since the discovery of the therapeutical potential of BACE1 inhibition in counteracting AD, many efforts have been undertaken to discover BACE1 targets aside APP in order to evaluate potential side effects of a BACE1-based therapy. While most studies on BACE1 target identification focussed on the nervous system [192][180] and few others on selected peripheral tissues [193][194], no studies have been performed on BACE1 cleaving targets in muscle or adipose tissue. To identify BACE1-cleaved peptides in these latter tissues, we utilised our C2C12$^{\Delta Bace1}$ model for a complementary proteomic approach: first ascertain enriched proteins on the cell surface of *Bace1* knock-out cells and then determine the lack of cleaved peptides in the medium of the same cell line.

4.9.1 *Bace1* knock-out exhibits accumulation of cell surface proteins from the PI3K/AKT-FGFR-EGFR signalling pathway

For the identification of cell surface proteins potentially targeted by BACE1, we used the cell surface capturing (CSC) technology [196]. This technology exploits the fact that most cell surface proteins are predicted to be glycosylated and covalently labels a chemical tag to these extracellular glycan moieties on living cells (Figure 4.9 a).
Relative quantitative comparison of the detected cell surface glycoproteins of C2C12$^{\Delta Bace1}$ and wild-type C2C12 revealed 79 differentially expressed proteins (Figure 4.9 b). Since the lack of BACE1 from C2C12 cells could allow detection of surface proteins otherwise cleaved by the β-scretase in wild-type cells, we focussed exclusively on the significantly up-regulated proteins in knock-out cells (45). The protein with the highest positive fold change was the pro-inflammatory amine oxidase, copper containing 3 (AOC3). However, over-representation and protein enrichment analysis performed on the up-regulated proteins using a publicly available online tool (consensuspathdb.org) depicted among the most affected the PI3K/AKT, FGFR and EGFR signalling pathway, including proteins like epidermal growth factor receptor (EGFR), beta-type platelet-derived growth factor

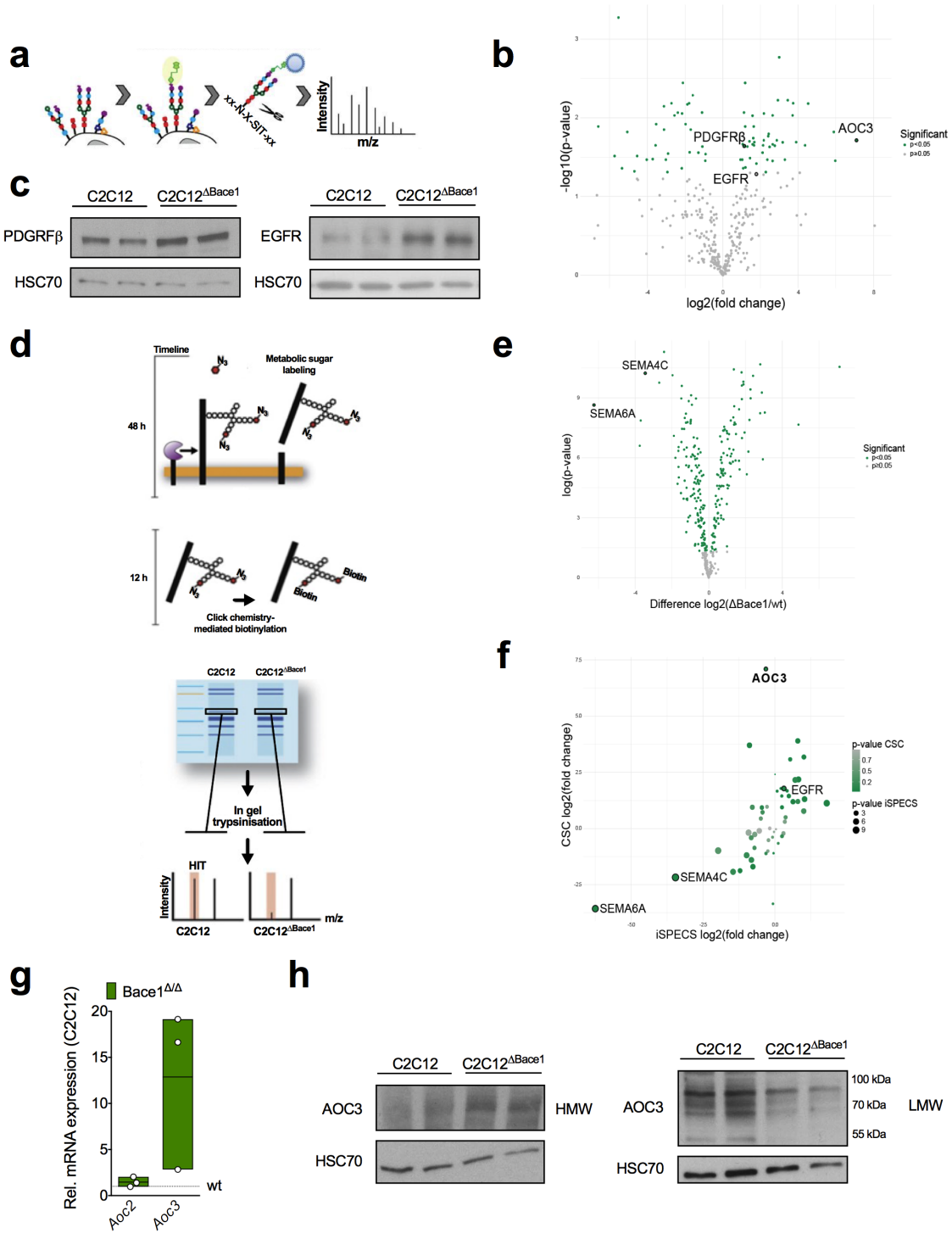

FIGURE 4.9. **Proteomic analysis of C2C12$^{\Delta Bace1}$ reveals potential BACE1 targets.** **a** Schematic representation of CSC method (adapted from [195]). **b** Volcano plot of C2C12

versus C2C12$^{\Delta Bace1}$ CSC results. Significant differentially expressed protein are represented in green. **c** Immunoblot analysis of indicated proteins in C2C12 and C2C12$^{\Delta Bace1}$ cells. Image is representative of two (EGFR) or three (PDGFRβ) independent experiments. **d** Schematic representation of iSPECS method (adapted from [180]). **e** Volcano plot of C2C12 versus C2C12$^{\Delta Bace1}$ iSPECS results. Significant differentially expressed protein are represented in green. **f** Bubble plot of results merged from differentially expressed proteins in CSC and iSPECS. Significance of CSC results is indicated by colour and significance of iSPECS results is indicated by size. **g** Relative expression of indicated genes in C2C12 and C2C12$^{\Delta Bace1}$ cells. **h** Immunoblot analysis of AOC3 in C2C12 and C2C12$^{\Delta Bace1}$ cells. Image is representative of three independent experiments. HMW, high molecular weight; LMW, low molecular weight.

receptor (PDGFRβ), kit ligand (KITLG) and members of the FGFR family (fibroblast growth factor receptors). The whole list of CSC-detected proteins in this pathway are listed in Table 6.1 (Appendix). Western blot validation of EGFR and PDGFRβ confirmed an up-regulation of these membrane proteins in C2C12$^{\Delta Bace1}$ cells (Figure 4.9 c).

4.9.2 Conditioned medium proteomic analysis reveals known and putative BACE1 targets

Having identified various proteins enriched on the cell surface of *Bace1* knock-out cells, we hypothesized that as true targets of BACE1 cleaving, peptides of those proteins should in turn be less detected in the cell supernatant.

Investigation of the sheddome of BACE1 via mass-spectrometry of cell medium encounters three main limitations [197]. First, secreted proteins can have very low concentrations in the media. Second, physiological media include supplements such as fetal calf serum containing albumin and other serum proteins at concentrations that could interfere with the mass-spec analysis. Third, secretome proteins can be masked by highly abundant cytosolic proteins released from broken or apoptotic cells. To circumvent these limitations and allow proteome-wide identification of shedding substrates and secreted proteins, we utilised the secretome protein enrichment with click sugars (SPECS) technique for the study of C2C12$^{\Delta Bace1}$ secretome (Figure 4.9 d). This technique was first developed by the laboratory of Prof. Stefan Lichtenthaler [180] and further improved [181]. For our study we utilised a further improved SPECS method (iSPECS) in collaboration with Prof. Stefan Lichtenthaler.

Results showed a total of 272 peptides at differential concentrations among the two analysed media (Figure 4.9 e), of which 155 were down-regulated upon knock-out of *Bace1* in C2C12. Some of these potential BACE1 substrates have also been found in other BACE1 sheddome analyses, such as members of the semaphorine family SEMA4C and SEMA6A [192].

4.9.3 AOC3 is a potential target of BACE1 and could trigger endocrine regulation of metabolism

To integrate our two proteomic approaches we selected significantly regulated peptides of both CSC and iSPECS analysis (Figure 4.9 f). Among proteins up-regulated on the surface of C2C12$^{\Delta Bace1}$ cells and down-regulated in the medium of the same cell line, we found AOC3, an amine oxidase with proinflammatory functions [198][199]. Interestingly, AOC3 (also known as VAP-1) exhibits a soluble form (soluble AOC3 or sVAP1) cleaved by metalloproteases [200], which can be found in serum, where concentrations are augmented in AD [201][202], diabetes and obesity [203][204]. Moreover, both the membrane-bound and soluble form of AOC3 have been reported to be expressed in murine and human adipocytes [200].
Notably, both AOC3 peptide sequences detected by iSPECS are shared by AOC3 and its homologous amine oxidase, copper containing 2 (AOC2), while another detected sequence was unique for AOC2. Unfortunately, due to the automatised procedure utilised for the standardisation, it was not possible to obtain standardised results for the single peptides. We therefore analysed the mRNA expression of the two amine oxidases in our cell model. While *Aoc2* expression was unaltered, *Aoc3* mRNA was surprisingly increased in C2C12$^{\Delta Bace1}$ cells (Figure 4.9 g), even correlating with an increase of the high molecular weight isoform of AOC3 protein (HMW in Figure 4.9 h). However, smaller isoforms of the protein, potentially cleaved by BACE1, were - in accordance with the iSPECS results - decreased in C2C12$^{\Delta Bace1}$ (LMW in Figure 4.9 h)

In conclusion we could show that throughput proteomic analysis of *Bace1* depleted surfaceome and medium identified AOC3 as putative novel target of the protease in peripheral tissues, with the potential of pursuing an endocrine regulation of metabolism and - perhaps - Alzheimer's disease.

CHAPTER 5

DISCUSSION

Obesity has become a major burden in modern society, with nowadays more than twice as many people affected as in 1980 [1]. The increased fat deposition and impaired glucose metabolism associated with obesity lead to a greater risk for co-morbidities, such as type 2 diabetes and dementia, in particular Alzheimer's disease [3] [4] [5].
To counteract the obesity pandemic and its sequelae, brown adipose tissue activation has been proposed as promising therapeutic target. Thanks to its thermogenic activity due to high enrichment of UCP1, BAT can significantly increase energy expenditure with beneficial effects on whole body metabolism. Despite previously considered to be present only in rodents and human newborns, this tissue has been recently detected as functional in adult humans as well. Similar thermogenic activity was also found in adipocytes within WAT, which were henceforth defined as beige or brite. Beige adipocytes are mainly located within murine subcutaneous and human visceral fat depots [205], which both arise from a white adipogenic lineage, contrarily to BAT which shares a precursor lineage with SM.
The activation of thermogenic potential has been shown to be also dependent on various noncoding RNAs, with lncRNAs [206] and especially miRNAs [154] being able to regulate brown adipogenesis, browning of white adipocytes and transdifferentiation between myocytes and brown adipocytes.

5.1 *MiR-328* regulation of BAT partially determines *Dicer1* knock-out *in vivo* phenotype

MicroRNAs are short noncoding RNAs able to block gene expression via targeting sequence-specific mRNAs. MiRNAs are generated in the nucleus and undergo two cleaving steps and exportation to the cytoplasm. DICER1 is one of the two ribonucleases III involved in miRNA biogenesis and is responsible for the final cleavage that leads to mature miRNA generation (1.5).

Control of miRNA expression by DICER1 was shown to have an important role in the regulation of AT homeostasis, with results from our group and others [151] indicating that a deficiency of *Dicer1* in pan- (AdicerKO mice) or brown adipose tissue (*Dicer1*$^{\Delta BAT/+}$) leads to a deteriorated glucose metabolism. AdicerKO mice exposed to HFD exhibit abnormal fat accumulation with an overall decrease in body weight and reduced WAT mass, while BAT mass is increased due to whitening of this tissue [151]. Our *Dicer1*$^{\Delta BAT/+}$ mouse model on the other hand shows no difference in body weight and a mere female-confined increase in fat mass [170]. These differences can be explained by discrepancies in the tissue distribution of *Dicer1* deficiency between the two mouse models: AdicerKO mice express Cre recombinase under control of the more abundant *Adiponectin* promotor which leads to a decrease in *Dicer1* expression by 60-80% in all adipose depots (SCAT, VAT, BAT) [151]. Au contraire *Dicer1*$^{\Delta BAT/+}$ mice express Cre recombinase under control of the BAT-specific *Ucp1* promotor, generating a 25% decrease in the ribonuclease expression exclusively in BAT. Notably, this mouse model exhibits a concomitant increase in *Dicer1* expression in WAT, possibly due to compensatory mechanisms [170]. Despite these differences, both mouse lines manifest a defective glucose homeostasis, suggesting that glucose intolerance and insulin desensitisation in these mice is dependent on the effects of *Dicer1* down-regulation specifically in BAT. The impairment of glucose metabolism observed in *Dicer1*$^{\Delta BAT/+}$ mice however, did not alter the blood levels of neither insulin nor leptin and was also not associated with any kind of adipose tissue redistribution (4.1.1), which is a characteristic of AdicerKO mice [151]. Moreover, *Dicer1*$^{\Delta BAT/+}$ mice exhibited no differences in BAT mass compared to controls, in line with observations made by Mudhasani *et al.* in aP2-Cre *Dicer1* knock-out mice [149].

To determine whether the *Dicer1* knock-out phenotype may be attributed to specific miRNAs, those miRNAs enriched in BAT with a correlation to BAT activity, were investigated for their potential in regulating brown adipocyte differentiation and function. *In vitro* loss- and gain-of-function studies revealed that the AT-enriched (4.2.1) *miR-328*,

could promote adipogenesis of brown adipocytes while inhibiting the myogenic potential of both myoblasts and PIBAs (4.2.2). Since *Dicer1*$^{\Delta BAT/+}$ mice show decreased expression of *miR-328* (4.2.1), the defective brown adipogenesis upon *miR-328* knock-down could explain the reduced UCP1 expression observed in this mouse line (4.1.1). Moreover, as *miR-328* does not alter differentiation and adipogenic marker expression in the white adipocytes 3T3-L1, the effects of the miRNA seem to be brown lineage-specific (4.2.4). This BAT-specificity was also confirmed by experiments investigating brown adipocyte activity: Indeed, *miR-328* over-expression was proven to increase maximal respiratory capacity of PIBA cells (4.2.3), which could attribute to the decreased EE observed in *Dicer1*$^{\Delta BAT/+}$ mice [170].
However, *miR-328* alone is not likely to explain the entire metabolic phenotype observed in *Dicer1*$^{\Delta BAT/+}$ mice considering the wide regulatory network of miRNAs, with these noncoding RNAs being able to regulate multiple gene targets and single genes being inhibited by multiple miRNAs [135]. Among the miRNAs that could have an additive effect on the *Dicer1*$^{\Delta BAT/+}$ phenotype, there are *miR-193b*, included as a positive control in our *in vitro* experiments (3, 4.2), and *miR-365*. These belong to the same miRNA cluster and were shown *in vitro* to regulate brown adipogenesis and myogenesis [168]. Analysis of their expression in our *Dicer1* knock-out model showed a defect in maturation of *miR-193b* and *miR-365* in the BAT of *Dicer1*$^{\Delta BAT/+}$ mice (4.2.1). *MiR-365* was also shown by Mori and colleagues to increase levels of *Ucp1* mRNA by 20-fold in AdicerKO pre-adipocytes, reversing the effects of *Dicer1* knock-out [151].
Taken together, *miR-328* is part of a miRNA regulatory network, possibly including the *miR-193b-miR-365*-cluster, involved in the regulation of brown adipocyte differentiation and activity, and obesity-related defects in this network function can lead to a deterioration of energy and glucose homeostasis.

5.2 *In vitro Bace1* inhibition resembles the *miR-328*-dependent pro-brown-adipogenic phenotype

Although *miR-328* is conserved in humans, its therapeutic use could imply complications due to three main reasons. First, given the broad spectrum of targets that a single miRNA can regulate, more information on the potential *miR-328* gene targets are needed. Second, given the positively correlated effects of *miR-328* on BAT function, an over-expression

approach would be needed for an enhancement in BAT activity. However, to date in the field of miRNA therapeutics, inhibition of miRNAs is the predominant approach in human studies, while an over-expression approach was limited to only one single study [207]. Third, selective and effective delivery of miRNAs into BAT are difficult to achieve with state of the art techniques and potential side effects of *miR-328* over-expression in other tissues would have to be determined. For these reasons, we set our focus onto the identification of targets of *miR-328* which may play an important role in peripheral metabolism via regulating BAT and SM activity.

Considering the inhibitory activity of miRNAs in regulating gene transcription, our findings of *miR-328* function in BAT suggest that the downstream gene targets of *miR-328*, instead of eliciting a pro-adipogenic phenotype, could in turn rather be related to SM homeostasis as seen - in a reverse way - with *miR-133* inhibition of *Prdm16* [166]. Our hypothesis is in line with the bidirectional regulation between BAT and SM due to their shared progenitor cells [208]. Gene candidates were selected based on their proposed role as myogenic regulators. In particular, we focused on those genes harbouring a potential miRNA binding site for both *miR-328* and *miR-193b*. Fulfilling these selection criteria the β-site amyloid precursor protein cleaving enzyme 1 (*Bace1*) was revealed as directly regulated by the two miRNAs (4.3.1-2). Interestingly, and in line with our hypothesis, *Bace1* knock-down was proven to regulate myogenesis and brown adipogenesis in a way that evoked *miR-328* action:

In C2C12 myoblasts reduced expression of *Bace1* or *miR-328*, inhibited or promoted differentiation, respectively. Furthermore, while the miRNA generally altered myogenic markers, the β-secretase affected exclusively late myogenic markers (4.4.1). This discrepancy could occur due to the inhibition by *miR-328* of various targets involved in muscle regulation, leading to additional early defects in myogenesis. For example, *miR-328* over-expression in the heart was shown to induce cardiac hypertrophy by targeting SERCA2a [209]. Another example is the proto-oncoprotein proviral integration site 1 (PIM-1), which in addition to its crucial role in tumorigenesis has also been implicated in vascular diseases and smooth muscle cell proliferation [210] [211]. Indeed, *miR-328*-mediated inhibition of *Pim-1* was shown to significantly reduce muscle cell proliferation through a mechanism involving the platelet-derived growth factor PDGFBB [212]. These results expand the knowledge on myogenic regulation by BACE1, whose function in this context was previously focused to its role, together with Neuregulin-1 (NRG1), in maintaining motor coordination through regulation of muscle spindle physiology [33].

Regarding brown adipogenesis, the exactly opposing effects of *Bace1* and *miR-328* as

its inhibitor appear more consistent. The inhibition of *Bace1* in PIBAs promoted brown adipocyte differentiation and lipid accumulation, which was associated with increased *Ucp1* expression (4.4.2), revealing in an opposite manner the effects observed upon *miR-328* knock-down in the same cell line (4.2.3). Moreover, both *Bace1* down-regulation and *miR-328* over-expression increased the maximal respiratory capacity of PIBA cells (4.4.2, 4.2.3), supporting a role for the *miR-328-Bace1* axis in enhancing BAT activity. Although *miR-328* has so far not been attributed any function in BAT - or even in any AT in general - BACE1 was recently suggested to play a role in brown fat homeostasis, with *Bace1* knock-out mice showing an increased expression of UCP1 in BAT [34]. Collectively, our results unveiled a novel *miR-328-Bace1* nexus that is able to prompt BAT activity *in vitro* via regulating both myogenesis and brown adipogenesis.

5.3 *In vivo* inhibition of BACE1 counteracts obesity-associated deterioration of glucose metabolism

Bace1 knock-out mice have been extensively studied since the discovery of BACE1 as the β-secretase involved in amyloid plaque formation in AD. However, only in recent years and in sparse studies this mouse model has been investigated from a metabolic point of view. Meakin and colleagues could show that mice lacking *Bace1* display decreased adiposity, higher energy expenditure and improved glucose and peripheral insulin metabolism compared to controls at 8-12 months of age [34]. These effects were observed upon both NCD and HFD feeding. Nevertheless, further studies utilising younger *Bace1*$^{-/-}$ mice could not reproduce the effects on glucose tolerance and insulin sensitivity, yet confirming the decrease in body weight and plasma insulin concentrations [213]. However, the *Bace1*$^{-/-}$ mouse model has been shown to manifest various side effects due to the numerous physiological substrates of BACE1 [17]. Our approach exploited the therapeutic potential of BACE1 in the context of obesity employing an inhibitor of BACE1 (RO5508887) which was toxicologically tested in mice for AD-related uses [43]. This approach was also based on our finding that BACE1 is over-expressed in BAT of obese mice (4.5), while previous reports showed no differences in its expression in the brain of HFD-fed mice [214]. By feeding RO5508887 mixed in the HFD to wild-type mice already exposed to diet-induced obesity for three weeks, we could assess beneficial effects of the inhibitor on obesity-dependent metabolic decline. In line with observations in the *Bace1*

knock-out mouse model, BACE1 inhibition led to a decrease in weight gain in already obese mice (4.6.1). These findings, together with our results on *Bace1* inhibition in PIBAs, hint to a role for the β-secretase in the obesity-dependent deterioration of BAT function (1.3.1.2).

BACE1 was shown to regulate glucose metabolism in muscle cells, with BACE1 inhibition in C2C12 cells leading to increased glucose uptake and oxidation, GLUT4 cell surface translocation and basal rate of oxygen consumption [35], whereas increased neuronal BACE1 was shown to be sufficient to impair systemic glucose metabolism [215]. In line with these and *Bace1*$^{-/-}$ [34] findings, BACE1 inhibition in our obese mouse model also enhanced glucose tolerance and insulin sensitivity (4.6.2), pinpointing BACE1 as a suitable target to counteract obesity-related impairment in glucose homeostasis. Our mice also showed unaltered insulin secretion upon BACE1 inhibition (4.6.2), in line with findings in *Bace1* knock-out mice [213] and in contrast to observations in *Bace2* whole body knock-out mice [188]. Although both BACE1 inhibition and *Bace1* global knock-out resulted in lower lean body mass, the protein inhibition in our mouse model led to decreased VAT mass and visceral adipocyte size (4.6.3), while *Bace1*$^{-/-}$ mice exhibit significantly increased VAT and SCAT depots [213].

The improved metabolism of BACE1-inhibited mice was associated with increased expression of brown fat-specific markers in both BAT and SCAT (4.6.4), indicating thermogenic activation as a possible mechanism to explain the enhanced glucose homeostasis. Notably, as suggested by our *in vitro* findings on adipogenic and myogenic regulation through BACE1, transcriptional networks associated with BAT differentiation were up-regulated in RO5508887-treated mice, while SM differentiation pathways were down-regulated (4.6.4).

These results point out that BACE1 inhibition *in vivo* protects from diet-induced obesity and impairment in glucose metabolism via activating thermogenesis in brown and white adipose tissue.

5.4 BACE1 sheddome regulates the switch between myogenesis and brown adipogenesis

It is known that some highly potent transcription factors such as PPARγ, C/EBPα [99] or more recently PRDM16 [70] are able to promote brown adipogenesis in SM due to the shared cell lineage of the two tissues. Since BACE1 inhibition was shown to promote brown adipogenesis to the detriment of myogenesis both *in vitro* and *in vivo*, our interest

focused on the potential ability of *Bace1* to stimulate a transdifferentiation process in myocytes/brown adipocytes, rather than focusing on single cell lineages. *Bace1* inhibition in C2C12 was already investigated by us and others [35] for its role in inhibiting myogenesis and promoting glucose uptake, but no studies have been performed so far on a *Bace1* potential to stimulate brown adipogenesis in this myogenic line. Complete knock-out of the β-secretase was therefore obtained in the C2C12 cell line (C2C12$^{\Delta Bace1}$) (4.7). This *in vitro* model was stronger than a mere inhibition of *Bace1* mRNA and could also be used for further proteomics analysis as it will be described in the next chapter (5.4).

BACE1 is known to have a role in muscle homeostasis *in vivo* with knock-out mice showing defects in the formation, maturation and maintenance of muscle spindles [33]. In line with these results, C2C12$^{\Delta Bace1}$ cells showed a block in myogenesis with an almost complete down-regulation of myogenic genes (4.8.1). Strikingly, the knock-out of *Bace1* affected the morphology of C2C12, which presented a round, adipocyte-like shape at confluence, showing a much stronger pro-adipogenic effect upon depletion of the β-secretase compared to our results using LNA inhibitors (4.4.1.

To investigate the adipogenic potential of C2C12$^{\Delta Bace1}$ cells, the cell line underwent a pro-adipogenic stimulation which was previously shown to promote an adipocyte-like phenotype in myocytes [70]. Forced adipogenic stimulation revealed that the changes in morphology of C2C12$^{\Delta Bace1}$ cells were associated with an increase in lipid droplet accumulation and up-regulation of both WAT- and BAT-related genes (4.8.2). Furthermore, prolonged adipogenic stimulation of C2C12$^{\Delta Bace1}$ cells increased the expression of brown adipocyte-specific genes even further, while the up-regulation of pan-adipogenic markers remained unchanged (4.4.2). These results suggest that *Bace1*-dependent regulation of myogenic and adipogenic transdifferentiation promotes specifically the brown lineage. For this purpose, experiments specifically targeting the thermogenic activity of C2C12$^{\Delta Bace1}$ cells would be required. However, further investigations are needed in this direction since it is not possible to unequivocally exclude a more general adipogenic role for *Bace1*. Having identified BACE1 as *in vitro* transdifferentiation effector between brown adipocytes and myocytes, it is worthy investigating, whether BACE1 may interact with other known proteins regulating cell fate decision of these two cell lines. Indeed *Pparg*, shown to be increased in C2C12$^{\Delta Bace1}$ cells, has been proposed as a repressor of *Bace1*, whose gene promoter contains a binding site for this transcription factor [216]. The up-regulation of *Pparg* upon *Bace1* knock-down could therefore establish a negative feedback loop leading to further repression of BACE1 and resulting in a subsequently

more pronounced adipocyte-like phenotype. However, whether this feedback loop holds true also for myocyte and brown adipocyte regulation remains to be elucidated.
With BACE1 being a protease of the sheddase family, its function is based on its cleaving activity on specific substrates. Although BACE1 cleavage of APP in the nervous system is the best characterised example of this sheddase's proteolytic function, different additional substrates have been discovered in the last years for BACE1 outside the brain [217]. Shedding by BACE1 in peripheral tissues could therefore generate a series of peptides able to activate brown adipogenesis through paracrine and endocrine regulation of tissues like SM, BAT end WAT. These peptides could be produced by BAT, which is a known endocrine tissue with different hormones, such as FGF21, shown to regulate thermogenesis and browning via peripheral and central signalling [65].
To investigate whether knock-out of *Bace1* affects the pool of peptides released by the cells and whether these in turn are responsible for the pro-adipogenic phenotype observed in C2C12$^{\Delta Bace1}$ cells, conditioned medium from C2C12$^{\Delta Bace1}$ and control cells was given to wild-type C2C12, which then underwent forced adipogenic differentiation. The BACE1-depleted conditioned medium was able to enhance the adipogenic potential of C2C12 myoblasts, as revealed by increased lipid accumulation and up-regulation of adipose tissue-specific genes (4.8.3), including *Pparg* which, as aforementioned, was able to promote adipogenesis in SM. The effect of C2C12$^{\Delta Bace1}$ conditioned medium hint to a potential role that BACE1 substrates could have in regulating BAT/SM shared cell fate. These results inquire about whether similar approaches could be valid in different *in vitro* models, such as various combinations of co-cultures. Further investigations are needed to study how BACE1-depleted medium from myocytes could regulate brown or white adipocytes or even neuronal populations.

5.5 Potential BACE1 substrates involved in peripheral metabolism regulation

Since the function of a protease is defined by its substrates, the identification and characterisation of novel BACE1 targets involved in adipogenic and myogenic homeostasis is fundamental to investigate their potential role in the regulation of metabolism. Although various substrates of the β-secretase have been identified, none of them were verified in adipocytes or myocytes. In light of our conditioned medium results, proteomic analysis were performed in our C2C12$^{\Delta Bace1}$ model and compared to wild-type cells. Our approach involved two distinct but complementary methods: cell surface capturing (CSC), which is

able to quantify proteins present specifically on the cell surface, and iSPECS, an improved proteomic analysis of conditioned media peptide contents (4.9). The latter is a state of the art technique which - in contrast to previous proteomic approaches [192] - is able to detect very small amount of cleaved or released proteins while avoiding interference with serum and cytosolic proteins and false positive substrate identification [181]. Both proteomic approaches showed various protein peptides significantly altered in C2C12$^{\Delta Bace1}$ cells (4.9), some of which could be directly targeted by BACE1 and could play a role in the various *in vitro* and *in vivo* phenotypes dependent on the β-secretase discussed in this thesis.

EGFR and PDGFRβ

CSC analysis of *Bace1* knock-out myoblasts revealed a total of 79 differentially expressed proteins, of which 45 were up-regulated on the surface of C2C12$^{\Delta Bace1}$ cells compared to C2C12 wild-type (4.9.1). Our focus on up-regulated proteins was based on the *in vitro* model used: depletion of *Bace1* in C2C12 should lead to lack of protein expression in the cell surface, decreasing substrate cleavage and retaining full-length proteins on the cell surface. To depict whether the proteins showed to be up-regulated by CSC belong to specific interaction networks, an online tool (consensuspathdb.org) was utilised which integrates data from 32 public resources for interactions and interactions curated from literature. Over-representation and protein enrichment analysis performed on the 45 up-regulated proteins depicted among the most affected the PI3K/AKT, FGFR and EGFR signalling pathway (Table 6.1, Appendix). The PI3K/AKT pathway was shown to be activated during VAT expansion and to regulate proliferation in VAT but not in SCAT [218]. Moreover, this pathway is a known interplayer in metabolic signalling control [219]. Both FGFR and EGFR singalling pathways have been involved in the regulation of metabolism [220] [221], with the latter playing a role in the neurometabolic signalling regulating obesity, T2D, AD, cancer and cardiorespiratory function [220]. Among the CSC-detected proteins up-regulated on the surface of C2C12$^{\Delta Bace1}$ cells and involved in this pathways, PDGFRβ and EGFR were validated as over-expressed in our cell model via WB analysis (4.9.1).

PDGFRβ is a receptor member of the PDGF family, whose downstream pathways regulate multiple cellular functions such as proliferation, migration and immediate early gene induction [222] and known to control vascular smooth muscle cell development [223]. Although little is known on whether PDGFRβ plays a role in adipocyte-myofibroblast transition, the other receptor of the PDGF family, PDGFRα, was identified in human and rodent SM as a marker of bipotent progenitors able to undergo differentiation into

adipocytes and myoblasts [224]. Furthermore, PDGFRβ up-regulation on C2C12$^{\Delta Bace1}$ cell surface could be a sign of the defective myogenic differentiation of C2C12: Indeed this receptor stimulates angiogenesis, but its expression is down-regulated as soon as vascular smooth muscle cells mature [225]. Moreover, PDGFRβ signalling in pre-adipocytes was shown to have an inhibitory effect on white adipocytes, with reduced lipids and increased undifferentiated cells, without altering brown adipogenesis [226]. This emphasizes a potential role for PDGFRβ in regulating both myogenic and adipogenic differentiation, with a differential regulation of white and brown adipocytes. However, subsequent iSPECS analysis of C2C12$^{\Delta Bace1}$ conditioned medium did not detect any peptide of PDGFRβ, making this candidate not suitable as potential BACE1 target (4.9.2).
EGFR, also known as ErbB1, is a transmembrane receptor for members of the epidermal growth factor (EGF) family of extracellular protein ligands, which was discovered many decades ago [227]. Since then, this tyrosine kinase has been thoroughly studied and has been shown to influence many cellular processes, especially tumour progression, but also wound healing and the maintenance of organ and cellular homeostasis, in particular in the cardiovascular system [228]. EGFR can be activated either directly by binding of EGF or EGF-like ligands, or it can be trans-activated by shedding of EGFR-ligands by a disintegrin and metalloproteases (ADAMs) or matrix metalloproteases (MMPs) [228]. The role for EGFR in adipose tissue is unclear, with contradictory studies showing an effect of EGFR in blocking maturation of adipocyte precursor cells into mature adipocytes [229] or in enhancing adipogenesis in differentiated adipocytes [230]. Although the expression of EGFR was increased on the surface of C2C12$^{\Delta Bace1}$ cells, as validated also by WB (4.9.1), a similar up-regulation was seen for the cleaved peptide in the cells' conditioned medium (4.9.2). This excludes the depletion of BACE1 as a regulator of EGFR cleavage and activity, marking this protein, as well as PDGFRβ, a not suitable candidate for BACE1-dependent peripheral metabolism regulation.

The sempahorines SEMA6A and SEMA4C

The two proteomic approaches utilised for this study, in particular iSPECS, revealed among the protein significantly altered in C2C12$^{\Delta Bace1}$ cells some previously proposed as BACE1 substrates. Of particular interest was the semaphorine family, some members of which were suggested in recent years to be cleaved by the β-secretase [192] [180] [181]. Semaphorines are a family of proteins that regulates key cellular functions, such as cell-cell interaction and communication, but also cell differentiation, morphology and function, mainly via interaction with the plexin transmembrane receptors [231].

Semaphorines are divided into 5 classes, all presenting a sema domain, yet harbouring different functions and ways of action. Class 3 semaphorines are soluble, classes 4-6 are transmembrane and SEMA7A is a GPI-anchored protein [231]. In our study iSPECS analysis revealed peptides from SEMA6A and SEMA4C to be the first and fourth most down-regulated ones respectively in the medium of C2C12$^{\Delta Bace1}$ cells (4.9.2).
SEMA6A deficiency in rodents was associated with various axonal guidance and neuronal migration defects [232] [233] and it was also shown to promote angiogenesis through regulation of endothelial cell survival and VEGF signalling [234]. In the context of adipose tissue, SEMA6A was proposed to regulate innervation of BAT through a mechanism involving expression of PlexinA4 - of the plexin family - in BAT-associated macrophages [235].
Of greater interest for our study was SEMA4C, a class 4 semaphorine that can be proteolytically cleaved to generate a soluble form [231]. Beyond its role in nervous system and angiogenesis regulation shared with other semaphorines, SEMA4C was shown to be important during myogenic differentiation [236] [237]. Using C2C12 and an *in vivo* model for muscle regeneration, Ko and colleagues could show an up-regulation of the semaphorine during *in vitro* differentiation and *in vivo* SM regeneration [236]. Moreover, RNAi depletion of Sema4c in C2C12 resulted in the inhibition of myotube formation and decreased expression of myogenic markers [236]. Further studies, testing both gain- and loss-of-function of Sema4c in C2C12, supported the previous findings and proposed the p38 MAPK pathway as responsible for SEMA4C enhancement of terminal myogenic differentiation [237]. Interestingly Sema4c was also found to be over-expressed in the brain of AD patients [238].
Although both semaphorines, but especially SEMA4C, could be interesting candidates for BACE1-dependent regulation of myocytes/adipocytes transition, CSC analysis showed the two proteins as being down-regulated also on the surface of C2C12$^{\Delta Bace1}$ cells (4.9.1). The decreased expression of SEMA4C and SEMA6A in both the surface and the conditioned medium of *Bace1* knock-out C2C12 could nonetheless be interpreted taking in consideration the intracellular activity of BACE1. Indeed, considering that the β-secretase activity is optimal in acidic environments, BACE1 is also present within the cell in endosomes and the trans-Golgi network [17]. Thus, the results of CSC and iSPECS analysis could be explained by intracellular cleavage of SEMA4C and SEMA6A by BACE1. However, further investigations including WB validation of the two semaphorines and cellular localisation analysis are needed to test this hypothesis.

The amine oxidase AOC3

The most promising candidate resulting from our proteomic analysis is certainly AOC3, which was shown to be highly up-regulated on the surface of C2C12$^{\Delta Bace1}$ cells, while being down-regulated in the same cells' conditioned medium (4.9.1-2). Other than for its role as a semicarbazide-sensitive amine oxidase (SSAO), AOC3 has been shown to regulate many cellular processes and has been proposed as therapeutic target for various diseases, including inflammatory diseases, T2D, atherosclerosis, neurodegenerative diseases, obesity, hypertension and cancer [239]. Its pro-inflammatory activity was demonstrated in liver where it promotes leukocyte recruitment and migration [199]. AOC3 was also shown to regulate glucose metabolism and a positive correlation was found between serum AOC3 levels and BMI and body weight in T2D patients [203]. Involvement in glucose regulation was demonstrated in the adipose tissue of rats, where AOC3 activity highly stimulated glucose transport via recruitment of GLUT4 to the plasma membrane of adipocytes [240]. Moreover, increased glucose transport was also found in GLUT4 vesicles from adipocytes and rat SM [240] and in human adipocytes [241]. Most of AOC3 functions throughout the body are carried out by its soluble form sAOC3, also known as sVAP1, which can be released into the bloodstream [239]. The main source of sAOC3 seem to be adipocytes or vascular endothelial cells [239]. The expression of this soluble form was also associated with AD, with sAOC3 being increased in the plasma of AD patients [201] [202]. Soluble AOC3 is generated via cleaving of the transmembrane full protein in a process that involves ADAM metalloproteases [200]. Indeed, Abella and colleagues could show decreased secretion of sAOC3 upon utilisation of batimastat, a matrix metalloprotease inhibitor. Interestingly, batimastat is also an inhibitor of BACE1 and was shown to reduce BACE1-dependent cleavage of APP [35]. These findings support the idea that the β-secretase could regulate the release of sAOC3 in BAT and SM, as also suggested by our results showing an increase in low molecular isoforms of AOC3 - possibly sAOC3 - in C2C12$^{\Delta Bace1}$ cells, despite increased expression of both protein and mRNA of the full length AOC3 (4.9.3). However further studies are needed to validate our hypothesis, in particularly regarding the possibility for BACE1 to cleave the amino oxidase. The terminal amine isotopic labelling of substrates (TAILS) technique could be utilised to determine the putative cleavage site for BACE1 [242].
Therefore, AOC3 could regulate inflammation and glucose metabolism via BACE1-dependent release of its soluble form in the blood. Moreover, considering that chronic inflammation, impairment in glucose homeostasis and energy metabolism are conditions associated with obesity, T2D and AD [22], a paracrine or endocrine role for AOC3 in the

regulation of these diseases cannot be excluded.

5.6 Perspectives

in vitro and *in vivo* inhibition of BACE1 showed beneficial effects on obesity-related deterioration of glucose and energy homeostasis, possibly due to enhanced differentiation and activation of BAT to the detriment of myogenesis. However, our *in vivo* results rely on a global effect of the protease, not allowing insights into specific tissue regulation. To investigate the *in vivo* relevance of the β-secretase in the regulation of BAT and SM homeostasis, conditional mouse models for *Bace1* gain- and loss-of-function need to be generated.

For the generation of a *Bace1* over-expressing mouse line, the Rosa26 knock-in plasmid [243] was utilised. This vector, which allows over-expression of target genes in a Cre-dependent manner, was generated in-house via cloning of the murine Bace1 cDNA (Bace1-LSL, Figure 6.1 a, Appendix). Validation of Bace1-LSL transfection in ES cells was performed via SB (Figure 6.1 b) and one of the positive clones was injected in the pro-nucleus of a fertilised egg. Unfortunately, the generated transgenic mice did not show high levels of chimerism and none of them transmitted the genetic modification to their progeny. For this reason, further pro-nuclear injections are needed to generate Bace1-LSL mice.

For the generation of a conditional knock-out of *Bace1*, a commercially available plasmid containing a promoter-driven cassette where exon 2 of the *Bace1* gene is flanked by two loxP sites (Bace1-flox) was utilised (Figure 6.1 c). The Bace1-flox vector generates a Cre-dependent deletion of BACE1 using the strategy first described by Luo et al. [32], which was also utilised for the generation of our C2C12$^{\Delta Bace1}$ cell line (4.7). Correct transfection of the plasmid was confirmed by SB analysis (Figure 6.1 d), however pronuclear injection for the generation of Bace1-flox mice have not been performed yet.

Both mouse models would be very useful to further investigate the role of BACE1 in metabolic and peripheral tissues regulation. This could be obtained via crossing of the newly generated mouse lines with tissue specific Cre recombinase lines. Of particular interest would be to utilise Cre recombinase *in vivo* lines specific for pan or brown adipose tissue, namely Adipoq-Cre [244] and Ucp1-Cre [245], respectively, and for skeletal muscle, Mck-Cre [246]. Moreover, in light of the proposed role for BACE1 in regulating the switch between myogenesis and brown adipogenesis, Bace1-LSL and Bace-flox mice could be crossed with Cre lines targeting the common precursors of this two lineages,

such as Myf5-Cre and Pax3-Cre [208]. Conditional *Bace1* knock-out mice should then be exposed to HFD to investigate potential beneficial effects of β-secretase depletion in diet-induced obesity, whereas the possible detrimental effects of *Bace1* over-expression could be investigated in a NCD condition.
To exploit the potential of peripheral BACE1 regulation in AD, the above described mouse lines could be also crossed with the established 3xTg-AD model, which harbours three AD-predisposing genetic lesions (APP Swedish Mutation, MAPT P301L and PSEN1 M146V) relevant for familial AD [247]. The generated *in vivo* models could then be characterised to investigate the effects of peripheral BACE1 down- or up-regulation on the pathophysiology of AD, performing behavioural tests and biochemical analysis of Aβ deposition.
Moreover, potential substrates of BACE1 (e.g AOC3) could be tested in all the aforementioned mouse models via over-expression (in Bace1-flox mice) or inhibition (in Bace1-LSL mice) of candidate recombinant proteins (e.g. recombinant sAOC3), to test if those rescue the expected BACE1-dependent phenotypes.

Clinical perspectives for BACE1 inhibition

BACE1 inhibition is to date the most promising approach in clinical trials to counteract the development and progression of AD [17]. However, no studies have been performed on the therapeutic potential of such an approach in other diseases. Our results support the idea that inhibition of BACE1 could have beneficial effects not only in AD patients, but also in the pathologies associated with obesity. Indeed, BACE1 inhibition in mice reduced body weight gain (4.6.2) and enhanced glucose tolerance and insulin sensitivity (4.6.2). Considering the high epidemiological correlation among AD, T2D and obesity [23], it cannot be excluded that these pathologies could share the same therapeutic targets involved in metabolism regulation. Moreover, identification of BACE1 substrates involved in metabolism and AD regulation could unveil new therapeutic approaches. Targeting proteins downstream of BACE1 could avoid the deleterious effects shown for BACE1 inhibitors *in vivo* [17] and could provide more specific targets to treat AD or obesity-related disease. These substrates, that could include AOC3, whose therapeutic function is yet to be investigated, could also be suitable biomarkers for AD. This neurodegenerative pathology to date does not have reliable biomarkers able to allow an early detection of the disease onset without high uncertainty. Classical AD biomarkers, such as Aβ deposition and tau phosphorylation, necessitate cerebrospinal fluid (CSF) analysis which are invasive for the patients and do not fully represent the pathophysiology of

AD [248]. Other circulating biomarkers on the other hand, including various miRNAs, have only recently been proposed and further investigations iare needed to validate their reliability [248]. AOC3, with its soluble blood-released form sAOC3, has already been proven as AD-relevant, showing to be increased in hippocampal blood vessels and being proposed as a therapeutic target for preventing/delaying the progress of AD-associated vasculopathy [201] [202]. Further studies are however needed to indicate a real potential for sAOC3 as an AD biomarker.

Taken together, BACE1 and its substrates (e.g. AOC3) can be claimed to be promising therapeutic targets for AD, obesity and their sequelae. This warrants the broadening of the scientific scope for BACE1 investigation beyond AD and towards brown adipose tissue and metabolism regulation.

CHAPTER 6

APPENDIX

Table 6.1: List of CSC-detected peptides in the PI3K/AKT, FGFR and EGFR signalling pathway up-regulated on the cell surface of C2C12$^{\Delta Bace1}$ cells compared to wild-type C2C12. Indicated in bold are the proteins which were validated via WB (4.9.1). FC = fold change, *nd* = not detectable.

Protein ID	Gene name		$\log_2$ FC	adj. *p*-value
P07141	*Csf1*	Macrophage colony-stimulating factor 1	1,64246	0,01290
Q01279	***Egfr***	**Epidermal growth factor receptor**	**1,77909**	**0,05211**
P21803	*Fgfr2*	Fibroblast growth factor receptor 2	4,08144	0,05003
Q03142	*Fgfr4*	Fibroblast growth factor receptor 4	1,12740	0,21831
P26952	*Il3ra*	Interleukin-3 receptor subunit alpha	1,61688	0,01814
Q3V3R4	*Itga1*	Integrin alpha-1	4,36586	0,02246
P61622	*Itga11*	Integrin alpha-11	5,96986	0,03519
Q62470	*Itga3*	Integrin alpha-3	1,20113	0,04282
P20826	*Kitlg*	Kit ligand	*nd* in C2C12	*nd*
Q8BLG2	*Lpar4*	Lysophosphatidic acid receptor 4	3,29353	0,03410
Q6VVW5	*Npr2*	Atrial natriuretic peptide receptor 2	2,11275	0,02776
P70180	*Npr3*	Atrial natriuretic peptide receptor 3	2,86614	0,01935
O70458	*Osmr*	Oncostatin-M-specific receptor subunit beta	1,41507	0,01995
P05622	***Pdgfrb***	**Platelet-derived growth factor receptor beta**	**1,13925**	**0,02288**
Q9QUN7	*Tlr2*	Toll-like receptor 2	2,36291	0,03410
Q9QUK6	*Tlr4*	Toll-like receptor 4	4,15034	0,23008

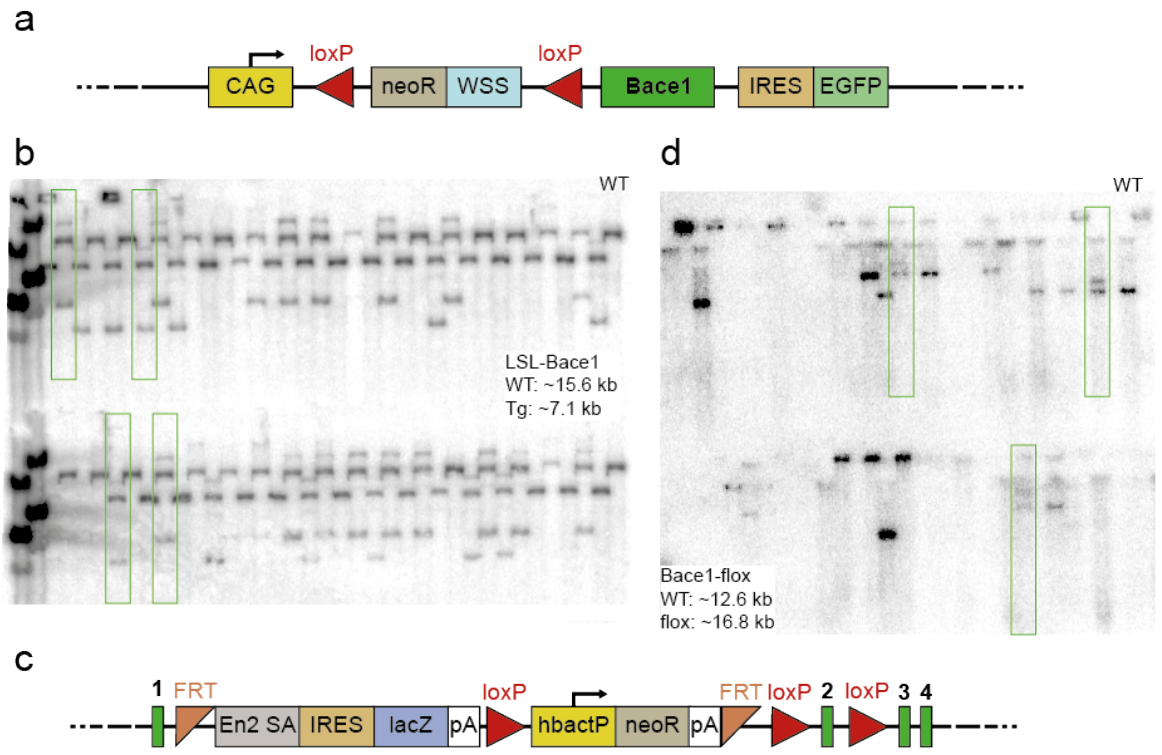

FIGURE 6.1. **Generation of *Bace1* gain- and loss-of-function mouse models.** **a** Schematic representation of Bace1-LSL (lox-STOP-lox) Rosa26 knock-in plasmid. **b** Southern blot for Bace1-LSL using the ROSA26 probe (details in 2.16). The wild-type control (WT) and a representative positive clone for each line (green boxes) are indicated. **c** Schematic representation of Bace1-flox exon 2 knock-out plasmid. **d** Southern blot for Bace1-flox using Bace1 exon 2 probe (details in 2.16). The wild-type control (WT) and positive clones (green boxes) are indicated. CAG, CAG promoter; loxP, Cre recombinase recognition site; NeoR, neomycin resistance cassette; WSS, Westphal stop sequence cassette; IRES, Internal ribosome entry site; EGFP, enhanced green fluorescent protein; FRT, Flp recombinase recognition target; En2 SA, En2 splice acceptor; lacZ, β-galactosidase reporter; pA, polyadenylation signal; hbactP, human β-actin promoter; Bace1, *Bace1* cDNA; numbers indicate exons of *Bace1*.

BIBLIOGRAPHY

[1] NCD Risk Factor Collaboration (NCD-RisC).
Trends in adult body-mass index in 200 countries from 1975 to 2014: a pooled analysis of 1698 population-based measurement studies with 19.2 million participants.
The Lancet, 387(10026):1377–96, 2016.

[2] M. C. Vogt, L. Paeger, S. Hess, S. M. Steculorum, M. Awazawa, B. Hampel, S. Neupert, H. T. Nicholls, J. Mauer, A. C. Hausen, R. Predel, P. Kloppenburg, T. L. Horvath, and J. C. Brüning.
Neonatal insulin action impairs hypothalamic neurocircuit formation in response to maternal high-fat feeding.
Cell, 156(3):495–509, 2014.

[3] R. T. Brookheart, C. I. Michel, and J. E. Schaffer.
As a matter of fat.
Cell Metab, 10(1):9–12, 2009.

[4] V. T. Samuel and G. I. Shulman.
Mechanisms for insulin resistance: common threads and missing links.
Cell, 148(5):852–71, 2012.

[5] E. D. Rosen and B. M. Spiegelman.
What we talk about when we talk about fat.
Cell, 156(1-2):20–44, 2014.

[6] A. Berrington de Gonzalez, P. Hartge, J. R. Cerhan, A. J. Flint, L. Hannan, R. J. MacInnis, S. C. Moore, G. S. Tobias, H. Anton-Culver, L. B. Freeman, W. L. Beeson, S. L. Clipp, D. R. English, A. R. Folsom, D. M. Freedman, G. Giles, N. Hakansson, K. D. Henderson, J. Hoffman-Bolton, J. A. Hoppin, K. L. Koenig, I. M. Lee, M. S. Linet, Y. Park, G. Pocobelli, A. Schatzkin, H. D. Sesso, E. Weiderpass, B. J. Willcox, A. Wolk, A. Zeleniuch-Jacquotte, W. C. Willett, and M. J. Thun.
Body-mass index and mortality among 1.46 million white adults.
N Engl J Med, 363(23):2211–9, 2010.

[7] NCD Risk Factor Collaboration (NCD-RisC).
Worldwide trends in diabetes since 1980: a pooled analysis of 751 population-based studies with 4.4 million participants.
The Lancet, 387(10027):1513–30, 2016.

[8] J. Boucher, A. Kleinridders, and C. R. Kahn.
Insulin receptor signaling in normal and insulin-resistant states.
Cold Spring Harb Perspect Biol, 6(1), 2014.

[9] S. K. Das and S. C. Elbein.
The genetic basis of type 2 diabetes.
Cellscience, 2(4):100–131, 2006.

[10] A. Doria, M. E. Patti, and C. R. Kahn.
The emerging genetic architecture of type 2 diabetes.
Cell Metab, 8(3):186–200, 2008.

[11] M. C. McKenna, H. S. Waagepetersen, A. Schousboe, and U. Sonnewald.
Neuronal and astrocytic shuttle mechanisms for cytosolic-mitochondrial transfer of reducing equivalents: current evidence and pharmacological tools.
Biochem Pharmacol, 71(4):399–407, 2006.

[12] C. Procaccini, M. Santopaolo, D. Faicchia, A. Colamatteo, L. Formisano, P. de Candia, M. Galgani, V. De Rosa, and G. Matarese.
Role of metabolism in neurodegenerative disorders.
Metabolism, 65(9):1376–90, 2016.

[13] J. N. Mazon, A. H. de Mello, G. K. Ferreira, and G. T. Rezin.
The impact of obesity on neurodegenerative diseases.
Life Sci, 182:22–28, 2017.

[14] J. Janson, T. Laedtke, J. E. Parisi, P. O'Brien, R. C. Petersen, and P. C. Butler.
Increased risk of type 2 diabetes in Alzheimer disease.
Diabetes, 53(2):474–81, 2004.

[15] M. Prince, A. Wimo, M. Guerchet, G.C. Ali, Y.Y. Wu, and M. Prina.
World alzheimer report 2015. the global impact of dementia: An analysis of prevalence, incidence, cost and trends.
London, 2015.

[16] K. Maurer, S. Volk, and H. Gerbaldo.
Auguste D and Alzheimer's disease.
Lancet, 349(9064):1546–9, 1997.

[17] R. Vassar, P. H. Kuhn, C. Haass, M. E. Kennedy, L. Rajendran, P. C. Wong, and S. F. Lichtenthaler.
Function, therapeutic potential and cell biology of BACE proteases: current status and future prospects.
J Neurochem, 130(1):4–28, 2014.

[18] S. Craft, E. Peskind, M. W. Schwartz, G. D. Schellenberg, M. Raskind, and Jr. Porte, D.
Cerebrospinal fluid and plasma insulin levels in Alzheimer's disease: relationship to severity of dementia and apolipoprotein E genotype.
Neurology, 50(1):164–8, 1998.

[19] S. I. Rapoport.
Functional brain imaging in the resting state and during activation in Alzheimer's disease. Implications for disease mechanisms involving oxidative phosphorylation.
Ann N Y Acad Sci, 893:138–53, 1999.

[20] L. Frölich, D. Blum-Degen, H. G. Bernstein, S. Engelsberger, J. Humrich, S. Laufer, D. Muschner, A. Thalheimer, A. Turk, S. Hoyer, R. Zochling, K. W. Boissl, K. Jellinger, and P. Riederer.
Brain insulin and insulin receptors in aging and sporadic Alzheimer's disease.
J Neural Transm (Vienna), 105(4-5):423–38, 1998.

[21] E. Steen, B. M. Terry, E. J. Rivera, J. L. Cannon, T. R. Neely, R. Tavares, X. J. Xu, J. R. Wands, and S. M. de la Monte.
Impaired insulin and insulin-like growth factor expression and signaling mechanisms in Alzheimer's disease–is this type 3 diabetes?
J Alzheimers Dis, 7(1):63–80, 2005.

[22] S. Kang, Y. H. Lee, and J. E. Lee.
Metabolism-centric overview of the pathogenesis of Alzheimer's disease.
Yonsei Med J, 58(3):479–488, 2017.

[23] K. L. Hildreth, R. E. Van Pelt, and R. S. Schwartz.
Obesity, insulin resistance, and Alzheimer's disease.
Obesity (Silver Spring), 20(8):1549–57, 2012.

[24] L. Ho, W. Qin, P. N. Pompl, Z. Xiang, J. Wang, Z. Zhao, Y. Peng, G. Cambareri, A. Rocher, C. V. Mobbs, P. R. Hof, and G. M. Pasinetti.
Diet-induced insulin resistance promotes amyloidosis in a transgenic mouse model of Alzheimer's disease.
FASEB J, 18(7):902–4, 2004.

[25] I. Hussain, D. Powell, D. R. Howlett, D. G. Tew, T. D. Meek, C. Chapman, I. S. Gloger, K. E. Murphy, C. D. Southan, D. M. Ryan, T. S. Smith, D. L. Simmons, F. S. Walsh, C. Dingwall, and G. Christie.
Identification of a novel aspartic protease (Asp 2) as beta-secretase.
Mol Cell Neurosci, 14(6):419–27, 1999.

[26] S. Sinha, J. P. Anderson, R. Barbour, G. S. Basi, R. Caccavello, D. Davis, M. Doan, H. F. Dovey, N. Frigon, J. Hong, K. Jacobson-Croak, N. Jewett, P. Keim, J. Knops, I. Lieberburg, M. Power, H. Tan, G. Tatsuno, J. Tung, D. Schenk, P. Seubert, S. M. Suomensaari, S. Wang, D. Walker, J. Zhao, L. McConlogue, and V. John.
Purification and cloning of amyloid precursor protein beta-secretase from human brain.
Nature, 402(6761):537–40, 1999.

[27] R. Vassar, B. D. Bennett, S. Babu-Khan, S. Kahn, E. A. Mendiaz, P. Denis, D. B. Teplow, S. Ross, P. Amarante, R. Loeloff, Y. Luo, S. Fisher, J. Fuller, S. Edenson, J. Lile, M. A. Jarosinski, A. L. Biere, E. Curran, T. Burgess, J. C. Louis, F. Collins, J. Treanor, G. Rogers, and M. Citron.
Beta-secretase cleavage of Alzheimer's amyloid precursor protein by the transmembrane aspartic protease BACE.
Science, 286(5440):735–41, 1999.

[28] R. Yan, M. J. Bienkowski, M. E. Shuck, H. Miao, M. C. Tory, A. M. Pauley, J. R. Brashier, N. C. Stratman, W. R. Mathews, A. E. Buhl, D. B. Carter, A. G. Tomasselli, L. A. Parodi, R. L. Heinrikson, and M. E. Gurney.
Membrane-anchored aspartyl protease with Alzheimer's disease beta-secretase activity.
Nature, 402(6761):533–7, 1999.

[29] X. Lin, G. Koelsch, S. Wu, D. Downs, A. Dashti, and J. Tang.
Human aspartic protease memapsin 2 cleaves the beta-secretase site of beta-amyloid precursor protein.
Proc Natl Acad Sci U S A, 97(4):1456–60, 2000.

[30] H. Cai, Y. Wang, D. McCarthy, H. Wen, D. R. Borchelt, D. L. Price, and P. C. Wong.
BACE1 is the major β-secretase for generation of Aβ peptides by neurons.
Nat Neurosci, 4(3):233–4, 2001.

[31] H. Fukumoto, B. S. Cheung, B. T. Hyman, and M. C. Irizarry.
Beta-secretase protein and activity are increased in the neocortex in Alzheimer disease.
Arch Neurol, 59(9):1381–9, 2002.

[32] Y. Luo, B. Bolon, S. Kahn, B. D. Bennett, S. Babu-Khan, P. Denis, W. Fan, H. Kha, J. Zhang, Y. Gong, L. Martin, J. C. Louis, Q. Yan, W. G. Richards, M. Citron, and R. Vassar.
Mice deficient in BACE1, the Alzheimer's β-secretase, have normal phenotype and abolished β-amyloid generation.
Nat Neurosci, 4(3):231–2, 2001.

[33] C. Cheret, M. Willem, F. R. Fricker, H. Wende, A. Wulf-Goldenberg, S. Tahirovic, K. A. Nave, P. Saftig, C. Haass, A. N. Garratt, D. L. Bennett, and C. Birchmeier.
Bace1 and Neuregulin-1 cooperate to control formation and maintenance of muscle spindles.
EMBO J, 32(14):2015–28, 2013.

[34] P. J. Meakin, A. J. Harper, D. L. Hamilton, J. Gallagher, A. D. McNeilly, L. A. Burgess, L. M. Vaanholt, K. A. Bannon, J. Latcham, I. Hussain, J. R. Speakman, D. R. Howlett, and M. L. Ashford.
Reduction in BACE1 decreases body weight, protects against diet-induced obesity and enhances insulin sensitivity in mice.
Biochem J, 441(1):285–96, 2012.

[35] D. L. Hamilton, J. A. Findlay, G. Montagut, P. J. Meakin, D. Bestow, S. M. Jalicy, and M. L. Ashford.
Altered amyloid precursor protein processing regulates glucose uptake and oxidation in cultured rodent myotubes.
Diabetologia, 57(8):1684–92, 2014.

[36] J. A. Findlay, D. L. Hamilton, and M. L. Ashford.
BACE1 activity impairs neuronal glucose oxidation: rescue by beta-hydroxybutyrate and lipoic acid.
Front Cell Neurosci, 9:382, 2015.

[37] Alzheimer's Association.
Changing the trajectory of alzheimer's disease: How a treatment by 2025 saves lives and dollars.
Chicago, 2015.

[38] H. W. Klafki, M. Staufenbiel, J. Kornhuber, and J. Wiltfang.
Therapeutic approaches to Alzheimer's disease.
Brain, 129(Pt 11):2840–55, 2006.

[39] S. Saito and M. Ihara.
New therapeutic approaches for Alzheimer's disease and cerebral amyloid angiopathy.
Front Aging Neurosci, 6:290, 2014.

[40] M. Ruthirakuhan, N. Herrmann, I. Suridjan, E. H. Abraham, I. Farber, and K. L. Lanctot.
Beyond immunotherapy: new approaches for disease modifying treatments for early Alzheimer's disease.
Expert Opin Pharmacother, 17(18):2417–2429, 2016.

[41] P. C. May, R. A. Dean, S. L. Lowe, F. Martenyi, S. M. Sheehan, L. N. Boggs, S. A. Monk, B. M. Mathes, D. J. Mergott, B. M. Watson, S. L. Stout, D. E. Timm, E. Smith Labell, C. R. Gonzales, M. Nakano, S. S. Jhee, M. Yen, L. Ereshefsky, T. D. Lindstrom, D. O. Calligaro, P. J. Cocke, D. Greg Hall, S. Friedrich, M. Citron, and J. E. Audia.
Robust central reduction of amyloid-beta in humans with an orally available, non-peptidic beta-secretase inhibitor.
J Neurosci, 31(46):16507–16, 2011.

[42] Z. Zhu, Z. Y. Sun, Y. Ye, J. Voigt, C. Strickland, E. M. Smith, J. Cumming, L. Wang, J. Wong, Y. S. Wang, D. F. Wyss, X. Chen, R. Kuvelkar, M. E. Kennedy, L. Favreau, E. Parker, B. A. McKittrick, A. Stamford, M. Czarniecki, W. Greenlee, and J. C. Hunter.
Discovery of cyclic acylguanidines as highly potent and selective beta-site amyloid cleaving enzyme (BACE) inhibitors: Part i–inhibitor design and validation.
J Med Chem, 53(3):951–65, 2010.

[43] H. Hilpert, W. Guba, T. J. Woltering, W. Wostl, E. Pinard, H. Mauser, A. V. Mayweg, M. Rogers-Evans, R. Humm, D. Krummenacher, T. Muser, C. Schnider, H. Jacobsen, L. Ozmen, A. Bergadano, D. W. Banner, R. Hochstrasser, A. Kuglstatter, P. David-Pierson, H. Fischer, A. Polara, and R. Narquizian.

β-Secretase (BACE1) inhibitors with high *in vivo* efficacy suitable for clinical evaluation in Alzheimer's disease.
J Med Chem, 56(10):3980–95, 2013.

[44] M. E. Kennedy, A. W. Stamford, X. Chen, K. Cox, J. N. Cumming, M. F. Dockendorf, M. Egan, L. Ereshefsky, R. A. Hodgson, L. A. Hyde, S. Jhee, H. J. Kleijn, R. Kuvelkar, W. Li, B. A. Mattson, H. Mei, J. Palcza, J. D. Scott, M. Tanen, M. D. Troyer, J. L. Tseng, J. A. Stone, E. M. Parker, and M. S. Forman.
The BACE1 inhibitor verubecestat (MK-8931) reduces CNS beta-amyloid in animal models and in Alzheimer's disease patients.
Sci Transl Med, 8(363):363ra150, 2016.

[45] A.W. Hetherington and S.W. Ranson.
Hypothalamic lesions and adiposity in the rat.
The Anatomical Record, 78(2):149–72, 1940.

[46] B. F. Belgardt and J. C. Brüning.
CNS leptin and insulin action in the control of energy homeostasis.
Ann N Y Acad Sci, 1212:97–113, 2010.

[47] N. R. Lenard and H. R. Berthoud.
Central and peripheral regulation of food intake and physical activity: pathways and genes.
Obesity (Silver Spring), 16 Suppl 3:S11–22, 2008.

[48] Sanchez-Gurmaches J, Hung CM, and Guertin DA.
Emerging complexities in adipocyte origins and identity.
Trends Cell Biol, 26(5):313–26, 2016.

[49] M. Furuhashi, S. Saitoh, K. Shimamoto, and T. Miura.
Fatty acid-binding protein 4 (FABP4): Pathophysiological insights and potent clinical biomarker of metabolic and cardiovascular diseases.
Clin Med Insights Cardiol, 8(Suppl 3):23–33, 2014.

[50] G. S. Hotamisligil, R. S. Johnson, R. J. Distel, R. Ellis, V. E. Papaioannou, and B. M. Spiegelman.
Uncoupling of obesity from insulin resistance through a targeted mutation in aP2, the adipocyte fatty acid binding protein.
Science, 274(5291):1377–9, 1996.

[51] R. Yang, G. Castriota, Y. Chen, M. A. Cleary, K. Ellsworth, M. K. Shin, J. L. Tran, T. F. Vogt, M. Wu, S. Xu, X. Yang, B. B. Zhang, J. P. Berger, and S. A. Qureshi.
RNAi-mediated germline knockdown of FABP4 increases body weight but does not improve the deranged nutrient metabolism of diet-induced obese mice.
Int J Obes (Lond), 35(2):217–25, 2011.

[52] W. Wang and P. Seale.
Control of brown and beige fat development.
Nat Rev Mol Cell Biol, 17(11):691–702, 2016.

[53] C. S. Hudak and H. S. Sul.
Pref-1, a gatekeeper of adipogenesis.
Front Endocrinol (Lausanne), 4:79, 2013.

[54] S. R. Farmer.
Transcriptional control of adipocyte formation.
Cell Metab, 4(4):263–73, 2006.

[55] I. Moreno-Indias and F. J. Tinahones.
Impaired adipose tissue expandability and lipogenic capacities as ones of the main causes of metabolic disorders.
J Diabetes Res, 2015:970375, 2015.

[56] V. Pellegrinelli, S. Carobbio, and A. Vidal-Puig.
Adipose tissue plasticity: how fat depots respond differently to pathophysiological cues.
Diabetologia, 59(6):1075–88, 2016.

[57] E. D. Rosen and B. M. Spiegelman.
Adipocytes as regulators of energy balance and glucose homeostasis.
Nature, 444(7121):847–53, 2006.

[58] S. M. Grundy.
Adipose tissue and metabolic syndrome: too much, too little or neither.
Eur J Clin Invest, 45(11):1209–17, 2015.

[59] T. T. Tran, Y. Yamamoto, S. Gesta, and C. R. Kahn.
Beneficial effects of subcutaneous fat transplantation on metabolism.
Cell Metab, 7(5):410–20, 2008.

[60] B. Cannon and J. Nedergaard.
Brown adipose tissue: function and physiological significance.
Physiol Rev, 84(1):277–359, 2004.

[61] J. Nedergaard, T. Bengtsson, and B. Cannon.
Unexpected evidence for active brown adipose tissue in adult humans.
Am J Physiol Endocrinol Metab, 293(2):E444–52, 2007.

[62] A. M. Cypess, S. Lehman, G. Williams, I. Tal, D. Rodman, A. B. Goldfine, F. C. Kuo, E. L. Palmer, Y. H. Tseng, A. Doria, G. M. Kolodny, and C. R. Kahn.
Identification and importance of brown adipose tissue in adult humans.
N Engl J Med, 360(15):1509–17, 2009.

[63] W. D. van Marken Lichtenbelt, J. W. Vanhommerig, N. M. Smulders, J. M. Drossaerts, G. J. Kemerink, N. D. Bouvy, P. Schrauwen, and G. J. Teule.
Cold-activated brown adipose tissue in healthy men.
N Engl J Med, 360(15):1500–8, 2009.

[64] A. M. Cypess, A. P. White, C. Vernochet, T. J. Schulz, R. Xue, C. A. Sass, T. L. Huang, C. Roberts-Toler, L. S. Weiner, C. Sze, A. T. Chacko, L. N. Deschamps, L. M. Herder, N. Truchan, A. L. Glasgow, A. R. Holman, A. Gavrila, P. O. Hasselgren, M. A. Mori, M. Molla, and Y. H. Tseng.
Anatomical localization, gene expression profiling and functional characterization of adult human neck brown fat.
Nat Med, 19(5):635–9, 2013.

[65] J. Villarroya, R. Cereijo, and F. Villarroya.
An endocrine role for brown adipose tissue?
Am J Physiol Endocrinol Metab, 305(5):E567–72, 2013.

[66] J. Nedergaard, V. Golozoubova, A. Matthias, A. Asadi, A. Jacobsson, and B. Cannon.
UCP1: the only protein able to mediate adaptive non-shivering thermogenesis and metabolic inefficiency.
Biochim Biophys Acta, 1504(1):82–106, 2001.

[67] J. Orava, P. Nuutila, M. E. Lidell, V. Oikonen, T. Noponen, T. Viljanen, M. Scheinin, M. Taittonen, T. Niemi, S. Enerback, and K. A. Virtanen.
Different metabolic responses of human brown adipose tissue to activation by cold and insulin.
Cell Metab, 14(2):272–9, 2011.

[68] S. F. Morrison and K. Nakamura.
Central neural pathways for thermoregulation.
Front Biosci (Landmark Ed), 16:74–104, 2011.

[69] Chechi K, Nedergaard J, and Richard D.
Brown adipose tissue as an anti-obesity tissue in humans.
Obes Rev, 15:92–106, 2014.

[70] P. Seale, B. Bjork, W. Yang, S. Kajimura, S. Chin, S. Kuang, A. Scime, S. Devarakonda, H. M. Conroe, H. Erdjument-Bromage, P. Tempst, M. A. Rudnicki, D. R. Beier, and B. M. Spiegelman.
PRDM16 controls a brown fat/skeletal muscle switch.
Nature, 454(7207):961–7, 2008.

[71] J. Sanchez-Gurmaches and D. A. Guertin.
Adipocytes arise from multiple lineages that are heterogeneously and dynamically distributed.
Nat Commun, 5:4099, 2014.

[72] C. Lepper and C. M. Fan.
Inducible lineage tracing of Pax7-descendant cells reveals embryonic origin of adult satellite cells.
Genesis, 48(7):424–36, 2010.

[73] R. Atit, S. K. Sgaier, O. A. Mohamed, M. M. Taketo, D. Dufort, A. L. Joyner, L. Niswander, and R. A. Conlon.
Beta-catenin activation is necessary and sufficient to specify the dorsal dermal fate in the mouse.
Dev Biol, 296(1):164–76, 2006.

[74] Lidell ME, Betz MJ, and Enerbäck S.
Brown adipose tissue and its therapeutic potential.
J Intern Med, 276(4):364–77, 2014.

[75] Bartelt A and Heeren J.
The holy grail of metabolic disease: brown adipose tissue.
Curr Opin Lipidol, 23:190–5, 2012.

[76] M. Saito, Y. Okamatsu-Ogura, M. Matsushita, K. Watanabe, T. Yoneshiro, J. Nio-Kobayashi, T. Iwanaga, M. Miyagawa, T. Kameya, K. Nakada, Y. Kawai, and M. Tsujisaki.
High incidence of metabolically active brown adipose tissue in healthy adult humans: effects of cold exposure and adiposity.
Diabetes, 58(7):1526–31, 2009.

[77] T. Yoneshiro, S. Aita, M. Matsushita, T. Kayahara, T. Kameya, Y. Kawai, T. Iwanaga, and M. Saito.
Recruited brown adipose tissue as an antiobesity agent in humans.
J Clin Invest, 123(8):3404–8, 2013.

[78] Lynes MD and Tseng YH.
The thermogenic circuit: Regulators of thermogenic competency and differentiation.
Genes Dis, 2(2):164–72, 2015.

[79] P. Young, J. R. Arch, and M. Ashwell.
Brown adipose tissue in the parametrial fat pad of the mouse.
FEBS Lett, 167(1):10–4, 1984.

[80] B. Cousin, S. Cinti, M. Morroni, S. Raimbault, D. Ricquier, L. Penicaud, and L. Casteilla.
Occurrence of brown adipocytes in rat white adipose tissue: molecular and morphological characterization.
J Cell Sci, 103 (Pt 4):931–42, 1992.

[81] C. Guerra, R. A. Koza, H. Yamashita, K. Walsh, and L. P. Kozak.
Emergence of brown adipocytes in white fat in mice is under genetic control. Effects on body weight and adiposity.
J Clin Invest, 102(2):412–20, 1998.

[82] J. Wu, P. Bostrom, L. M. Sparks, L. Ye, J. H. Choi, A. H. Giang, M. Khandekar, K. A. Virtanen, P. Nuutila, G. Schaart, K. Huang, H. Tu, W. D. van Marken Lichtenbelt, J. Hoeks, S. Enerback, P. Schrauwen, and B. M. Spiegelman.
Beige adipocytes are a distinct type of thermogenic fat cell in mouse and human.
Cell, 150(2):366–76, 2012.

[83] A. Bartelt and J. Heeren.
Adipose tissue browning and metabolic health.
Nat Rev Endocrinol, 10(1):24–36, 2014.

[84] J. M. de Jong, O. Larsson, B. Cannon, and J. Nedergaard.
A stringent validation of mouse adipose tissue identity markers.
Am J Physiol Endocrinol Metab, 308(12):E1085–105, 2015.

[85] R. A. DeFronzo, E. Jacot, E. Jequier, E. Maeder, J. Wahren, and J. P. Felber.
The effect of insulin on the disposal of intravenous glucose. Results from indirect calorimetry and hepatic and femoral venous catheterization.
Diabetes, 30(12):1000–7, 1981.

[86] C. S. Stump, E. J. Henriksen, Y. Wei, and J. R. Sowers.
The metabolic syndrome: role of skeletal muscle metabolism.
Ann Med, 38(6):389–402, 2006.

[87] J. O. Holloszy and E. F. Coyle.
Adaptations of skeletal muscle to endurance exercise and their metabolic consequences.
J Appl Physiol Respir Environ Exerc Physiol, 56(4):831–8, 1984.

[88] R. L. Perry and M. A. Rudnick.
Molecular mechanisms regulating myogenic determination and differentiation.
Front Biosci, 5:D750–67, 2000.

[89] H. Weintraub, S. J. Tapscott, R. L. Davis, M. J. Thayer, M. A. Adam, A. B. Lassar, and A. D. Miller.
Activation of muscle-specific genes in pigment, nerve, fat, liver, and fibroblast cell lines by forced expression of myoD.
Proc Natl Acad Sci U S A, 86(14):5434–8, 1989.

[90] P. Hasty, A. Bradley, J. H. Morris, D. G. Edmondson, J. M. Venuti, E. N. Olson, and W. H. Klein.
Muscle deficiency and neonatal death in mice with a targeted mutation in the myogenin gene.
Nature, 364(6437):501–6, 1993.

[91] T. Braun, M. A. Rudnicki, H. H. Arnold, and R. Jaenisch.
Targeted inactivation of the muscle regulatory gene Myf-5 results in abnormal rib development and perinatal death.
Cell, 71(3):369–82, 1992.

[92] M. A. Rudnicki, T. Braun, S. Hinuma, and R. Jaenisch.
Inactivation of MyoD in mice leads to up-regulation of the myogenic HLH gene Myf-5 and results in apparently normal muscle development.
Cell, 71(3):383–90, 1992.

[93] T. Wallimann, M. Wyss, D. Brdiczka, K. Nicolay, and H. M. Eppenberger.
Intracellular compartmentation, structure and function of creatine kinase isoenzymes in tissues with high and fluctuating energy demands: the 'phosphocreatine circuit' for cellular energy homeostasis.
Biochem J, 281 (Pt 1):21–40, 1992.

[94] U. B. Rosenberg, G. Kunz, A. Frischauf, H. Lehrach, R. Mahr, H. M. Eppenberger, and J. C. Perriard.
Molecular cloning and expression during myogenesis of sequences coding for M-creatine kinase.
Proc Natl Acad Sci U S A, 79(21):6589–92, 1982.

[95] B. Wei and J. P. Jin.
TNNT1, TNNT2, and TNNT3: Isoform genes, regulation, and structure-function relationships.
Gene, 582(1):1–13, 2016.

[96] B. Wei and J. P. Jin.
Troponin T isoforms and posttranscriptional modifications: Evolution, regulation and function.
Arch Biochem Biophys, 505(2):144–54, 2011.

[97] C. Pellegrino and C. Franzini.
An electron microscope study of denervation atrophy in red and white skeletal muscle fibers.
J Cell Biol, 17(2):327–49, 1963.

[98] M. A. Egerman and D. J. Glass.
Signaling pathways controlling skeletal muscle mass.
Crit Rev Biochem Mol Biol, 49(1):59–68, 2014.

[99] E. Hu, P. Tontonoz, and B. M. Spiegelman.
Transdifferentiation of myoblasts by the adipogenic transcription factors PPAR gamma and C/EBPalpha.
Proc Natl Acad Sci U S A, 92(21):9856–60, 1995.

[100] C. Sciorati, E. Clementi, A. A. Manfredi, and P. Rovere-Querini.
Fat deposition and accumulation in the damaged and inflamed skeletal muscle: cellular and molecular players.
Cell Mol Life Sci, 72(11):2135–56, 2015.

[101] R. Vettor, G. Milan, C. Franzin, M. Sanna, P. De Coppi, R. Rizzuto, and G. Federspil.
The origin of intermuscular adipose tissue and its pathophysiological implications.
Am J Physiol Endocrinol Metab, 297(5):E987–98, 2009.

[102] T. J. Schulz, T. L. Huang, T. T. Tran, H. Zhang, K. L. Townsend, J. L. Shadrach, M. Cerletti, L. E. McDougall, N. Giorgadze, T. Tchkonia, D. Schrier, D. Falb, J. L. Kirkland, A. J. Wagers, and Y. H. Tseng.
Identification of inducible brown adipocyte progenitors residing in skeletal muscle and white fat.
Proc Natl Acad Sci U S A, 108(1):143–8, 2011.

[103] Y. Zhang, R. Proenca, M. Maffei, M. Barone, L. Leopold, and J. M. Friedman.
Positional cloning of the mouse obese gene and its human homologue.
Nature, 372(6505):425–32, 1994.

[104] H. Larsson, S. Elmstahl, G. Berglund, and B. Ahren.
Evidence for leptin regulation of food intake in humans.
J Clin Endocrinol Metab, 83(12):4382–5, 1998.

[105] J. Friedman.
Leptin and the regulation of food intake and body weight.
J Nutr Sci Vitaminol (Tokyo), 61 Suppl:S202, 2015.

[106] C. H. Lee, Y. C. Woo, Y. Wang, C. Y. Yeung, A. Xu, and K. S. Lam.
Obesity, adipokines and cancer: an update.
Clin Endocrinol (Oxf), 83(2):147–56, 2015.

[107] X. Huang and Z. Yang.
Resistin's, obesity and insulin resistance: the continuing disconnect between rodents and humans.
J Endocrinol Invest, 39(6):607–15, 2016.

[108] C. R. Kahn.
Banting lecture. Insulin action, diabetogenes, and the cause of type ii diabetes.
Diabetes, 43(8):1066–84, 1994.

[109] A. C. Könner and J. C. Brüning.
Selective insulin and leptin resistance in metabolic disorders.
Cell Metab, 16(2):144–52, 2012.

[110] B. Cannon and J. Nedergaard.
Thermogenesis challenges the adipostat hypothesis for body-weight control.
Proc Nutr Soc, 68(4):401–7, 2009.

[111] J. E. Silva and P. R. Larsen.
Adrenergic activation of triiodothyronine production in brown adipose tissue.
Nature, 305(5936):712–3, 1983.

[112] K. N. Saraswathy, M. Asghar, R. Samtani, B. Murry, P. R. Mondal, P. K. Ghosh, and M. P. Sachdeva.
Spectrum of MTHFR gene SNPs C677T and A1298C: a study among 23 population groups of India.
Mol Biol Rep, 39(4):5025–31, 2012.

[113] S. C. Gunawardana and D. W. Piston.
Reversal of type 1 diabetes in mice by brown adipose tissue transplant.
Diabetes, 61(3):674–82, 2012.

[114] G. Li, R. L. Klein, M. Matheny, M. A. King, E. M. Meyer, and P. J. Scarpace.
Induction of uncoupling protein 1 by central interleukin-6 gene delivery is dependent on sympathetic innervation of brown adipose tissue and underlies one mechanism of body weight reduction in rats.
Neuroscience, 115(3):879–89, 2002.

[115] H. Ellingsgaard, I. Hauselmann, B. Schuler, A. M. Habib, L. L. Baggio, D. T. Meier, E. Eppler, K. Bouzakri, S. Wueest, Y. D. Muller, A. M. Hansen, M. Reinecke, D. Konrad, M. Gassmann, F. Reimann, P. A. Halban, J. Gromada, D. J. Drucker, F. M. Gribble, J. A. Ehses, and M. Y. Donath.
Interleukin-6 enhances insulin secretion by increasing glucagon-like peptide-1 secretion from L cells and alpha cells.
Nat Med, 17(11):1481–9, 2011.

[116] E. Hondares, R. Iglesias, A. Giralt, F. J. Gonzalez, M. Giralt, T. Mampel, and F. Villarroya.
Thermogenic activation induces FGF21 expression and release in brown adipose tissue.
J Biol Chem, 286(15):12983–90, 2011.

[117] P. Lee, C. D. Werner, E. Kebebew, and F. S. Celi.
Functional thermogenic beige adipogenesis is inducible in human neck fat.
Int J Obes (Lond), 38(2):170–6, 2014.

[118] D. A. Sarruf, J. P. Thaler, G. J. Morton, J. German, J. D. Fischer, K. Ogimoto, and M. W. Schwartz.
Fibroblast growth factor 21 action in the brain increases energy expenditure and insulin sensitivity in obese rats.
Diabetes, 59(7):1817–24, 2010.

[119] A. Planavila, I. Redondo, E. Hondares, M. Vinciguerra, C. Munts, R. Iglesias, L. A. Gabrielli, M. Sitges, M. Giralt, M. van Bilsen, and F. Villarroya.
Fibroblast growth factor 21 protects against cardiac hypertrophy in mice.
Nat Commun, 4:2019, 2013.

[120] F. M. Fisher, J. L. Estall, A. C. Adams, P. J. Antonellis, H. A. Bina, J. S. Flier, A. Kharitonenkov, B. M. Spiegelman, and E. Maratos-Flier.
Integrated regulation of hepatic metabolism by fibroblast growth factor 21 (FGF21) *in vivo*.
Endocrinology, 152(8):2996–3004, 2011.

[121] S. A. Byron, K. R. Van Keuren-Jensen, D. M. Engelthaler, J. D. Carpten, and D. W. Craig.
Translating RNA sequencing into clinical diagnostics: opportunities and challenges.
Nat Rev Genet, 17(5):257–71, 2016.

[122] M. Esteller.
Non-coding RNAs in human disease.
Nat Rev Genet, 12(12):861–74, 2011.

[123] P. Bertone, V. Stolc, T. E. Royce, J. S. Rozowsky, A. E. Urban, X. Zhu, J. L. Rinn, W. Tongprasit, M. Samanta, S. Weissman, M. Gerstein, and M. Snyder.
Global identification of human transcribed sequences with genome tiling arrays.
Science, 306(5705):2242–6, 2004.

[124] J. Cheng, P. Kapranov, J. Drenkow, S. Dike, S. Brubaker, S. Patel, J. Long, D. Stern, H. Tammana, G. Helt, V. Sementchenko, A. Piccolboni, S. Bekiranov, D. K. Bailey, M. Ganesh, S. Ghosh, I. Bell, D. S. Gerhard, and T. R. Gingeras.
Transcriptional maps of 10 human chromosomes at 5-nucleotide resolution.
Science, 308(5725):1149–54, 2005.

[125] P. Kapranov, J. Cheng, S. Dike, D. A. Nix, R. Duttagupta, A. T. Willingham, P. F. Stadler, J. Hertel, J. Hackermuller, I. L. Hofacker, I. Bell, E. Cheung, J. Drenkow, E. Dumais, S. Patel, G. Helt, M. Ganesh, S. Ghosh, A. Piccolboni, V. Sementchenko, H. Tammana, and T. R. Gingeras.
RNA maps reveal new RNA classes and a possible function for pervasive transcription.
Science, 316(5830):1484–8, 2007.

[126] S. Djebali, C. A. Davis, A. Merkel, A. Dobin, T. Lassmann, A. Mortazavi, A. Tanzer, J. Lagarde, W. Lin, F. Schlesinger, C. Xue, G. K. Marinov, J. Khatun, B. A. Williams, C. Zaleski, J. Rozowsky, M. Roder, F. Kokocinski, R. F. Abdelhamid, T. Alioto, I. Antoshechkin, M. T. Baer, N. S. Bar, P. Batut, K. Bell, I. Bell, S. Chakrabortty, X. Chen, J. Chrast, J. Curado, T. Derrien, J. Drenkow, E. Dumais, J. Dumais, R. Duttagupta, E. Falconnet, M. Fastuca, K. Fejes-Toth, P. Ferreira, S. Foissac, M. J. Fullwood, H. Gao, D. Gonzalez, A. Gordon, H. Gunawardena, C. Howald, S. Jha, R. Johnson, P. Kapranov, B. King, C. Kingswood, O. J. Luo, E. Park, K. Persaud, J. B. Preall, P. Ribeca, B. Risk, D. Robyr, M. Sammeth, L. Schaffer, L. H. See, A. Shahab, J. Skancke, A. M. Suzuki, H. Takahashi, H. Tilgner, D. Trout, N. Walters, H. Wang, J. Wrobel, Y. Yu, X. Ruan, Y. Hayashizaki, J. Harrow, M. Gerstein, T. Hubbard, A. Reymond, S. E. Antonarakis, G. Hannon, M. C. Giddings, Y. Ruan, B. Wold, P. Carninci, R. Guigo, and T. R. Gingeras.
Landscape of transcription in human cells.
Nature, 489(7414):101–8, 2012.

[127] Encode Project Consortium.
An integrated encyclopedia of dna elements in the human genome.
Nature, 489(7414):57–74, 2012.

[128] K. Yamada, J. Lim, J. M. Dale, H. Chen, P. Shinn, C. J. Palm, A. M. Southwick, H. C. Wu, C. Kim, M. Nguyen, P. Pham, R. Cheuk, G. Karlin-Newmann, S. X. Liu, B. Lam, H. Sakano, T. Wu, G. Yu, M. Miranda, H. L. Quach, M. Tripp, C. H. Chang, J. M. Lee, M. Toriumi, M. M. Chan, C. C. Tang, C. S. Onodera, J. M. Deng, K. Akiyama, Y. Ansari, T. Arakawa, J. Banh, F. Banno, L. Bowser, S. Brooks, P. Carninci, Q. Chao, N. Choy, A. Enju, A. D. Goldsmith, M. Gurjal, N. F. Hansen, Y. Hayashizaki, C. Johnson-Hopson, V. W. Hsuan, K. Iida, M. Karnes, S. Khan, E. Koesema, J. Ishida, P. X. Jiang, T. Jones, J. Kawai, A. Kamiya, C. Meyers, M. Nakajima, M. Narusaka, M. Seki, T. Sakurai, M. Satou, R. Tamse, M. Vaysberg, E. K. Wallender, C. Wong, Y. Yamamura, S. Yuan, K. Shinozaki, R. W. Davis, A. Theologis, and J. R. Ecker.
Empirical analysis of transcriptional activity in the Arabidopsis genome.
Science, 302(5646):842–6, 2003.

[129] J. L. Tupy, A. M. Bailey, G. Dailey, M. Evans-Holm, C. W. Siebel, S. Misra, S. E. Celniker, and G. M. Rubin.
Identification of putative noncoding polyadenylated transcripts in Drosophila melanogaster.
Proc Natl Acad Sci U S A, 102(15):5495–500, 2005.

[130] Consortium Honeybee Genome Sequencing.
Insights into social insects from the genome of the honeybee Apis mellifera.
Nature, 443(7114):931–49, 2006.

[131] M. Baker.
Long noncoding RNAs: the search for function.
Nat Methods, 8(5):379–83, 2011.

[132] M. J. Hangauer, I. W. Vaughn, and M. T. McManus.
Pervasive transcription of the human genome produces thousands of previously unidentified long intergenic noncoding RNAs.
PLoS Genet, 9(6):e1003569, 2013.

[133] M. E. Dinger, K. C. Pang, T. R. Mercer, and J. S. Mattick.
Differentiating protein-coding and noncoding RNA: challenges and ambiguities.
PLoS Comput Biol, 4(11):e1000176, 2008.

[134] J. L. Rinn and H. Y. Chang.
Genome regulation by long noncoding RNAs.
Annu Rev Biochem, 81:145–66, 2012.

[135] K. C. Miranda, T. Huynh, Y. Tay, Y. S. Ang, W. L. Tam, A. M. Thomson, B. Lim, and I. Rigoutsos.
A pattern-based method for the identification of microRNA binding sites and their corresponding heteroduplexes.
Cell, 126(6):1203–17, 2006.

[136] T. H. King, B. Liu, R. R. McCully, and M. J. Fournier.
Ribosome structure and activity are altered in cells lacking snornps that form pseudouridines in the peptidyl transferase center.
Mol Cell, 11(2):425–35, 2003.

[137] J. Salzman.
Circular RNA expression: Its potential regulation and function.
Trends Genet, 32(5):309–16, 2016.

[138] A. A. Aravin, R. Sachidanandam, A. Girard, K. Fejes-Toth, and G. J. Hannon.
Developmentally regulated piRNA clusters implicate MILI in transposon control.
Science, 316(5825):744–7, 2007.

[139] S. Memczak, M. Jens, A. Elefsinioti, F. Torti, J. Krueger, A. Rybak, L. Maier, S. D. Mackowiak, L. H. Gregersen, M. Munschauer, A. Loewer, U. Ziebold, M. Landthaler, C. Kocks, F. le Noble, and N. Rajewsky.
Circular RNAs are a large class of animal RNAs with regulatory potency.
Nature, 495(7441):333–8, 2013.

[140] R. C. Lee, R. L. Feinbaum, and V. Ambros.
The C. elegans heterochronic gene lin-4 encodes small RNAs with antisense complementarity to lin-14.
Cell, 75(5):843–54, 1993.

[141] B. Wightman, I. Ha, and G. Ruvkun.
Posttranscriptional regulation of the heterochronic gene lin-14 by lin-4 mediates temporal pattern formation in C. elegans.
Cell, 75(5):855–62, 1993.

[142] M. Ha and V. N. Kim.
Regulation of microRNA biogenesis.
Nat Rev Mol Cell Biol, 15(8):509–24, 2014.

[143] J. G. Ruby, C. H. Jan, and D. P. Bartel.
Intronic microRNA precursors that bypass Drosha processing.
Nature, 448(7149):83–6, 2007.

[144] K. Okamura, J. W. Hagen, H. Duan, D. M. Tyler, and E. C. Lai.
The mirtron pathway generates microRNA-class regulatory RNAs in drosophila.
Cell, 130(1):89–100, 2007.

[145] J. S. Yang and E. C. Lai.
Alternative miRNA biogenesis pathways and the interpretation of core miRNA pathway mutants.
Mol Cell, 43(6):892–903, 2011.

[146] S. Cheloufi, C. O. Dos Santos, M. M. Chong, and G. J. Hannon.
A dicer-independent miRNA biogenesis pathway that requires Ago catalysis.
Nature, 465(7298):584–9, 2010.

[147] D. Cifuentes, H. Xue, D. W. Taylor, H. Patnode, Y. Mishima, S. Cheloufi, E. Ma, S. Mane, G. J. Hannon, N. D. Lawson, S. A. Wolfe, and A. J. Giraldez.
A novel miRNA processing pathway independent of Dicer requires Argonaute2 catalytic activity.
Science, 328(5986):1694–8, 2010.

[148] J. S. Yang, T. Maurin, N. Robine, K. D. Rasmussen, K. L. Jeffrey, R. Chandwani, E. P. Papapetrou, M. Sadelain, D. O'Carroll, and E. C. Lai.
Conserved vertebrate miR-451 provides a platform for Dicer-independent, Ago2-mediated microRNA biogenesis.
Proc Natl Acad Sci U S A, 107(34):15163–8, 2010.

[149] R. Mudhasani, A. N. Imbalzano, and S. N. Jones.
An essential role for Dicer in adipocyte differentiation.
J Cell Biochem, 110(4):812–6, 2010.

[150] M. A. Mori, P. Raghavan, T. Thomou, J. Boucher, S. Robida-Stubbs, Y. Macotela, S. J. Russell, J. L. Kirkland, T. K. Blackwell, and C. R. Kahn.
Role of microRNA processing in adipose tissue in stress defense and longevity.
Cell Metab, 16(3):336–47, 2012.

[151] M. A. Mori, T. Thomou, J. Boucher, K. Y. Lee, S. Lallukka, J. K. Kim, M. Torriani, H. Yki-Jarvinen, S. K. Grinspoon, A. M. Cypess, and C. R. Kahn.
Altered miRNA processing disrupts brown/white adipocyte determination and associates with lipodystrophy.
J Clin Invest, 124(8):3339–51, 2014.

[152] F. C. Reis, J. L. Branquinho, B. B. Brandao, B. A. Guerra, I. D. Silva, A. Frontini, T. Thomou, L. Sartini, S. Cinti, C. R. Kahn, W. T. Festuccia, A. J. Kowaltowski, and M. A. Mori.
Fat-specific Dicer deficiency accelerates aging and mitigates several effects of dietary restriction in mice.
Aging (Albany NY), 8(6):1201–22, 2016.

[153] M. Trajkovski and H. Lodish.
MicroRNA networks regulate development of brown adipocytes.
Trends Endocrinol Metab, 24(9):442–50, 2013.

[154] F. Shamsi, H. Zhang, and Y. H. Tseng.
MicroRNA regulation of brown adipogenesis and thermogenic energy expenditure.
Front Endocrinol (Lausanne), 8:205, 2017.

[155] Q. Lin, Z. Gao, R. M. Alarcon, J. Ye, and Z. Yun.
A role of miR-27 in the regulation of adipogenesis.
FEBS J, 276(8):2348–58, 2009.

[156] L. Sun and M. Trajkovski.
MiR-27 orchestrates the transcriptional regulation of brown adipogenesis.
Metabolism, 63(2):272–82, 2014.

[157] T. Kang, W. Lu, W. Xu, L. Anderson, M. Bacanamwo, W. Thompson, Y. E. Chen, and D. Liu.
MicroRNA-27 (miR-27) targets prohibitin and impairs adipocyte differentiation and mitochondrial function in human adipose-derived stem cells.
J Biol Chem, 288(48):34394–402, 2013.

[158] H. Ding, S. Zheng, D. Garcia-Ruiz, D. Hou, Z. Wei, Z. Liao, L. Li, Y. Zhang, X. Han, K. Zen, C. Y. Zhang, J. Li, and X. Jiang.
Fasting induces a subcutaneous-to-visceral fat switch mediated by microRNA-149-3p and suppression of PRDM16.
Nat Commun, 7:11533, 2016.

[159] Y. Chen, F. Siegel, S. Kipschull, B. Haas, H. Fröhlich, G. Meister, and A. Pfeifer.
miR-155 regulates differentiation of brown and beige adipocytes via a bistable circuit.
Nat Commun, 4:1769, 2013.

[160] M. Mori, H. Nakagami, G. Rodriguez-Araujo, K. Nimura, and Y. Kaneda.
Essential role for miR-196a in brown adipogenesis of white fat progenitor cells.
PLoS Biol, 10(4):e1001314, 2012.

[161] M. Karbiener, C. Neuhold, P. Opriessnig, A. Prokesch, J. G. Bogner-Strauss, and M. Scheideler.
MicroRNA-30c promotes human adipocyte differentiation and co-represses PAI-1 and ALK2.
RNA Biol, 8(5):850–60, 2011.

[162] F. Hu, M. Wang, T. Xiao, B. Yin, L. He, W. Meng, M. Dong, and F. Liu.
miR-30 promotes thermogenesis and the development of beige fat by targeting RIP140.
Diabetes, 64(6):2056–68, 2015.

[163] I. Guller, S. McNaughton, T. Crowley, V. Gilsanz, S. Kajimura, M. Watt, and A. P. Russell.
Comparative analysis of microRNA expression in mouse and human brown adipose tissue.
BMC Genomics, 16:820, 2015.

[164] H. Zhang, M. Guan, K. L. Townsend, T. L. Huang, D. An, X. Yan, R. Xue, T. J. Schulz, J. Winnay, M. Mori, M. F. Hirshman, K. Kristiansen, J. S. Tsang, A. P. White, A. M. Cypess, L. J. Goodyear, and Y. H. Tseng.
MicroRNA-455 regulates brown adipogenesis via a novel HIF1an-AMPK-PGC1alpha signaling network.
EMBO Rep, 16(10):1378–93, 2015.

[165] R. Ng, N. A. Hussain, Q. Zhang, C. Chang, H. Li, Y. Fu, L. Cao, W. Han, W. Stunkel, and F. Xu.
miRNA-32 drives brown fat thermogenesis and trans-activates subcutaneous white fat browning in mice.
Cell Rep, 19(6):1229–1246, 2017.

[166] M. Trajkovski, K. Ahmed, C. C. Esau, and M. Stoffel.
MyomiR-133 regulates brown fat differentiation through prdm16.
Nat Cell Biol, 14(12):1330–5, 2012.

[167] W. Liu, P. Bi, T. Shan, X. Yang, H. Yin, Y. X. Wang, N. Liu, M. A. Rudnicki, and S. Kuang.
miR-133a regulates adipocyte browning in vivo.
PLoS Genet, 9(7):e1003626, 2013.

[168] L. Sun, H. Xie, M. A. Mori, R. Alexander, B. Yuan, S. M. Hattangadi, Q. Liu, C. R. Kahn, and H. F. Lodish.
MiR-193b-365 is essential for brown fat differentiation.
Nat Cell Biol, 13(8):958–65, 2011.

[169] Y. Feuermann, K. Kang, O. Gavrilova, N. Haetscher, S. J. Jang, K. H. Yoo, C. Jiang, F. J. Gonzalez, G. W. Robinson, and L. Hennighausen.
MiR-193b and miR-365-1 are not required for the development and function of brown fat in the mouse.
RNA Biol, 10(12):1807–14, 2013.

[170] M. Oliverio, E. Schmidt, J. Mauer, C. Baitzel, N. Hansmeier, S. Khani, S. Konieczka, M. Pradas-Juni, S. Brodesser, T. M. Van, D. Bartsch, H. S. Brönneke, M. Heine, H. Hilpert, E. Tarcitano, G. A. Garinis, P. Frommolt, J. Heeren, M. A. Mori, J. C. Brüning, and J. W. Kornfeld.
Dicer1-miR-328-Bace1 signalling controls brown adipose tissue differentiation and function.
Nat Cell Biol, 18(3):328–36, 2016.

[171] S. M. Turpin, H. T. Nicholls, D. M. Willmes, A. Mourier, S. Brodesser, C. M. Wunderlich, J. Mauer, E. Xu, P. Hammerschmidt, H. S. Brönneke, A. Trifunovic, G. LoSasso, F. T. Wunderlich, J. W. Kornfeld, M. Blüher, M. Krönke, and J. C. Brüning.
Obesity-induced CerS6-dependent C16:0 ceramide production promotes weight gain and glucose intolerance.
Cell Metab, 20(4):678–86, 2014.

[172] B. F. Belgardt, J. Mauer, F. T. Wunderlich, M. B. Ernst, M. Pal, G. Spohn, H. S. Brönneke, S. Brodesser, B. Hampel, A. C. Schauss, and J. C. Brüning.
Hypothalamic and pituitary c-Jun N-terminal kinase 1 signaling coordinately regulates glucose metabolism.
Proc Natl Acad Sci U S A, 107(13):6028–33, 2010.

[173] S. M. Steculorum, J. Ruud, I. Karakasilioti, H. Backes, L. Engstrom Ruud, K. Timper, M. E. Hess, E. Tsaousidou, J. Mauer, M. C. Vogt, L. Paeger, S. Bremser, A. C. Klein, D. A. Morgan, P. Frommolt, P. T. Brinkkotter, P. Hammerschmidt, T. Benzing, K. Rahmouni, F. T. Wunderlich, P. Kloppenburg, and J. C. Brüning.

AgRP Neurons Control Systemic Insulin Sensitivity via Myostatin Expression in Brown Adipose Tissue.
Cell, 165(1):125–138, 2016.

[174] L. Cong, F. A. Ran, D. Cox, S. Lin, R. Barretto, N. Habib, P. D. Hsu, X. Wu, W. Jiang, L. A. Marraffini, and F. Zhang.
Multiplex genome engineering using CRISPR/Cas systems.
Science, 339(6121):819–23, 2013.

[175] M. Zhang, C. D'Aniello, A. O. Verkerk, E. Wrobel, S. Frank, D. Ward-van Oostwaard, I. Piccini, C. Freund, J. Rao, G. Seebohm, D. E. Atsma, E. Schulze-Bahr, C. L. Mummery, B. Greber, and M. Bellin.
Recessive cardiac phenotypes in induced pluripotent stem cell models of Jervell and Lange-Nielsen syndrome: disease mechanisms and pharmacological rescue.
Proc Natl Acad Sci U S A, 111(50):E5383–92, 2014.

[176] J. Gao, D. Schatton, P. Martinelli, H. Hansen, D. Pla-Martin, E. Barth, C. Becker, J. Altmueller, P. Frommolt, M. Sardiello, and E. I. Rugarli.
CLUH regulates mitochondrial biogenesis by binding mRNAs of nuclear-encoded mitochondrial proteins.
J Cell Biol, 207(2):213–23, 2014.

[177] X. Mao, Y. Fujiwara, and S. H. Orkin.
Improved reporter strain for monitoring Cre recombinase-mediated DNA excisions in mice.
Proc Natl Acad Sci U S A, 96(9):5037–42, 1999.

[178] A. Keller, J. Eng, N. Zhang, X. J. Li, and R. Aebersold.
A uniform proteomics MS/MS analysis platform utilizing open XML file formats.
Mol Syst Biol, 1:2005 0017, 2005.

[179] M. Choi, C. Y. Chang, T. Clough, D. Broudy, T. Killeen, B. MacLean, and O. Vitek.
MSstats: an R package for statistical analysis of quantitative mass spectrometry-based proteomic experiments.
Bioinformatics, 30(17):2524–6, 2014.

[180] P. H. Kuhn, K. Koroniak, S. Hogl, A. Colombo, U. Zeitschel, M. Willem, C. Volbracht, U. Schepers, A. Imhof, A. Hoffmeister, C. Haass, S. Rossner, S. Brase, and S. F. Lichtenthaler.
Secretome protein enrichment identifies physiological BACE1 protease substrates in neurons.
EMBO J, 31(14):3157–68, 2012.

[181] A. Serdaroglu, S. A. Muller, U. Schepers, S. Brase, W. Weichert, S. F. Lichtenthaler, and P. H. Kuhn.
An optimised version of the secretome protein enrichment with click sugars (SPECS) method leads to enhanced coverage of the secretome.
Proteomics, 17(5), 2017.

[182] T. Fromme and M. Klingenspor.
Uncoupling protein 1 expression and high-fat diets.
Am J Physiol Regul Integr Comp Physiol, 300(1):R1–8, 2011.

[183] I. Karakasilioti, I. Kamileri, G. Chatzinikolaou, T. Kosteas, E. Vergadi, A. R. Robinson, I. Tsamardinos, T. A. Rozgaja, S. Siakouli, C. Tsatsanis, L. J. Niedernhofer, and G. A. Garinis.
DNA damage triggers a chronic autoinflammatory response, leading to fat depletion in NER progeria.
Cell Metab, 18(3):403–15, 2013.

[184] J. Darcy and A. Bartke.
Functionally enhanced brown adipose tissue in Ames dwarf mice.
Adipocyte, 6(1):62–67, 2017.

[185] V. Boissonneault, I. Plante, S. Rivest, and P. Provost.
MicroRNA-298 and microRNA-328 regulate expression of mouse beta-amyloid precursor protein-converting enzyme 1.
J Biol Chem, 284(4):1971–81, 2009.

[186] B. D. Bennett, S. Babu-Khan, R. Loeloff, J. C. Louis, E. Curran, M. Citron, and R. Vassar.
Expression analysis of BACE2 in brain and peripheral tissues.
J Biol Chem, 275(27):20647–51, 2000.

[187] X. Sun, G. He, and W. Song.
BACE2, as a novel APP theta-secretase, is not responsible for the pathogenesis of Alzheimer's disease in Down syndrome.
FASEB J, 20(9):1369–76, 2006.

[188] D. Esterhazy, I. Stutzer, H. Wang, M. P. Rechsteiner, J. Beauchamp, H. Dobeli, H. Hilpert, H. Matile, M. Prummer, A. Schmidt, N. Lieske, B. Boehm, L. Marselli, D. Bosco, J. Kerr-Conte, R. Aebersold, G. A. Spinas, H. Moch, C. Migliorini, and M. Stoffel.
Bace2 is a beta cell-enriched protease that regulates pancreatic beta cell function and mass.
Cell Metab, 14(3):365–77, 2011.

[189] S. L. Roberds, J. Anderson, G. Basi, M. J. Bienkowski, D. G. Branstetter, K. S. Chen, S. B. Freedman, N. L. Frigon, D. Games, K. Hu, K. Johnson-Wood, K. E. Kappenman, T. T. Kawabe, I. Kola, R. Kuehn, M. Lee, W. Liu, R. Motter, N. F. Nichols, M. Power, D. W. Robertson, D. Schenk, M. Schoor, G. M. Shopp, M. E. Shuck, S. Sinha, K. A. Svensson, G. Tatsuno, H. Tintrup, J. Wijsman, S. Wright, and L. McConlogue.
BACE knockout mice are healthy despite lacking the primary β-secretase activity in brain: implications for Alzheimer's disease therapeutics.
Hum Mol Genet, 10(12):1317–24, 2001.

[190] M. Jinek, K. Chylinski, I. Fonfara, M. Hauer, J. A. Doudna, and E. Charpentier.
A programmable dual-RNA-guided DNA endonuclease in adaptive bacterial immunity.
Science, 337(6096):816–21, 2012.

[191] S. Chira, D. Gulei, A. Hajitou, A. A. Zimta, P. Cordelier, and I. Berindan-Neagoe.
CRISPR/Cas9: Transcending the Reality of Genome Editing.
Mol Ther Nucleic Acids, 7:211–222, 2017.

[192] M. L. Hemming, J. E. Elias, S. P. Gygi, and D. J. Selkoe.
Identification of β-secretase (BACE1) substrates using quantitative proteomics.
PLoS One, 4(12):e8477, 2009.

[193] A. Hoffmeister, G. Dietz, U. Zeitschel, J. Mossner, S. Rossner, and T. Stahl.
BACE1 is a newly discovered protein secreted by the pancreas which cleaves enteropeptidase *in vitro*.
JOP, 10(5):501–6, 2009.

[194] I. Stutzer, N. Selevsek, D. Esterhazy, A. Schmidt, R. Aebersold, and M. Stoffel.
Systematic proteomic analysis identifies β-site amyloid precursor protein cleaving enzyme 2 and 1 (BACE2 and BACE1) substrates in pancreatic β-cells.
J Biol Chem, 288(15):10536–47, 2013.

[195] P. Mirkowska, A. Hofmann, L. Sedek, L. Slamova, E. Mejstrikova, T. Szczepanski, M. Schmitz, G. Cario, M. Stanulla, M. Schrappe, V. H. van der Velden, B. C. Bornhauser, B. Wollscheid, and J. P. Bourquin.
Leukemia surfaceome analysis reveals new disease-associated features.
Blood, 121(25):e149–59, 2013.

[196] D. Bausch-Fluck, A. Hofmann, T. Bock, A. P. Frei, F. Cerciello, A. Jacobs, H. Moest, U. Omasits, R. L. Gundry, C. Yoon, R. Schiess, A. Schmidt, P. Mirkowska, A. Hartlova, J. E. Van Eyk, J. P. Bourquin, R. Aebersold, K. R. Boheler, P. Zandstra, and B. Wollscheid.
A mass spectrometric-derived cell surface protein atlas.
PLoS One, 10(3):e0121314, 2015.

[197] M. Makridakis and A. Vlahou.
Secretome proteomics for discovery of cancer biomarkers.
J Proteomics, 73(12):2291–305, 2010.

[198] P. F. Lalor, C. Tuncer, C. Weston, A. Martin-Santos, D. J. Smith, and D. H. Adams.
Vascular adhesion protein-1 as a potential therapeutic target in liver disease.
Ann N Y Acad Sci, 1110:485–96, 2007.

[199] C. J. Weston, E. L. Shepherd, L. C. Claridge, P. Rantakari, S. M. Curbishley, J. W. Tomlinson, S. G. Hubscher, G. M. Reynolds, K. Aalto, Q. M. Anstee, S. Jalkanen, M. Salmi, D. J. Smith, C. P. Day, and D. H. Adams.
Vascular adhesion protein-1 promotes liver inflammation and drives hepatic fibrosis.
J Clin Invest, 125(2):501–20, 2015.

[200] A. Abella, S. Garcia-Vicente, N. Viguerie, A. Ros-Baro, M. Camps, M. Palacin, A. Zorzano, and L. Marti.
Adipocytes release a soluble form of VAP-1/SSAO by a metalloprotease-dependent process and in a regulated manner.
Diabetologia, 47(3):429–438, 2004.

[201] T. Valente, A. Gella, M. Sole, N. Durany, and M. Unzeta.
Immunohistochemical study of semicarbazide-sensitive amine oxidase/vascular adhesion protein-1 in the hippocampal vasculature: pathological synergy of Alzheimer's disease and diabetes mellitus.
J Neurosci Res, 90(10):1989–96, 2012.

[202] M. Sole, A. J. Minano-Molina, and M. Unzeta.
Cross-talk between Abeta and endothelial SSAO/VAP-1 accelerates vascular damage and Abeta aggregation related to CAA-AD.
Neurobiol Aging, 36(2):762–75, 2015.

[203] Z. Meszaros, T. Szombathy, L. Raimondi, I. Karadi, L. Romics, and K. Magyar.
Elevated serum semicarbazide-sensitive amine oxidase activity in non-insulin-dependent diabetes mellitus: correlation with body mass index and serum triglyceride.
Metabolism, 48(1):113–7, 1999.

[204] N. Yoshikawa, K. Noda, H. Shinoda, A. Uchida, Y. Ozawa, K. Tsubota, Y. Mashima, and S. Ishida.
Serum vascular adhesion protein-1 correlates with vascular endothelial growth factor in patients with type ii diabetes.
J Diabetes Complications, 27(2):162–6, 2013.

[205] E. Sondergaard, L. C. Gormsen, M. H. Christensen, S. B. Pedersen, P. Christiansen, S. Nielsen, P. L. Poulsen, and N. Jessen.
Chronic adrenergic stimulation induces brown adipose tissue differentiation in visceral adipose tissue.
Diabet Med, 32(2):e4–8, 2015.

[206] L. Sun, L. A. Goff, C. Trapnell, R. Alexander, K. A. Lo, E. Hacisuleyman, M. Sauvageau, B. Tazon-Vega, D. R. Kelley, D. G. Hendrickson, B. Yuan, M. Kellis, H. F. Lodish, and J. L. Rinn.
Long noncoding RNAs regulate adipogenesis.
Proc Natl Acad Sci U S A, 110(9):3387–92, 2013.

[207] A. F. Christopher, R. P. Kaur, G. Kaur, A. Kaur, V. Gupta, and P. Bansal.
MicroRNA therapeutics: Discovering novel targets and developing specific therapy.
Perspect Clin Res, 7(2):68–74, 2016.

[208] J. Sanchez-Gurmaches and D. A. Guertin.
Adipocyte lineages: tracing back the origins of fat.
Biochim Biophys Acta, 1842(3):340–51, 2014.

[209] C. Li, X. Li, X. Gao, R. Zhang, Y. Zhang, H. Liang, C. Xu, W. Du, Y. Zhang, X. Liu, N. Ma, Z. Xu, L. Wang, X. Chen, Y. Lu, J. Ju, B. Yang, and H. Shan.
MicroRNA-328 as a regulator of cardiac hypertrophy.
Int J Cardiol, 173(2):268–76, 2014.

[210] N. Katakami, H. Kaneto, H. Hao, Y. Umayahara, Y. Fujitani, K. Sakamoto, S. Gorogawa, T. Yasuda, D. Kawamori, Y. Kajimoto, M. Matsuhisa, C. Yutani, M. Hori, and Y. Yamasaki.
Role of pim-1 in smooth muscle cell proliferation.
J Biol Chem, 279(52):54742–9, 2004.

[211] J. Meloche, R. Paulin, A. Courboulin, C. Lambert, M. Barrier, P. Bonnet, M. Bisserier, M. Roy, M. A. Sussman, M. Agharazii, and S. Bonnet.
RAGE-dependent activation of the oncoprotein Pim1 plays a critical role in systemic vascular remodeling processes.
Arterioscler Thromb Vasc Biol, 31(9):2114–24, 2011.

[212] Z. Qian, L. Zhang, J. Chen, Y. Li, K. Kang, J. Qu, Z. Wang, Y. Zhai, L. Li, and D. Gou.
MiR-328 targeting PIM-1 inhibits proliferation and migration of pulmonary arterial smooth muscle cells in PDGFBB signaling pathway.
Oncotarget, 7(34):54998–55011, 2016.

[213] A. Hoffmeister, J. Tuennemann, I. Sommerer, J. Mossner, A. Rittger, D. Schleinitz, J. Kratzsch, J. Rosendahl, N. Kloting, T. Stahl, S. Rossner, F. Paroni, K. Maedler, P. Kovacs, and M. Bluher.
Genetic and biochemical evidence for a functional role of BACE1 in the regulation of insulin mRNA expression.
Obesity (Silver Spring), 21(12):E626–33, 2013.

[214] M. Maesako, K. Uemura, M. Kubota, A. Kuzuya, K. Sasaki, M. Asada, K. Watanabe, N. Hayashida, M. Ihara, H. Ito, S. Shimohama, T. Kihara, and A. Kinoshita.
Environmental enrichment ameliorated high-fat diet-induced Abeta deposition and memory deficit in APP transgenic mice.
Neurobiol Aging, 33(5):1011 e11–23, 2012.

[215] K. Plucinska, R. Dekeryte, D. Koss, K. Shearer, N. Mody, P. D. Whitfield, M. K. Doherty, M. Mingarelli, A. Welch, G. Riedel, M. Delibegovic, and B. Platt.
Neuronal human BACE1 knockin induces systemic diabetes in mice.
Diabetologia, 59(7):1513–23, 2016.

[216] M. Sastre, I. Dewachter, S. Rossner, N. Bogdanovic, E. Rosen, P. Borghgraef, B. O. Evert, L. Dumitrescu-Ozimek, D. R. Thal, G. Landreth, J. Walter, T. Klockgether, F. van Leuven, and M. T. Heneka.
Nonsteroidal anti-inflammatory drugs repress beta-secretase gene promoter activity by the activation of PPARgamma.
Proc Natl Acad Sci U S A, 103(2):443–8, 2006.

[217] B. Dislich and S. F. Lichtenthaler.
The membrane-bound aspartyl protease BACE1: Molecular and functional properties in Alzheimer's disease and beyond.

Front Physiol, 3:8, 2012.

[218] E. Jeffery, C. D. Church, B. Holtrup, L. Colman, and M. S. Rodeheffer.
Rapid depot-specific activation of adipocyte precursor cells at the onset of obesity.
Nat Cell Biol, 17(4):376–85, 2015.

[219] P. S. Ward and C. B. Thompson.
Signaling in control of cell growth and metabolism.
Cold Spring Harb Perspect Biol, 4(7):a006783, 2012.

[220] S. Siddiqui, M. Fang, B. Ni, D. Lu, B. Martin, and S. Maudsley.
Central role of the EGF receptor in neurometabolic aging.
Int J Endocrinol, 2012:739428, 2012.

[221] V. J. Nies, G. Sancar, W. Liu, T. van Zutphen, D. Struik, R. T. Yu, A. R. Atkins, R. M. Evans, J. W. Jonker, and M. R. Downes.
Fibroblast growth factor signaling in metabolic regulation.
Front Endocrinol (Lausanne), 6:193, 2015.

[222] C. H. Heldin and B. Westermark.
Mechanism of action and in vivo role of platelet-derived growth factor.
Physiol Rev, 79(4):1283–316, 1999.

[223] M. D. Tallquist, W. J. French, and P. Soriano.
Additive effects of PDGF receptor beta signaling pathways in vascular smooth muscle cell development.
PLoS Biol, 1(2):E52, 2003.

[224] A. Uezumi, S. Fukada, N. Yamamoto, M. Ikemoto-Uezumi, M. Nakatani, M. Morita, A. Yamaguchi, H. Yamada, I. Nishino, Y. Hamada, and K. Tsuchida.
Identification and characterization of PDGFRalpha+ mesenchymal progenitors in human skeletal muscle.
Cell Death Dis, 5:e1186, 2014.

[225] M. Hellstrom, M. Kalen, P. Lindahl, A. Abramsson, and C. Betsholtz.
Role of PDGF-B and PDGFR-beta in recruitment of vascular smooth muscle cells and pericytes during embryonic blood vessel formation in the mouse.
Development, 126(14):3047–55, 1999.

[226] L. E. Olson and P. Soriano.
PDGFRbeta signaling regulates mural cell plasticity and inhibits fat development.
Dev Cell, 20(6):815–26, 2011.

[227] S. A. Prigent and N. R. Lemoine.
The type 1 (EGFR-related) family of growth factor receptors and their ligands.
Prog Growth Factor Res, 4(1):1–24, 1992.

[228] B. Schreier, M. Gekle, and C. Grossmann.
Role of epidermal growth factor receptor in vascular structure and function.
Curr Opin Nephrol Hypertens, 23(2):113–21, 2014.

[229] G. Serrero and D. Mills.
Physiological role of epidermal growth factor on adipose tissue development in vivo.
Proc Natl Acad Sci U S A, 88(9):3912–6, 1991.

[230] H. Adachi, H. Kurachi, H. Homma, K. Adachi, T. Imai, K. Morishige, Y. Matsuzawa, and A. Miyake.
Epidermal growth factor promotes adipogenesis of 3T3-L1 cell in vitro.
Endocrinology, 135(5):1824–30, 1994.

[231] T. Worzfeld and S. Offermanns.
Semaphorins and plexins as therapeutic targets.
Nat Rev Drug Discov, 13(8):603–21, 2014.

[232] G. Kerjan, J. Dolan, C. Haumaitre, S. Schneider-Maunoury, H. Fujisawa, K. J. Mitchell, and A. Chedotal.
The transmembrane semaphorin Sema6A controls cerebellar granule cell migration.
Nat Neurosci, 8(11):1516–24, 2005.

[233] J. Renaud, G. Kerjan, I. Sumita, Y. Zagar, V. Georget, D. Kim, C. Fouquet, K. Suda, M. Sanbo, F. Suto, S. L. Ackerman, K. J. Mitchell, H. Fujisawa, and A. Chedotal.
Plexin-A2 and its ligand, Sema6A, control nucleus-centrosome coupling in migrating granule cells.
Nat Neurosci, 11(4):440–9, 2008.

[234] M. Segarra, H. Ohnuki, D. Maric, O. Salvucci, X. Hou, A. Kumar, X. Li, and G. Tosato.
Semaphorin 6A regulates angiogenesis by modulating VEGF signaling.
Blood, 120(19):4104–15, 2012.

[235] Y. Wolf, S. Boura-Halfon, N. Cortese, Z. Haimon, H. Sar Shalom, Y. Kuperman, V. Kalchenko, A. Brandis, E. David, Y. Segal-Hayoun, L. Chappell-Maor, A. Yaron, and S. Jung.
Brown-adipose-tissue macrophages control tissue innervation and homeostatic energy expenditure.
Nat Immunol, 18(6):665–674, 2017.

[236] J. A. Ko, T. Gondo, S. Inagaki, and M. Inui.
Requirement of the transmembrane semaphorin Sema4C for myogenic differentiation.
FEBS Lett, 579(10):2236–42, 2005.

[237] H. Wu, X. Wang, S. Liu, Y. Wu, T. Zhao, X. Chen, L. Zhu, Y. Wu, X. Ding, X. Peng, J. Yuan, X. Wang, W. Fan, and M. Fan.
Sema4C participates in myogenic differentiation in vivo and in vitro through the p38 MAPK pathway.
Eur J Cell Biol, 86(6):331–44, 2007.

[238] N. Puthiyedth, C. Riveros, R. Berretta, and P. Moscato.
Identification of Differentially Expressed Genes through Integrated study of alzheimer's disease affected brain regions.
PLoS One, 11(4):e0152342, 2016.

[239] P. Dunkel, A. Gelain, D. Barlocco, N. Haider, K. Gyires, B. Sperlagh, K. Magyar, E. Maccioni, A. Fadda, and P. Matyus.
Semicarbazide-sensitive amine oxidase/vascular adhesion protein 1: recent developments concerning substrates and inhibitors of a promising therapeutic target.
Curr Med Chem, 15(18):1827–39, 2008.

[240] G. Enrique-Tarancon, L. Marti, N. Morin, J. M. Lizcano, M. Unzeta, L. Sevilla, M. Camps, M. Palacin, X. Testar, C. Carpene, and A. Zorzano.
Role of semicarbazide-sensitive amine oxidase on glucose transport and GLUT4 recruitment to the cell surface in adipose cells.
J Biol Chem, 273(14):8025–32, 1998.

[241] N. Morin, J. M. Lizcano, E. Fontana, L. Marti, F. Smih, P. Rouet, D. Prevot, A. Zorzano, M. Unzeta, and C. Carpene.
Semicarbazide-sensitive amine oxidase substrates stimulate glucose transport and inhibit lipolysis in human adipocytes.
J Pharmacol Exp Ther, 297(2):563–72, 2001.

[242] A. Doucet, O. Kleifeld, J. N. Kizhakkedathu, and C. M. Overall.
Identification of proteolytic products and natural protein N-termini by Terminal Amine Isotopic Labeling of Substrates (TAILS).
Methods Mol Biol, 753:273–87, 2011.

[243] P. Hohenstein, J. Slight, D. D. Ozdemir, S. F. Burn, R. Berry, and N. D. Hastie.
High-efficiency Rosa26 knock-in vector construction for Cre-regulated overexpression and RNAi.
Pathogenetics, 1(1):3, 2008.

[244] Z. V. Wang, Y. Deng, Q. A. Wang, K. Sun, and P. E. Scherer.
Identification and characterization of a promoter cassette conferring adipocyte-specific gene expression.
Endocrinology, 151(6):2933–9, 2010.

[245] C. Guerra, P. Navarro, A. M. Valverde, M. Arribas, J. Bruning, L. P. Kozak, C. R. Kahn, and M. Benito.
Brown adipose tissue-specific insulin receptor knockout shows diabetic phenotype without insulin resistance.
J Clin Invest, 108(8):1205–13, 2001.

[246] J. J. McCarthy, R. Srikuea, T. J. Kirby, C. A. Peterson, and K. A. Esser.
Inducible Cre transgenic mouse strain for skeletal muscle-specific gene targeting.
Skelet Muscle, 2(1):8, 2012.

[247] J. L. Jankowsky, D. J. Fadale, J. Anderson, G. M. Xu, V. Gonzales, N. A. Jenkins, N. G. Copeland, M. K. Lee, L. H. Younkin, S. L. Wagner, S. G. Younkin, and D. R. Borchelt.
Mutant presenilins specifically elevate the levels of the 42 residue beta-amyloid peptide in vivo: evidence for augmentation of a 42-specific gamma secretase.
Hum Mol Genet, 13(2):159–70, 2004.

[248] N. El Kadmiri, N. Said, I. Slassi, B. El Moutawakil, and S. Nadifi.
Biomarkers for Alzheimer disease: Classical and novel candidates' review.
Neuroscience, 2017.

Acknowledgements

I would like to thank Dr. Jan-Wilhelm Kornfeld (a.k.a. Jan) for the great opportunity that he gave me and all the help and support shown during these four years.

Thanks to Prof. Dr. Thomas Langer, Prof. Dr. Matthias Hammerschmidt and Dr. Ursula Lichtenberg for being part of my thesis committee.

I would also like to thank my collaborators Maik Müller, Prof. Dr. Bernd Wollscheid, Johanna Tüshaus and Prof. Dr. Stefan Lichtenthaler for their help with proteomic analysis.

Special thanks to the SpecialKs, current and former members of the AG Kornfeld, for making the time spent in the lab worth much more than the experiments only. In particular, thanks to Elena Schmidt, with whom I shared from the beginning this crazy adventure called PhD.

Many thanks to the members of the Brüning, Wunderlich and Steculorum groups for making the MPI-MR such a nice place where to go to work and for all the scientific support. In particular Thomas (Dr. F. T. Wunderlich, the master of cloning), Cathy Baitzel and Anke Lietzau for the immense help in everything concerning cloning, ES cell culture and southern blots. I am grateful for Brigitte Hampel, Pia Scholl and Christiane Schäfer for everything concerning immunohistochemistry.

Huge thanks to Tim and Erica for coping with the hard life of a scientist and feeding me when the lab hours were too long. And a very huge thanks to Galen, first of my not-scientist friends here in Cologne, always supportive and helping with graphic-related matters, including this thesis.

I have to thank Copes (named Francesco) and the Nikita's Filippo (a.k.a. Golden) and Lorenzo with whom I shared laughters and knowledge in the first years of my scientific career.

Immense thanks go to my relatives, in particular nonna Anna and my stars looking from above, for always supporting me although understanding nothing of what I was - and I am - doing.
There will never be enough thanks to my parents for all they have done and the many ways they supported me.

The biggest thanks of all is for Isabella for the immeasurable help she gave for this thesis, the scientific discussions, the awesome moments spent together, the daily support and love, in other words, for everything. Thank you.

Erklärung

Die vorliegende Arbeit wurde in der Zeit von Februar 2014 bis Dezember 2017 am Max-Planck-Institut für Stoffwechselforschung Köln, Forschungsgruppe Noncoding RNAs and Energy Homeostasis unter Anleitung von Herrn Dr. Jan-Wilhelm Kornfeld angefertigt.

Ich versichere hiermit, dass ich die von mir vorgelegte Dissertation selbstständig angefertigt, die benutzten Quellen und Hilfsmittel vollständig angegeben und die Stellen der Arbeit - einschließlich Tabellen, Karten und Abbildungen -, die anderen Werken im Wortlaut oder dem Sinn nach entnommen sind, in jedem Einzelfall als Entlehnung kenntlich gemacht habe; dass diese Dissertation noch keiner anderen Fakultät oder Universität zur Prüfung vorgelegen hat; dass sie - abgesehen von unten angegebenen Teilpublikationen - noch nicht veröffentlicht worden ist sowie, dass ich eine solche Veröffentlichung vor Abschluss des Promotionsverfahrens nicht vornehmen werde. Die Bestimmungen dieser Promotionsordnung sind mir bekannt.

Köln, 15. August 2018

Matteo Oliverio

TEILPUBLIKATIONEN

Oliverio, M., E. Schmidt, J. Mauer, C. Baitzel, N. Hansmeier, S. Khani, S. Konieczka, M. Pradas-Juni, S. Brodesser, T. M. Van, D. Bartsch, H. S. Brönneke, M. Heine, H. Hilpert, E. Tarcitano, G. A. Garinis, P. Frommolt, J. Heeren, M. A. Mori, J. C. Brüning, and J. W. Kornfeld.

Dicer1-miR-328-Bace1 signalling controls brown adipose tissue differentiation and function.

Nat Cell Biol, 18(3):328–36, 2016.

Matteo Oliverio

Curriculum Vitae

Work Experience

Feb 2014 - Dec 2017 **Graduate Student at the University of Cologne**, *Laboratory of Non-Coding Principles of Energy Homeostasis (headed by Dr. Jan-Wilhelm Kornfeld), Max-Planck Institute for Metabolism Research* , Köln (Germany).
Project: "A novel *miR-328*-Bace1 axis ensures brown adipose tissue homeostasis and energy metabolism in mice".

Jan 2013 - Dec 2013 **Assistant Researcher**, *Laboratory of Molecular and Cellular Biology of the Nucleus (headed by Dr. Alessandra Montecucco), Institute of Molecular Genetics - CNR*, Pavia (Italy).
Project: Influence of post-trascriptional modulations on gene expression in Alzheimer's Disease (AD). This project included the creation and characterisation of neuroblastoma SH-SY5Y cells and consequent differentiation and β-Amyloid treatment.

Education and Training

Master's degree in Molecular Biology and Genetics

Oct 2012 **Final evaluation 110/110 cum laude**, *University of Pavia*, Pavia (Italy).
Advanced Molecular Biology, Molecular Genetics, Cellular Biochemistry, Developmental Biology, Microbial Genetics and Molecular Microbiology, Molecular Pharmacology, Structural Biology and Pharmacology, Bioinformatics.
The Master's courses were all conducted in English language.
Master's thesis in Molecular Biology and Genetics. Title: "The cellular response to DNA damage affects the expression of genes involved in cell motility and migration".

Internship for experimental thesis (Master's degree)

Jan 2011 - Oct 2012 **Laboratory Internship**, *Laboratory of Molecular and Cellular Biology of the Nucleus (headed by Dr. Alessandra Montecucco), Institute of Molecular Genetics - CNR*, Pavia (Italy).
Project: The influence of DNA damage response (DDR) on morphology and adhesion properties of cells. This project worked with the cell model 46BR.1G1, characterised by endogenous and chronic activation of DDR. My work included RT-qPCR validation of differential gene expression involved in cell motility and migration in 46BR.1G1 and investigation of DDR induced checkpoint kinases.

Kleiner Griechenmarkt 26 – 50676 Köln
+49 176 89277790
Matteo.Oliverio@sf.mpg.de; matteoliverio@gmail.com

Bachelor's degree in Biological Sciences

Sep 2010 **Final evaluation 109/110**, *University of Pavia*, Pavia (Italy).
Molecular biology, Genetics, Microbiology, Biochemistry, General and Inorganic, Chemistry Organic Chemistry, Cytology and Histology, Developmental biology, Bioinformatics.
Degree Thesis in Biological Sciences. Title: "Analisi di un polimorfismo di sequenza (SNP) nel gene oncosoppressore CDH1 codificante per E-caderina" [Analyses of a sequence polymorphism (SNP) in the oncosuppressor gene CDH1 coding for E-cadherin]

Internship for experimental thesis (Bachelor's degree)

Nov 2009 - Sep 2010 **Laboratory Internship**, *Laboratory of Human Genetics (headed by Prof. Guglielmina Nadia Ranzani), Department of Biology and Biotechnology "Lazzaro Spallanzani"*, Pavia (Italy).

Science High School Diploma

Jul 2007 **Final evaluation 92/100** , *Liceo ginnasio statale "Melchiorre Gioia"*, Piacenza (Italy).

Languages

Italian	Mothertongue	
English	Very good knowledge	*First Certificate in English (FCE), level C (2006)*
German	Good knowledge	

Additional Information

Publications

Oliverio M*, Schmidt E*, Mauer J, Baitzel C, Hansmeier N, Khani S, Konieczka S, Pradas-Juni M, Brodesser S, Van TM, Bartsch D, Brönneke HS, Heine M, Hilpert H, Tarcitano E, Garinis GA, Frommolt P, Heeren J, Mori MA, Brüning JC, Kornfeld JW. Dicer1-miR-328-Bace1 signalling controls brown adipose tissue differentiation and function. *Nature Cell Biology*. 2016. doi: 10.1038/ncb3316. * Equal contribution

Cremaschi P*, **Oliverio M***, Leva V, Bione S, Carriero R, Mazzucco G, Palamidessi A, Scita G, Biamonti G, Montecucco A. Chronic Replication Problems Impact Cell Morphology and Adhesion of DNA Ligase I Defective Cells. *PLoS One*. 2015. doi: 10.1371/journal.pone.0130561. * Equal contribution

Brodarac A, Saric T, Oberwallner B, Mahmoodzadeh S, Neef K, Albrecht J, Burkert K, **Oliverio M**, Nguemo F, Choi YH, Neiss WF, Morano I, Hescheler J, Stamm C. Susceptibility of murine induced pluripotent stem cell-derived cardiomyocytes to hypoxia and nutrient deprivation. *Stem Cell Research & Therapy*. 2015. doi: 10.1186/s13287-015-0057-6.

Kleiner Griechenmarkt 26 – 50676 Köln
+49 176 89277790
Matteo.Oliverio@sf.mpg.de; matteoliverio@gmail.com

Conferences

- **Cell Symposia: Metabolic Disease Therapies**, San Diego (USA), 15-17.10.2017
  Poster: Bace1: a new link between neurodegenerative diseases and obesity.
- **6th PhD students/PostDocs CECAD Retreat**, St. Goar (Germany), 13-14.03.2017
  Talk: Bace1: a new link between neurodegenerative diseases and obesity.
- **1st joint MPI Scientific Retreat**, Köln (Germany), 13.09.2016
  Poster: Dicer1-miR-328-Bace1 signalling controls brown adipose tissue differentiation and function.
- **Cell Symposia: Aging and Metabolism**, Sitges (Spain), 10-12.07.2016
  Poster: Dicer1-miR-328-Bace1 signalling controls brown adipose tissue differentiation and function.
- **5th PhD students/PostDocs CECAD Retreat**, Trier (Germany), 03-04.03.2016
  Poster: Dicer1-miR-328-Bace1 signaling controls brown adipose tissue differentiation and function.
- **EMBO|EMBL Symposium: The Non-coding Genome**, Heidelberg (Germany), 18-21.10.2015
  Poster: Age- and Obesity-Induced Decline of Brown Fat Function as Consequence of Impaired miR-328 Dependent Silencing of Bace1.*
  *Winner of a Seahorse Bioscience (Agilent) Travel Grant.
- **4th PhD students/PostDocs CECAD Retreat**, Maastricht (Neederland), 02-03.03.2015
  Talk: Age- and Obesity-Induced Decline of Brown Fat Function as Consequence of Impaired miR-328 dependent Silencing of Bace1.
- **EMBO|EMBL Symposium: Frontiers in Metabolism: From Molecular Physiology to Systems Medicine**, Heidelberg (Germany), 17-20.11.2014
- **CECAD/IRCAN PhD student Postdoc Retreat**, Nizza (France), 01-03.10.2014
  Talk: microRNA-328 in brown fat controls glucose homeostasis via silencing of Bace1.
- **SIBBM Frontiers in Molecular Biology seminar -Revisiting the central dogma: emerging new concepts in replication, transcription and translation**, Pavia (Italy), 05-07.10.2013
  Poster: The cell response to replication defects affects alternative splicing programs and cell morphology.

Courses

- **Education and training of persons carrying out animal experiments (Category B) (FELASA)**, 2014. Interfakultäre Biomedizinische Forschungseinrichtung (IBF) - University of Heidelberg, Germany.
- **Scientific writing**, 2014. Cluster of Excellence in Aging-associated Diseases (CECAD), Cologne, Germany.
- **Scientific poster design**, 2016. Cluster of Excellence in Aging-associated Diseases (CECAD), Cologne, Germany.

Kleiner Griechenmarkt 26 – 50676 Köln
+49 176 89277790
Matteo.Oliverio@sf.mpg.de; matteoliverio@gmail.com